The spatiotemporal control of cell divisions in Physcomitrella development Han Tang 2020

The spatiotemporal control of cell divisions in Physcomitrella development

Han Tang

Propositions

1. Different subunits of the exocyst complex can individually contribute to cell divisions in terms of cell plate formation and the orientation of the division plane. (this thesis)

2. Changes in cell polarity and geometry can be both a prerequisite for and a consequence of cell fate change during the 2D-to-3D growth transition in moss. (this thesis)

3. The level of stress hormone does not represent the level of stress we encounter.

4. The different opinions about regulating CRISPR-Cas edited plants as GMO food in different countries reflect the living quality of citizens.

5. Feeding of mind and body are equally important, and junk foods are present in both scenarios.

6. The travel mate is more important than the destination.

Propositions belonging to the thesis, entitled

The spatiotemporal control of cell divisions in Physcomitrella development

Han Tang

Wageningen, 24 Jan 2020

The spatiotemporal control of cell divisions in Physcomitrella development

Han Tang

Thesis committee

Promotors

Prof. Dr Ben Scheres
Professor of Plant Developmental Biology
Wageningen University & Research

Prof. Dr Joop E.M. Vermeer
Professor of Cell and Molecular Biology
University of Neuchâtel

Co-promotors

Dr Viola Willemsen
Assistant Professor, Laboratory of Plant Developmental Biology
Wageningen University & Research

Dr Tijs Ketelaar
Assistant Professor, Laboratory of Cell Biology
Wageningen University & Research

Other members

Prof. Dr D. van Damme, VIB Ghent / Ghent University, Belgium
Dr Y. Coudert, ENS Lyon, France
Prof. Dr J Xu, Radboud University, Nijmegen
Prof. Dr D Weijers, Wageningen University & Research

This research was conducted under the auspices of the Graduate School Experimental Plant Sciences.

The spatiotemporal control of cell divisions in Physcomitrella development

Han Tang

Thesis

submitted in fulfilment of the requirements for the degree of doctor
at Wageningen University
by the authority of the Rector Magnificus
Prof. Dr A.P.J.Mol,
in the presence of the
Thesis Committee appointed by the Academic Board
to be defended in public
on Friday 24 Jan 2020
at 1:30 p.m. in the Aula.

Han Tang
The spatiotemporal control of cell divisions in Physcomitrella development. 144 pages.

PhD thesis, Wageningen University, Wageningen, the Netherlands (2020)
With references, with summary in English

ISBN: 978-94-6395-221-7

DOI: https://doi.org/10.18174/507481

For my beloved family

Table of contents

Abstract

Cell division is fundamental in the development of all living organisms. In plants, cells are caged in rigid cell walls, thus plant cell shape is solely determined by cell expansion and the orientation of the cell division plane. Additionally, a newly divided cell can acquire a different cell fate through an asymmetric cell division, which is essential for tissue innovations. During my PhD, I used *Physcomitrella patens*, a model moss system with powerful genetic toolkits and single-cell-layer tissues, to investigate cell division control in plant development. During cytokinesis, the last step of cell division when cells are physically separated, two antiparallel sets of microtubules overlap at the midline where cell plate formation takes place. I found that subunit Sec6 of the exocyst complex is positioned to the microtubule overlaps before membranous vesicles arrive, suggesting that Sec6 bridges the cytoskeletal network and membranous compartments in cytokinesis. During moss development, cells grow as branching filaments to form a 2D filamentous network. Filaments then start to generate initial cells with a new fate, becoming gametophore initial cells. These commence growth of a 3D leafy gametophore. I identified markers that can predict the fate of initial cells, providing a new tool to investigate the early stages of the 2D-to-3D growth transition. Next, I investigated the contribution of Rho-GTPase proteins, Rho-of-Plant (ROP), to gametophore formation. I demonstrated that deletion of ROP2 results in defects in filamentous cell type transition, gametophore initiation, and leaf development. Additive deletion of ROP's effector, RIC, in *rop2* mutants only rescued phenotypes in gametophore development, suggesting that the ROP2-RIC module is functional in a tissue-specific manner. Finally, I developed a controllable wounding system to study cell reprogramming in excised moss leaves as a start to elucidate the interplay of cell reprogramming and cell division control in the early land plant lineage.

Chapter 1

General introduction

Han Tang[1,2]

[1] Laboratory of Plant Developmental Biology, Wageningen University & Research, Wageningen, The Netherlands
[2] Laboratory of Cell Biology, Wageningen University & Research, Wageningen, The Netherlands

General introduction

All living organisms grow through successive rounds of coordinated cell growth and cell division. Upon division, dividing cells partition their cytoplasm and genetic materials to daughter cells. Proliferative symmetric divisions that produce identical daughter cells are essential and account for the majority of divisions to increase the size of the population and expand body plan growth across kingdoms. Alternatively, formative asymmetric divisions that produce daughter cells possessing different cell fates are crucial to generate cell diversity during development (Kaiser *et al.*, 2007). Additionally, asymmetric divisions are also common to perform to survive harsh environmental stimuli, e.g. *Bacillus subtilis* generates spores under nutrients starvation (Kunkel, 1991). In multicellular organisms, cells acquire distinct identities from asymmetric divisions to initiate tissue patterning and organ formation, while proliferative divisions participate in this developmental progress as well. The coordination of cell division and differentiation permit proper growth and development of any organism.

Plant cells are caged in stiff cell walls that lead to a fixed position in the developing body plan after a cell is newly generated from a cell division. The immobility of plant cells dictates that the cell fate of a daughter cell must be determined at the position where it is formed during cell division (Shao & Dong, 2016; Facette *et al.*, 2019). The decision of when, where, and how to divide is sophistically regulated. Information about tissue identity, relative position, and developmental stages are coordinated by internal gene expression and external signal perception and eventually lead to the correct orientation of cell divisions and the proper specification of daughter cell fates. In plant development, asymmetric cell divisions are used to generate cell diversity that forms new tissues while maintaining self-renewing stem cell populations for additional growth (Pillitteri *et al.*, 2016). In the bryophyte lineage, moss plants use a series of asymmetric divisions to generate an apical meristem cell that initiates the formation of 3-dimensional leafy shoots. This structure allows mosses to survive harsh environmental conditions such as drought, fluctuating temperature, and radiation (Harrison *et al.*, 2009). In angiosperms, most studies regarding asymmetric divisions were performed in the model plant *Arabidopsis* and revealed that asymmetric divisions are critical in a wide spectrum of developmental programs including embryo, root, and leaf development (Rasmussen *et al.*, 2011).

I will first briefly introduce the intracellular mechanisms of **cell cycle** control that serve as the primary gatekeeper of cell proliferation and **cytokinesis**, where the orientation of the division plane is fixed. Next, the tissue level control of formative cell divisions will be discussed including control components involved in **asymmetric cell division**. Finally, I will discuss division strategies in early land plants and the advantages of using the model bryophyte ***Physcomitrella patens*** for investigating the spatiotemporal control of cell division.

1. Intracellular control of cell division

1.1 Cell cycle

Once a cell reaches a minimum size (Jones *et al.*, 2017) and perceives developmental cues including nutrients and growth factors, the cell passes the G1 cell cycle checkpoint and is ready to initiate DNA replication (Inzé & Veylder, 2006). Later cell cycle checkpoints act as gates to ensure the accuracy of DNA replication and chromosome segregation. When DNA damage or incomplete replication occurs, progression to mitosis is arrested by a series of phosphorylation events at the G2-M checkpoint for DNA repair. Later, to ensure proper segregation of the duplicated chromosomes, the spindle

attachment to each sister chromatid is safeguarded at the mitotic checkpoint. Cell cycle checkpoints are mainly controlled by cyclins, a family of proteins that integrate cellular cues and regulate cyclin-dependent kinase (CDK) activity by phosphorylation. Association with different cyclin partners determines the activity and substrate specificity of CDKs. The phosphorylation of CDK substrates subsequently activates proteins and genes that are specifically required for the progression of distinct cell cycle phases (De Veylder *et al.*, 2007). CDKs can also be directly inhibited by binding with inhibitor proteins in response to abiotic and biotic stresses to cease cell cycle (De Veylder *et al.*, 2007; Peres *et al.*, 2007).

Once a cell passes the G2-M checkpoint and proceeds to the mitosis, the cell starts to physically separate duplicated chromosomes and fixes the location and orientation of the future division plane. To separate sister chromosomes, all eukaryotic cells reorganize the microtubule cytoskeleton by forming bipolar spindles that attach and pull sister chromatids toward opposite directions (Oliferenko *et al.*, 2009; Li *et al.*, 2015). During plant cell division, in addition to the spindle, two specialized structures called preprophase band (PPB) and phragmoplast are also established by microtubules and actin filaments (Lipka *et al.*, 2015).

1.2 Cytokinesis

To determine the orientation of the division plane, plant cells build a belt-like structure, the **PPB** by assembling cortical microtubules and actin filaments at the G2-to-M phase (Mineyuki, 1999; Vos *et al.*, 2004). The PPB marks the insertion site of the future cell plate in the existing parental membrane. The PPB disassembles before mitosis, indicating that the cell plate insertion site marked by the PPB needs to be memorized throughout mitosis (Lloyd & Buschmann, 2007; Lipka *et al.*, 2015). A number of microtubule-associated proteins and polarity proteins e.g. MAP65-4, TANGLED, and RanGAP1 are recruited and persist at the cortical division site, where they assist as landmark proteins that remember and define the cortical division zone (CDZ) after the PPB has disappeared (Cleary & Smith, 1998; Walker, Keely L *et al.*, 2007; Xu *et al.*, 2008; Li *et al.*, 2017). Mutants of these landmarks or specific kinesins required for their residence reveal misaligned PPBs and phragmoplasts or oblique division planes, demonstrating their role in phragmoplast guidance function (Cleary & Smith, 1998; Muller *et al.*, 2006; Walker, K. L. *et al.*, 2007; Xu *et al.*, 2008).

At the final step of mitosis, **cytokinesis**, the dividing cell physically partitions cytoplasmic contents and duplicated chromosomes to daughter cells by forming cell plate in between. The CDZ is narrowed by distinct localization patterns of resident proteins and defined as the cell division site (CDS), where cell plate insertion takes place. The cell plate forms *de novo* between two dividing cells. Vesicles carrying materials of new membrane and cell wall accumulate and fuse with each other to centrifugally build up the cell plate (Mueller & Juergens, 2016). To precisely locate these vesicles to the correct site where the future cell plate forms, another specialized microtubule structure is developed, the **phragmoplast**. At the initial phase of cytokinesis, the phragmoplast is developed by reorganizing microtubules into two antiparallel sets. The plus ends of each set of microtubules overlap in the middle via crosslinker proteins and the interdigitating region, where vesicles are immobilized and fused to accurately position the division site (Lee & Liu, 2013; de Keijzer *et al.*, 2017). Arrival vesicles centrifugally expand the cell plate towards the guidance cues at parental membranes (Lipka *et al.*, 2015). The lateral expansion along with the disassembly of microtubules at the trailing edges of the phragmoplast is required for cell plate maturation. Mutation of the key kinesin HINKEL that drives the depolymerization of the

trailing edges of phragmoplast results in incomplete cell walls and multiple nuclei (Nishihama *et al.*, 2002; Strompen *et al.*, 2002). The lateral expansion of the phragmoplast leading edge is guided toward the CDS. In addition to the landmark proteins mentioned above, myosin VIII resides at the CDS and also at the phragmoplast microtubule plus ends of the leading edge, where its motor activity along actin filaments is proposed to guide the expanding phragmoplast toward the CDS (Wu & Bezanilla, 2014). Golgi-derived vesicles are transported along the aligned phragmoplast microtubule arrays towards the central overlapping region, where tethering complexes and mitosis-specific membrane anchoring proteins are required to perform homologous vesicles fusion (Waizenegger *et al.*, 2000; Fendrych *et al.*, 2010b).

While heterologous vesicle fusion uses landmark cues on target membranes to guide vesicle trafficking, homologous vesicle fusion may demand different control in the absence of the guidance of a target membrane. Two tethering complexes, the exocyst complex and the transport protein particle II complex, have been identified to contribute to homologous vesicle fusion during cell plate formation in plant (Fendrych *et al.*, 2010a; Rybak *et al.*, 2014). In addition to tethering, cytokinesis-specific membrane anchoring proteins KNOLLE and its interacting partner KEULE are also essential for homologous vesicle fusion, as mutations in either gene lead to an incomplete cell plate (Lukowitz *et al.*, 1996; Assaad *et al.*, 2001). The fusion of arrival vesicles builds a tubular membranous structure, which ultimately develops into a continuous cell plate. Once the expanding cell plate attaches and fuses with the parental membrane, excess membrane materials are removed from the newly formed cell wall to complete cell division.

2. Whole organism control of cell division

The cell cycle program and cytokinesis use common mechanisms in diverse cells during plant cell division. However, the orientation of division planes that leads to volumetric asymmetry and asymmetric division that generates a daughter cell with a different cell fate relies on diverse mechanisms in distinct developmental programs.

2.1 Symmetric cell division

How to specify zones of cell division in an intact plant? At different tissues and positions within tissues, the cells receive positional cues such as growth hormones and mobile transcriptional factors that activate genes for cell division (Murray *et al.*, 2012; Santuari *et al.*, 2016). The gradient distribution of different hormones may facilitate or antagonize cell division at different tissues, indicating that tissue-specific components can change the cell division response to hormones (Schaller *et al.*, 2015).

Once a cell is activated to divide, the cell needs to determine the orientation of the division to position daughter cells at the appropriate place in the tissue. Many symmetric divisions follow the “shortest wall” rule, originally proposed by Errera., *et al* (Errera, 1888). The shortest wall rule is a logical way to position divisions to optimally partition a growing tissue and posits that at the G1 phase, the nucleus moves to the geometric centre of the cell, where the division plane is aligned with the shortest wall within the cell (Errera, 1888). This rule implicates that the cell division plane is determined by cell geometry. How do cells sense and integrate geometric cues into growth? Throughout the interphase of the cell cycle, the orientation of cortical microtubules in the so-called cortical microtubule array (CMT) often correlates with the orientation of the future cell plate. The CMT is therefore a likely relevant structure to guide cell division orientation (Ehrhardt & Shaw, 2006). Moreover, in the

Arabidopsis shoot apex, a mutation in microtubule severing protein KATANIN results in changes in CMT orientation, mis-positioning of the PPB and non-responsiveness to mechanical stress, suggesting that mechanical force is transmitted through microtubules to direct proper division planes (Uyttewaal *et al.*, 2012). Additionally, recent computational modelling study in *Arabidopsis* embryogenesis demonstrated that the auxin-mediated stabilization and the geometrically favoured orientation of cortical microtubule array associated with cell shape and cell edge stability are sufficient to predict the division planes of the first four divisions (Chakrabortty *et al.*, 2018). These studies begin to provide mechanistic explanations on how cells translate geometric information into the orientation of cell division plane.

2.2 Asymmetric cell division

Asymmetric cell division is defined as any cell division where a daughter cell gains a different fate from its parent (Horvitz & Herskowitz, 1992). A daughter cell can intrinsically acquire a different cell fate from the moment it is generated, implicating that particular cues are already present in the mother cell and facilitate asymmetric division in the parental cell by segregating into one but not the other daughter. Alternatively, two identical daughter cells can be initially generated and acquire different cell fates after divisions by unequally perceiving different external cues after divisions (Pillitteri *et al.*, 2016). In animals and plants, both intrinsic and extrinsic cues are commonly used to execute asymmetric divisions for tissue patterning and organ formation. Notably, intrinsic and extrinsic regulatory networks are not mutually exclusive. Two-step processes that intrinsically produce different daughter cells and then reinforce the differences by cell-cell interactions between them after division have been described in bacteria and budding yeast, while both intrinsic and extrinsic cues are required during nematode embryogenesis (Horvitz & Herskowitz, 1992). In *Arabidopsis*, several developmental processes provide examples for both types of control in a few critical divisions.

Stomatal development starts when a protodermal cell activated by transcription factor SPEECHLESS (SPCH) undergoes an asymmetric division to generate a small meristemoid cell and a large stomata-lineage cell (Dong *et al.*, 2009), where stomata development is initiated. Prior to this first asymmetric division, an intrinsic protein BREAKING ASYMMETRY IN THE STOMATA LINEAGE (BASL) is polarly localized to the cortex distal from the division plane, where it marks polarity and presumably alters the position and orientation of division plane that generates daughter cells unequally in size and identity. The polarization of BASL is disrupted in mutants the for leucine-rich repeat receptor TOO MANY MOUTHs (TMM), suggesting the polarity of BASL is in response to external cues (Dong *et al.*, 2009). In addition to the intrinsic factor BASL, extrinsic auxin signalling is also involved in stomatal divisions. Live imaging of auxin markers and auxin efflux carrier PIN-FORMED (PIN family) PIN3-GFP reveals that high auxin levels are associated with following asymmetric divisions; whereas auxin depletion is associated with the final guard cell differentiation (Le *et al.*, 2014). Consistent with an instructive role of auxin in stomatal patterning, mutations in auxin efflux carrier result in overproduction and clustering of stomata (Le *et al.*, 2014).

Due to the fixed tissue position, plant cells demand high flexibility to acquire new cell fates, which can be achieved by coordinating intrinsic cues with diverse extrinsic cues. The growth hormones auxin (Benková *et al.*, 2003), cytokinin (Ioio *et al.*, 2008), mechanical force (Louveaux & Hamant, 2013), and mobile transcription factors (Bernhardt *et al.*, 2005; Sarkar *et al.*, 2007; Schlereth *et al.*, 2010) have

been demonstrated to facilitate cell fate decisions in different developmental steps during *Arabidopsis* root development.

The root meristem contains a small group of cells with slow division rate called the quiescent centre (QC), which inhibits differentiation of the surrounding cells to maintain their stem cell function. For example, in columella root cap development, stem cells undergo asymmetric divisions to repetitively generate one cell always in contact with QC, which maintains its stem cell activity. The other daughter cell grows and differentiates to columella root cap fate. To generate two cells fated to different identities, the mobile transcription factor WUSCHEL-RELATED HOMEOBOX 5 (WOX5), produced in the QC, is transported to the adjacent cell where it maintains stem cell identity and represses differentiation (Sarkar *et al.*, 2007). Additionally, two NAC domain transcription factors sequentially activated in columella stem cells and differentiating cells coordinate the orientation of division planes during root cap differentiation (Willemsen *et al.*, 2008).

In addition to the control of stem cell identity, epidermis, cortex, and endodermis layers in the root also demand sophisticated regulation of asymmetric divisions. The cortex/endodermis stem cell that is in contact with QC first undergoes an asymmetric division to generate a cortex/endodermis initial cell. This cell divides asymmetrically to generate two cells fated to cortex and endodermis. Stele-expressed mobile protein SHORT-ROOT (SHR) moves to the initial cell where it activates SCARECROW (SCR), which sequesters SHR in the nucleus to restrict its movement to one cell layer. The SHR-SCR complex promotes cell division in the cortex/endodermis initial cell and specifies the identity of endodermal cells, while a mutation in each gene leads to defects in the division and/or the specification of endodermis (Di Laurenzio *et al.*, 1996; Helariutta *et al.*, 2000).

Asymmetric cell division also plays an important role in root branching. Lateral root formation originates from auxin-responsive asymmetric divisions in pericycle cells, specific cell files located opposite to the xylem poles. In response to auxin, the nuclei of two adjacent pericycle cells move toward each other, and these cells then asymmetrically divide transversely to the cell axis to generate the founder cells for lateral root primordia (Casimiro *et al.*, 2001). In these cells, many of the genes required for embryonic patterning and asymmetric divisions are re-initiated (Du & Scheres, 2017), underpinning the importance of tight control in asymmetric divisions throughout plant development.

To compensate for their fixed position in plant tissues, plant cells possess the ability to re-initiate divisions and change fate during the repair of tissues or the re-construction of organs upon physical wounding (Sugimoto *et al.*, 2019). Regeneration processes in response to wounding can replace lost tissue, e.g. *Arabidopsis* root tip regeneration (Xu *et al.*, 2006); *de novo* organ regeneration takes place to produce tissues that were not present at the regeneration site before. In extreme cases, such as during somatic embryogenesis, a committed cell de-differentiates followed by acquiring the ability to form an embryo that gives rise to an entire plant (Mordhorst *et al.*, 1997; Kadokura *et al.*, 2018). To repair damaged tissue, cells must undergo reprogramming and re-activation of cell division. The requirement of hormones including auxin, cytokinin, jasmonate and of key transcription factors has been clarified in different forms of regeneration (Xu *et al.*, 2006; Liu *et al.*, 2014; Ikeuchi *et al.*, 2017; Zhou *et al.*, 2019). Cell regeneration leading to different organ formation likely depends on positional cues and cell-cell communication, since the new tissue has to connect to previously established tissue. However, our knowledge on the mechanisms underlying cell reprogramming and accompanied asymmetric divisions still remain fragmentary.

2.3 Symmetry breaking

How do cells unevenly partition internal information e.g. BASL that leads to different daughter cells? Breaking of symmetry in an asymmetrically dividing cell can be achieved by alteration of intrinsic polarity. The asymmetry can be generated by polar localization of proteins, unequal distribution of determinants (e.g. transcription factors, proteases, receptors), or directly by spindle positioning to produce daughter cells of different sizes (Horvitz & Herskowitz, 1992). Throughout the evolution of eukaryotes, a conserved central actor in cell polarity is the Rho family of small GTPases. In budding yeast, small GTPase Cdc42p-mediated polarity control underlies morphogenesis and cell division, while the depletion of Cdc42p results in non-polarized cell growth without budding/division (Adams *et al.*, 1990). Cdc42p has been demonstrated to be essential for septin assembly, a ring at the mother-bud neck that serves as a scaffold for the recruitment of proteins for the division. Notably, the recruitment of septins to the presumptive bud site is dependent on Cdc42p (Caviston *et al.*, 2003). The interaction of Rho GTPases with their GTP/GDP exchange factors has been shown to be sufficient for symmetry breaking, such that active Rho is partitioned only on one side of the plasma membrane (Kozubowski *et al.*, 2008). The regulation of Rho-GTPases is evolutionarily conserved and involves activation and polar localization to the plasma membrane in response to diverse extracellular stimuli. Downstream signals are transduced to corresponding signalling pathways e.g. cytoskeleton organization, membrane trafficking, polarized growth by interacting with effectors (Etienne-Manneville, 2004).

In plant cells, the establishment and maintenance of intracellular polarity is mainly investigated in tip cell growing root hair and pollen tube in angiosperms (Cole & Fowler, 2006) and filamentous cells of moss (Vidali & Bezanilla, 2012). To maintain polarized growth, Rho-of-Plant (ROP) GTPases are actively localized at the apex, where they interact with plant-specific effectors RICs (ROP-Interacting CRIB-containing). This interaction leads to the rearrangement of the cytoskeleton and boosts tip growth by promoting polar exocytosis (Gu *et al.*, 2003). Additionally, ROPs are also functioning in cell shape regulation. In *Arabidopsis,* the jigsaw puzzle-like appearance of pavement cell is dependent on ROPs mediated cytoskeleton reorganization that leads to anisotropic polar outgrowth (Craddock *et al.*, 2012). ROP polarization can be under the influence of external cues: high levels of extracellular auxin activate ROPs and subsequently induce ROPs-mediated local inhibition of PIN1 endocytosis, leading to the consistent polarization of PIN1 to the lobe region of a pavement cell (Nagawa *et al.*, 2012).

Although conserved functions of ROPs in cell growth and morphogenesis have been demonstrated across species, the regulatory role in plant asymmetric divisions e.g. polarity establishment in a dividing descent cell or division plane orientation remains to be elucidated. The obstacle to investigating ROPs in divisional control in the model plant *Arabidopsis* is that there are multiple ROP and RIC paralogs, each with different expression patterns and diverse functions in specific tissues. The combination of functional redundancy and tissue complexity makes it difficult to identify which ROP may be involved in specific asymmetric cell divisions. Moreover, numerous upstream regulators and downstream effectors have been identified, which multiply the possibilities of mechanisms in polarity alteration for the asymmetric division. In the early land plants, smaller gene families and relatively simpler developmental progression may provide an opportunity to investigate the involvement of ROPs in asymmetric cell division (Eklund *et al.*, 2010).

3. *Physcomitrella patens* as a model system for cell division orientation

3.1 Life cycle of *P. patens*

To deepen our understanding of the spatiotemporal regulation of cell division in basal land plants, *Physcomitrella patens* has been put forward as a new model system. In the life cycle of *P. patens*, filamentous chloronema cells emerge from germinated haploid spores and commence polarized cell growth driven by the apical stem cell. In an auxin-dependent manner, the growing apical cell of a chloronema filament gradually transitions to a caulonema cell, which possesses a smaller diameter and fewer chloroplasts compared to chloronema cells (Prigge & Bezanilla, 2010). Moreover, the cell division plane is perpendicular to the cell axis in chloronema cell, whereas it is oblique in caulonema cells, implying distinct cell division plane orientation mechanisms in these two types of filaments.

Protonema filaments develop by tip growth of apical cells along with branch emergence in subapical cells. About 87% of the emerging initial cells grow and elongate as a secondary chloronema cell, whereas approximately 5% of the emerging cell form gametophore initial cells that give rise to buds and ultimately develop to gametophores (Cove & Knight, 1993). After branching off from a filamentous cell, a gametophore initial cell appears to swell and performs an oblique cell division, while a branch initial cell elongates and performs a perpendicular division instead. The oblique division is followed by a series of asymmetric divisions to form a bud with a specified single stem cell residing at the apex. The stem cell divides in characteristic patterns to form leaflets and ultimately generate a 3D gametophore (Harrison *et al.*, 2009), where the sexual organs are formed and fertilized to produce a zygote. The diploid zygote develops into a sporophyte that eventually releases spores and completes the moss life cycle (Prigge & Bezanilla, 2010).

Given that the entire reproductive organs originate after a 2D-to-3D growth transition, where the gametophore initial cell divides and gains a new identity, the question of how this asymmetric transition division is controlled is pivotal for understanding moss development.

3.2 Cell regeneration in *P. patens*

Cell divisions not only take place during the development of the plan body but also happen during tissue repair. In *P. patens*, the excision of leaves induces leaf cells to regenerate into new protonema cells through cell reprogramming and is accompanied by reactivation of cell divisions (Ishikawa & Hasebe, 2015). Complications that arise during the investigation of cell reprogramming in vascular plants are the complexity of multiple cell layers and tissues, crosstalk between signalling pathways around the damaged area, and the technical imaging limitation caused by the embedding of a wounding site in deeper tissues. Moss possesses a single cell layer leaf that can be imaged at high resolution and is easy to manipulate for introducing wound to a target area. The high competence to regenerate and available genetic tools make moss leaves a suitable system to study the generality of regeneration mechanisms discovered in angiosperms.

3.3 The evolutionary conservation of cell division control in *P. patens*

The colonization of land by early land plant bryophytes has likely been a key trigger for the evolution of the complex coordination of cell divisions needed to generate 3D shoot tissues (Buschmann & Zachgo, 2016). The coincidence of 3D tissues with the utilization of a PPB reinforces the hypothesis that bryophytes incorporated new division control machinery to develop 3D tissues for survival on land (see below).

Despite their simpler morphology, accumulating evidence indicates that the moss *P. patens* shares common and conserved elements in cell division control with vascular plants. For example, during phragmoplast development, the formation of antiparallel microtubule overlaps is essential for vesicle delivery and fusion. Cytokinesis-specific microtubule bundling proteins establish and maintain the microtubule overlaps in both moss and angiosperms (Kosetsu *et al.*, 2013). In the control of the orientation of division plane, a group of landmark proteins (Stockle *et al.*, 2016), non-cell-autonomous peptides (Whitewoods *et al.*, 2018), and cytoskeleton organizers (Kosetsu *et al.*, 2017) share common roles to orient the division plane in *Physcomitrella* and *Arabidopsis*. Finally, for the activation of asymmetric divisions, homologs of AP2-type ANT/PLETHORA/BABYBOOM transcription factors, required for stem cell activity in *Arabidopsis*, have been demonstrated to control moss gametophore formation (Aoyama *et al.*, 2012).

4. The regulation of cell division in basal land plants

4.1 cellular perspective

To control the orientation of the cell division plane, PPB and phragmoplast are essential and present in all land plants (Buschmann & Zachgo, 2016). However, the spindle and PPB in the bryophyte basal land plant lineage are initiated from different types of polar organizing centres. In liverworts, astral microtubules spread out from γ-Tubulin to form polar organizers (PO) that subsequently precedes the organization of PPB, while in hornworts the unique axial microtubule system (AMS) that forms in concert with dividing plastid leads to unusual PPB configuration (Brown & Lemmon, 2011). Remarkably, not all cell divisions rely on the PPB. Exceptions occur in certain cell types of bryophyte mosses. The mosses *Physcomitrella* and *Funaria* execute divisions in the absence of PPB in the 2D filamentous protonemata (Doonan *et al.*, 1987; Sawidis *et al.*, 1991; Graham *et al.*, 2000). PPB is formed by transient narrowing of interphase CMTs at G2 phase in the cortical region of nucleus (Cyr, 1994). However, CMTs in protonema cells of mosses *Physcomitrella* and *Funaria* have not been observed (Doonan *et al.*, 1987; Sawidis *et al.*, 1991), implicating that there must be other mechanisms that control the orientation of the division plane to compensate for the lacking of PPB and cortical microtubule arrays. Notably, the gametophores of *Physcomitrella* and *Funaria* possess cortical microtubules and are capable of forming the PPB, which has led to the idea that PPB formation might be essential to develop a 3D body plan but is dispensable for 2D filamentous growth (Graham *et al.*, 2000). Whether the correlation of the presence of CMTs and PPB in leafy shoots implies a causal relationship in the control of cell division remains to be clarified. In filamentous protonemata, some motor proteins are identified to reside on the cell division site prior to cytokinesis, where a division plane is marked (Miki *et al.*, 2014; Wu & Bezanilla, 2014). This implies that a guidance mechanism may still take place in the absence of the PPB. As a filament continues to grow, the apical cell daughters gradually transition from chloronema cell with perpendicular division plane to caulonema cell with oblique division plane (Prigge & Bezanilla, 2010). It has been shown that the expansion of the cell plate along with tilting movement *per se* that eventually reaches parental membranes to form an oblique division plane (Tang *et al.*, 2019). What force drives the tilting of the cell plate and why it exhibits differences in the two types of protonemata that do not establish PPBs is still mysterious.

Recent studies in *Arabidopsis* show that a PPB-lacking mutant has a subtle effect on the orientation of the division plane in the root, indicating that the PPB may not be strictly necessary but is instead fine-tunes the orientation of the divisional plane (Schaefer *et al.*, 2017). Additionally, the presence of CMTs

and the localization of landmark proteins was not influenced in this PPB-lacking mutant, suggesting other mechanisms to guide the resident proteins to the correct site in the presence of CMTs. The absence and presence of CMTs and PPB in mosses and *Arabidopsis* raise further questions: How do landmark proteins localize to and mark the division site with or without CMTs and PPB? Is there an evolutionarily conserved mechanism to allocate these proteins to the correct place where the future cell plate attachment takes place?

4.2 Whole organism perspective

During moss tissue development, polarity is established and maintained in apical cells to support polar growth (Decker *et al.*, 2006; Eklund *et al.*, 2010). Additionally, polarity is re-established in dividing subapical cells that generate branches. In non-dividing filamentous cells, nuclei are steadily positioned in the middle of the cells, while in a subapical cell that is undergoing division the nucleus is allocated to the protrusion site of the emerging initial cell, where cytokinesis takes place (Conrad *et al.*, 1986). This nuclear reallocation reflects a transient polarity change during divisions. How subapical cells change their polarity and mobilize their nuclei toward the future division site remains to be elucidated.

The 2D-to-3D developmental transition is initiated by an asymmetric division (Prigge & Bezanilla, 2010). How is a filamentous parent cell specified to perform this asymmetric division? The plant hormone cytokinin has been shown to trigger this process (Brandes & Kende, 1968; Ashton *et al.*, 1979). Accumulation of isotope-labelled cytokinin was detected in bud-parental cells (Brandes & Kende, 1968), whereas auxin has been suggested to sensitize the parental cell to cytokinin (Ashton *et al.*, 1979; Cove & Ashton, 1984). Although the necessity of asymmetric divisions to create new cell types for tissue innovation are evolutionarily conserved to a high degree, studies of asymmetric divisions in basal land plants have obtained little attention compared to vascular plants.

5. Scope of this thesis

In **Chapter 1**, I briefly review the control mechanisms of plant cell divisions throughout development from the viewpoint of the individual cell to the tissue level. Most studies about plant cell division control including the orientation of division plane, polarity establishment, and cell identity acquirement in asymmetric divisions have been carried out in angiosperms. To broaden our understanding in the generality and difference of cell division control in an evolutionary manner, this thesis describes studies on the spatiotemporal control of cell divisions in different moss tissues (Fig. **1**). We first investigate cell division within a short time frame, during cytokinesis in a dividing caulonema cell where we illustrate the localization patterns and functioning of the tethering exocyst complex **(Chapter 2)**. To begin addressing mechanisms underlying the asymmetric division during *P. patens* gametophore initiation, geometric differences between gametophore and branch initial cells are described in **Chapter 3**. In **Chapter 4** the requirement of polarity protein Rho-GTPases for bud formation and gametophore development are examined. To explore cell reprogramming that demands the reactivation of cell divisions in excised moss leaves, we describe wounding induced cell reprogramming in **Chapter 5**. A brief outline of the rationale for the experimental sections follows below.

Cytoskeleton and membranous materials orchestrate *de novo* cell plate formation during cytokinesis. To unravel how the microtubule overlaps are bridged to vesicles during cell plate formation in moss, we hypothesize in **Chapter 2** that exocyst complex may play a central role as a missing link. To test this

possibility, we illustrate localization patterns of different subunits of the exocyst complex during cytokinesis (Tang *et al.*, 2019). Further, to verify if the microtubule overlaps participate in exocyst accumulation, we monitor the recruitment of exocyst subunit Sec6 under the mutant background with collapse microtubule overlaps. Lastly, the requirement of Sec6 in vesicle accumulation is examined by transiently repression of Sec6.

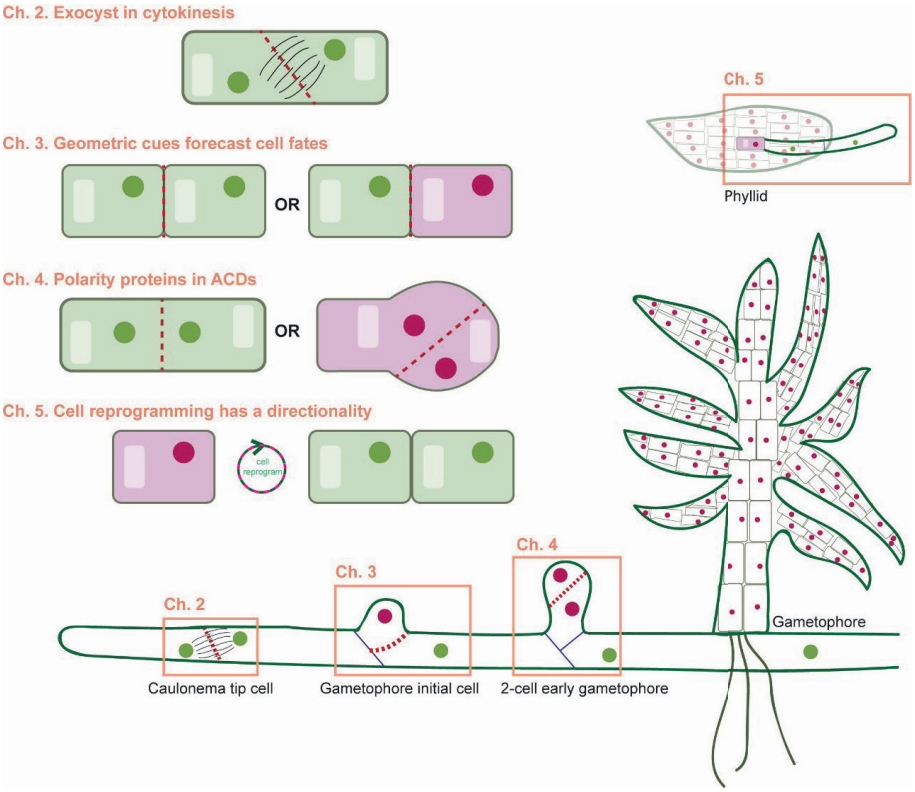

Figure 1. Schematic overview of the objectives of the indicated chapters. Cells coloured with green represent filamentous protonema cell types, and cells coloured with pink represent gametophore cells. ACDs, asymmetric cell divisions. Drawing not to scale.

To integrate cell division control into developmental progress, we study the transition division that gives rise to a gametophore initial cell rather a branch filament. Because the swelling of a gametophore initial cell reflects as a consequence of a cellular polarity/property change, we suspect that a gametophore initial cell may already gain new properties prior to swelling. We test this hypothesis in **Chapter 3**. We observe and quantify two geometric characters in budding initial cells, the width of initial cells and the orientation of division plane, before visible swelling. Additionally, a florescent marker is monitored to test if the expression level exhibits a difference in protonema and gametophore initial cells. We then attempt to predict cell fates of initial cells based on these parameters.

The swelling of a gametophore initial cell indicates an alteration of intracellular polarity, which could serve as an intrinsic cue for the asymmetric division. In **Chapter 4,** we aim to address if alteration of cellular polarity is necessary for gametophore initiation and development. To answer this question, we

first characterize the localization patterns of widely conserved polarity proteins Rho-GTPases (PpROPs) in the young stage of a gametophore, the bud formation. In loss-of-function analyses, we investigate which ROPs play a dominant role in bud formation. Moreover, a putative effector PpRIC is taken along to obtain mechanistic insight of polarity establishment via a potential ROP-RIC interaction that may contribute to the cell swelling of a gametophore initial cell, the subsequent oblique division, and further gametophore development.

Wounding-induced cell reprogramming is usually accompanied by reactivation of cell division to regenerate tissues. In **Chapter 5,** we aim to develop a controllable system in moss excised leaves to gain knowledge about cell reprogramming in basal land plants. We induce wounding in excised leaves by laser ablation, which allows us to control the damage area precisely. By this way, we obtain information about the timing and location of cell reprogramming. The potential role of cytoskeleton rearrangement in cell reprogramming is investigated by tracking cytoskeleton upon wounding.

In **Chapter 6**, finally, the findings presented in this thesis are summarized and discussed. The control of the orientation of division plane in related to tethering complex and asymmetric division will be discussed and compared to other studies. Based on the characterization of cytoskeleton patterns in this research, We compare and propose the role of cytoskeleton during cytokinesis, fate transition, and cell reprogramming. We relate our findings and previous research to discuss the interplay of tethering complex and polarity proteins in cell polarity establishment and division control.

References

Adams A, Johnson DI, Longnecker RM, Sloat BF, Pringle JR. 1990. CDC42 and CDC43, two additional genes involved in budding and the establishment of cell polarity in the yeast Saccharomyces cerevisiae. *The Journal of Cell Biology* **111**(1): 131-142.

Aoyama T, Hiwatashi Y, Shigyo M, Kofuji R, Kubo M, Ito M, Hasebe M. 2012. AP2-type transcription factors determine stem cell identity in the moss Physcomitrella patens. *Development* **139**(17): 3120-3129.

Ashton NW, Grimsley NH, Cove DJ. 1979. Analysis of gametophytic development in the moss, Physcomitrella patens, using auxin and cytokinin resistant mutants. *Planta* **144**(5): 427-435.

Assaad FF, Huet Y, Mayer U, Jürgens G. 2001. The cytokinesis gene KEULE encodes a Sec1 protein that binds the syntaxin KNOLLE. *The Journal of Cell Biology* **152**(3): 531-544.

Benková E, Michniewicz M, Sauer M, Teichmann T, Seifertová D, Jürgens G, Friml J. 2003. Local, efflux-dependent auxin gradients as a common module for plant organ formation. *Cell* **115**(5): 591-602.

Bernhardt C, Zhao M, Gonzalez A, Lloyd A, Schiefelbein J. 2005. The bHLH genes GL3 and EGL3 participate in an intercellular regulatory circuit that controls cell patterning in the Arabidopsis root epidermis. *Development* **132**(2): 291-298.

Brandes H, Kende H. 1968. Studies on cytokinin-controlled bud formation in moss protonemata. *Plant Physiol* **43**(5): 827-837.

Brown RC, Lemmon BE. 2011. Dividing without centrioles: innovative plant microtubule organizing centres organize mitotic spindles in bryophytes, the earliest extant lineages of land plants. *AoB PLANTS* **2011**: plr028-plr028.

Buschmann H, Zachgo S. 2016. The evolution of cell division: from streptophyte algae to land plants. *Trends Plant Sci* **21**(10): 872-883.

Casimiro I, Marchant A, Bhalerao RP, Beeckman T, Dhooge S, Swarup R, Graham N, Inzé D, Sandberg G, Casero PJ. 2001. Auxin transport promotes Arabidopsis lateral root initiation. *The Plant Cell* **13**(4): 843-852.

Caviston JP, Longtine M, Pringle JR, Bi E. 2003. The role of Cdc42p GTPase-activating proteins in assembly of the septin ring in yeast. *Molecular biology of the cell* **14**(10): 4051-4066.

Chakrabortty B, Willemsen V, de Zeeuw T, Liao C-Y, Weijers D, Mulder B, Scheres B. 2018. A plausible microtubule-based mechanism for cell division orientation in plant embryogenesis. *Current Biology* **28**(19): 3031-3043. e3032.

Cleary AL, Smith LG. 1998. The Tangled1 gene is required for spatial control of cytoskeletal arrays associated with cell division during maize leaf development. *The Plant Cell* **10**(11): 1875-1888.

Cole RA, Fowler JE. 2006. Polarized growth: maintaining focus on the tip. *Curr Opin Plant Biol* **9**(6): 579-588.

Conrad PA, Steucek GL, Hepler PK. 1986. Bud formation inFunaria: Organelle redistribution following cytokinin treatment. *Protoplasma* **131**(3): 211-223.

Cove D, Ashton N. 1984. Hormonal regulation of gametophytic development in bryophytes. *Experimental biology of bryophytes/edited by AF Dyer, JG Duckett*.

Cove DJ, Knight CD. 1993. The moss Physcomitrella patens, a model system with potential for the study of plant reproduction. *The Plant Cell* **5**(10): 1483.

Craddock C, Lavagi I, Yang Z. 2012. New insights into Rho signaling from plant ROP/Rac GTPases. *Trends Cell Biol* **22**(9): 492-501.

Cyr RJ. 1994. Microtubules in plant morphogenesis: role of the cortical array. *Annual Review of Cell Biology* **10**(1): 153-180.

de Keijzer J, Kieft H, Ketelaar T, Goshima G, Janson ME. 2017. Shortening of microtubule overlap regions defines membrane delivery sites during plant cytokinesis. *Current Biology* **27**(4): 514-520.

De Veylder L, Beeckman T, Inzé D. 2007. The ins and outs of the plant cell cycle. *Nature Reviews Molecular Cell Biology* **8**(8): 655.

Decker EL, Frank W, Sarnighausen E, Reski R. 2006. Moss systems biology en route: phytohormones in Physcomitrella development. *Plant Biol (Stuttg)* **8**(3): 397-405.

Di Laurenzio L, Wysocka-Diller J, Malamy JE, Pysh L, Helariutta Y, Freshour G, Hahn MG, Feldmann KA, Benfey PN. 1996. The SCARECROW gene regulates an asymmetric cell division that is essential for generating the radial organization of the Arabidopsis root. *Cell* **86**(3): 423-433.

Dong J, MacAlister CA, Bergmann DC. 2009. BASL controls asymmetric cell division in Arabidopsis. *Cell* **137**(7): 1320-1330.

Doonan JH, Cove DJ, Corke FMK, Lloyd CW. 1987. Pre-prophase band of microtubules, absent from tip-growing moss filaments, arises in leafy shoots during transition to intercalary growth. *Cell Motility* **7**(2): 138-153.

Du Y, Scheres B. 2017. Lateral root formation and the multiple roles of auxin. *J Exp Bot* **69**(2): 155-167.

Ehrhardt DW, Shaw SL. 2006. Microtubule dynamics and organization in the plant cortical array. *Annu. Rev. Plant Biol.* **57**: 859-875.

Eklund DM, Svensson EM, Kost B. 2010. Physcomitrella patens: a model to investigate the role of RAC/ROP GTPase signalling in tip growth. *J Exp Bot* **61**(7): 1917-1937.

Errera L. 1888. Uber zellformen und seifenblasen. *Bot. Centralbl.* **34**: 395-398.

Etienne-Manneville S. 2004. Cdc42 - the centre of polarity. *Journal of Cell Science* **117**(8): 1291-1300.

Facette MR, Rasmussen CG, Van Norman JM. 2019. A plane choice: coordinating timing and orientation of cell division during plant development. *Curr Opin Plant Biol* **47**: 47-55.

Fendrych M, Synek L, Pečenková T, Toupalová H, Cole R, Drdová E, Nebesářová J, Šedinová M, Hála M, Fowler JE. 2010a. The Arabidopsis exocyst complex is involved in cytokinesis and cell plate maturation. *The Plant Cell* **22**(9): 3053-3065.

Fendrych M, Synek L, Pečenková T, Toupalová H, Cole R, Drdová E, Nebesářová J, Šedinová M, Hála M, Fowler JE. 2010b. The Arabidopsis exocyst complex is involved in cytokinesis and cell plate maturation. *The Plant Cell*: tpc. 110.074351.

Graham LE, Cook ME, Busse JS. 2000. The origin of plants: body plan changes contributing to a major evolutionary radiation. *Proceedings of the National Academy of Sciences* **97**(9): 4535-4540.

Gu Y, Vernoud V, Fu Y, Yang Z. 2003. ROP GTPase regulation of pollen tube growth through the dynamics of tip-localized F-actin. *J Exp Bot* **54**(380): 93-101.

Harrison CJ, Roeder AH, Meyerowitz EM, Langdale JA. 2009. Local cues and asymmetric cell divisions underpin body plan transitions in the moss Physcomitrella patens. *Curr Biol* **19**(6): 461-471.

Helariutta Y, Fukaki H, Wysocka-Diller J, Nakajima K, Jung J, Sena G, Hauser M-T, Benfey PN. 2000. The SHORT-ROOT gene controls radial patterning of the Arabidopsis root through radial signaling. *Cell* **101**(5): 555-567.

Horvitz HR, Herskowitz I. 1992. Mechanisms of asymmetric cell division: two Bs or not two Bs, that is the question. *Cell* **68**(2): 237-255.

Ikeuchi M, Iwase A, Rymen B, Lambolez A, Kojima M, Takebayashi Y, Heyman J, Watanabe S, Seo M, De Veylder L. 2017. Wounding triggers callus formation via dynamic hormonal and transcriptional changes. *Plant Physiol* **175**(3): 1158-1174.

Inzé D, Veylder LD. 2006. Cell Cycle Regulation in Plant Development. *Annual Review of Genetics* **40**(1): 77-105.

Ioio RD, Nakamura K, Moubayidin L, Perilli S, Taniguchi M, Morita MT, Aoyama T, Costantino P, Sabatini S. 2008. A genetic framework for the control of cell division and differentiation in the root meristem. *Science* **322**(5906): 1380-1384.

Ishikawa M, Hasebe M. 2015. Cell cycle reentry from the late S phase: implications from stem cell formation in the moss Physcomitrella patens. *J Plant Res* **128**(3): 399-405.

Jones AR, Forero-Vargas M, Withers SP, Smith RS, Traas J, Dewitte W, Murray JA. 2017. Cell-size dependent progression of the cell cycle creates homeostasis and flexibility of plant cell size. *Nat Commun* **8**: 15060.

Kadokura S, Sugimoto K, Tarr P, Suzuki T, Matsunaga S. 2018. Characterization of somatic embryogenesis initiated from the Arabidopsis shoot apex. *Dev Biol* **442**(1): 13-27.

Kaiser CA, Krieger M, Lodish H, Berk A. 2007. *Molecular cell biology*: WH Freeman.

Kosetsu K, de Keijzer J, Janson ME, Goshima G. 2013. MICROTUBULE-ASSOCIATED PROTEIN65 is essential for maintenance of phragmoplast bipolarity and formation of the cell plate in Physcomitrella patens. *The Plant Cell*: tpc. 113.117432.

Kosetsu K, Murata T, Yamada M, Nishina M, Boruc J, Hasebe M, Van Damme D, Goshima G. 2017. Cytoplasmic MTOCs control spindle orientation for asymmetric cell division in plants. *Proc Natl Acad Sci U S A* **114**(42): E8847-E8854.

Kozubowski L, Saito K, Johnson JM, Howell AS, Zyla TR, Lew DJ. 2008. Symmetry-breaking polarization driven by a Cdc42p GEF-PAK complex. *Current Biology* **18**(22): 1719-1726.

Kunkel B. 1991. Compartmentalized gene expression during sporulation in Bacillus subtilis. *Trends in Genetics* **7**(5): 167-172.

Le J, Liu X-G, Yang K-Z, Chen X-L, Zou J-J, Wang H-Z, Wang M, Vanneste S, Morita M, Tasaka M. 2014. Auxin transport and activity regulate stomatal patterning and development. *Nat Commun* **5**: 3090.

Lee Y-RJ, Liu B. 2013. The rise and fall of the phragmoplast microtubule array. *Curr Opin Plant Biol* **16**(6): 757-763.

Li H, Sun B, Sasabe M, Deng X, Machida Y, Lin H, Julie Lee YR, Liu B. 2017. Arabidopsis MAP65-4 plays a role in phragmoplast microtubule organization and marks the cortical cell division site. *New Phytol* **215**(1): 187-201.

Li S, Sun T, Ren H. 2015. The functions of the cytoskeleton and associated proteins during mitosis and cytokinesis in plant cells. *Frontiers in Plant Science* **6**(282).

Lipka E, Herrmann A, Mueller S. 2015. Mechanisms of plant cell division. *Wiley Interdiscip Rev Dev Biol* **4**(4): 391-405.

Liu J, Sheng L, Xu Y, Li J, Yang Z, Huang H, Xu L. 2014. WOX11 and 12 are involved in the first-step cell fate transition during de novo root organogenesis in Arabidopsis. *The Plant Cell* **26**(3): 1081-1093.

Lloyd C, Buschmann H. 2007. Plant division: remembering where to build the wall. *Curr Biol* **17**(24): R1053-1055.

Louveaux M, Hamant O. 2013. The mechanics behind cell division. *Curr Opin Plant Biol* **16**(6): 774-779.

Lukowitz W, Mayer U, Jürgens G. 1996. Cytokinesis in the Arabidopsis embryo involves the syntaxin-related KNOLLE gene product. *Cell* **84**(1): 61-71.

Miki T, Naito H, Nishina M, Goshima G. 2014. Endogenous localizome identifies 43 mitotic kinesins in a plant cell. *Proceedings of the National Academy of Sciences*: 201311243.

Mineyuki Y 1999. The preprophase band of microtubules: its function as a cytokinetic apparatus in higher plants. *International review of cytology*: Elsevier, 1-49.

Mordhorst AP, Toonen MA, de Vries SC, Meinke D. 1997. Plant embryogenesis. *Critical Reviews in Plant Sciences* **16**(6): 535-576.

Mueller S, Juergens G 2016. Plant cytokinesis—No ring, no constriction but centrifugal construction of the partitioning membrane. *Seminars in cell & developmental biology*: Elsevier. 10-18.

Muller S, Han S, Smith LG. 2006. Two kinesins are involved in the spatial control of cytokinesis in Arabidopsis thaliana. *Curr Biol* **16**(9): 888-894.

Murray JAH, Jones A, Godin C, Traas J. 2012. Systems Analysis of Shoot Apical Meristem Growth and Development: Integrating Hormonal and Mechanical Signaling. *The Plant Cell* **24**(10): 3907-3919.

Nagawa S, Xu T, Lin D, Dhonukshe P, Zhang X, Friml J, Scheres B, Fu Y, Yang Z. 2012. ROP GTPase-dependent actin microfilaments promote PIN1 polarization by localized inhibition of clathrin-dependent endocytosis. *PLoS biology* **10**(4): e1001299.

Nishihama R, Soyano T, Ishikawa M, Araki S, Tanaka H, Asada T, Irie K, Ito M, Terada M, Banno H. 2002. Expansion of the cell plate in plant cytokinesis requires a kinesin-like protein/MAPKKK complex. *Cell* **109**(1): 87-99.

Oliferenko S, Chew TG, Balasubramanian MK. 2009. Positioning cytokinesis. *Genes & development* **23**(6): 660-674.

Peres A, Churchman ML, Hariharan S, Himanen K, Verkest A, Vandepoele K, Magyar Z, Hatzfeld Y, Van Der Schueren E, Beemster GT. 2007. Novel plant-specific cyclin-dependent kinase inhibitors induced by biotic and abiotic stresses. *Journal of Biological Chemistry*.

Pillitteri LJ, Guo X, Dong J. 2016. Asymmetric cell division in plants: mechanisms of symmetry breaking and cell fate determination. *Cell Mol Life Sci* **73**(22): 4213-4229.

Prigge MJ, Bezanilla M. 2010. Evolutionary crossroads in developmental biology: Physcomitrella patens. *Development* **137**(21): 3535-3543.

Rasmussen CG, Humphries JA, Smith LG. 2011. Determination of symmetric and asymmetric division planes in plant cells. *Annual Review of Plant Biology* **62**: 387-409.

Rybak K, Steiner A, Synek L, Klaeger S, Kulich I, Facher E, Wanner G, Kuster B, Zarsky V, Persson S. 2014. Plant cytokinesis is orchestrated by the sequential action of the TRAPPII and exocyst tethering complexes. *Dev Cell* **29**(5): 607-620.

Santuari L, Sanchez-Perez GF, Luijten M, Rutjens B, Terpstra I, Berke L, Gorte M, Prasad K, Bao D, Timmermans-Hereijgers JLPM, et al. 2016. The PLETHORA Gene Regulatory Network Guides Growth and Cell Differentiation in Arabidopsis Roots. *The Plant Cell* **28**(12): 2937-2951.

Sarkar AK, Luijten M, Miyashima S, Lenhard M, Hashimoto T, Nakajima K, Scheres B, Heidstra R, Laux T. 2007. Conserved factors regulate signalling in Arabidopsis thaliana shoot and root stem cell organizers. *Nature* **446**(7137): 811.

Sawidis T, Quader H, Bopp M, Schnepf E. 1991. Presence and absence of the preprophase band of microtubules in moss protonemata: a clue to understanding its function? *Protoplasma* **163**(2): 156-161.

Schaefer E, Belcram K, Uyttewaal M, Duroc Y, Goussot M, Legland D, Laruelle E, de Tauzia-Moreau M-L, Pastuglia M, Bouchez D. 2017. The preprophase band of microtubules controls the robustness of division orientation in plants. *Science* **356**(6334): 186-189.

Schaller GE, Bishopp A, Kieber JJ. 2015. The Yin-Yang of Hormones: Cytokinin and Auxin Interactions in Plant Development. *The Plant Cell* **27**(1): 44-63.

Schlereth A, Möller B, Liu W, Kientz M, Flipse J, Rademacher EH, Schmid M, Jürgens G, Weijers D. 2010. MONOPTEROS controls embryonic root initiation by regulating a mobile transcription factor. *Nature* **464**(7290): 913.

Shao W, Dong J. 2016. Polarity in plant asymmetric cell division: Division orientation and cell fate differentiation. *Dev Biol* **419**(1): 121-131.

Stockle D, Herrmann A, Lipka E, Lauster T, Gavidia R, Zimmermann S, Muller S. 2016. Putative RopGAPs impact division plane selection and interact with kinesin-12 POK1. *Nat Plants* **2**: 16120.

Strompen G, El Kasmi F, Richter S, Lukowitz W, Assaad FF, Jürgens G, Mayer U. 2002. The Arabidopsis HINKEL gene encodes a kinesin-related protein involved in cytokinesis and is expressed in a cell cycle-dependent manner. *Current Biology* **12**(2): 153-158.

Sugimoto K, Temman H, Kadokura S, Matsunaga S. 2019. To regenerate or not to regenerate: factors that drive plant regeneration. *Curr Opin Plant Biol* **47**: 138-150.

Tang H, de Keijzer J, Overdijk EJ, Sweep E, Steentjes M, Vermeer JE, Janson ME, Ketelaar T. 2019. Exocyst subunit Sec6 is positioned by microtubule overlaps in the moss phragmoplast prior to cell plate membrane arrival. *J Cell Sci* **132**(3): jcs222430.

Uyttewaal M, Burian A, Alim K, Landrein B, Borowska-Wykręt D, Dedieu A, Peaucelle A, Ludynia M, Traas J, Boudaoud A. 2012. Mechanical stress acts via katanin to amplify differences in growth rate between adjacent cells in Arabidopsis. *Cell* **149**(2): 439-451.

Vidali L, Bezanilla M. 2012. Physcomitrella patens: a model for tip cell growth and differentiation. *Curr Opin Plant Biol* **15**(6): 625-631.

Vos JW, Dogterom M, Emons AMC. 2004. Microtubules become more dynamic but not shorter during preprophase band formation: A possible "search-and-capture" mechanism for microtubule translocation. *Cell motility and the cytoskeleton* **57**(4): 246-258.

Waizenegger I, Lukowitz W, Assaad F, Schwarz H, Jürgens G, Mayer U. 2000. The Arabidopsis KNOLLE and KEULE genes interact to promote vesicle fusion during cytokinesis. *Current Biology* **10**(21): 1371-1374.

Walker KL, Muller S, Moss D, Ehrhardt DW, Smith LG. 2007. Arabidopsis TANGLED identifies the division plane throughout mitosis and cytokinesis. *Curr Biol* **17**(21): 1827-1836.

Walker KL, Müller S, Moss D, Ehrhardt DW, Smith LG. 2007. Arabidopsis TANGLED identifies the division plane throughout mitosis and cytokinesis. *Current Biology* **17**(21): 1827-1836.

Whitewoods CD, Cammarata J, Nemec Venza Z, Sang S, Crook AD, Aoyama T, Wang XY, Waller M, Kamisugi Y, Cuming AC, et al. 2018. CLAVATA Was a Genetic Novelty for the Morphological Innovation of 3D Growth in Land Plants. *Curr Biol*.

Willemsen V, Bauch M, Bennett T, Campilho A, Wolkenfelt H, Xu J, Haseloff J, Scheres B. 2008. The NAC domain transcription factors FEZ and SOMBRERO control the orientation of cell division plane in Arabidopsis root stem cells. *Dev Cell* **15**(6): 913-922.

Wu S-Z, Bezanilla M. 2014. Myosin VIII associates with microtubule ends and together with actin plays a role in guiding plant cell division. *Elife* **3**: e03498.

Xu J, Hofhuis H, Heidstra R, Sauer M, Friml J, Scheres B. 2006. A Molecular Framework for Plant Regeneration. *Science* **311**(5759): 385-388.

Xu XM, Zhao Q, Rodrigo-Peiris T, Brkljacic J, He CS, Müller S, Meier I. 2008. RanGAP1 is a continuous marker of the Arabidopsis cell division plane. *Proceedings of the National Academy of Sciences* **105**(47): 18637-18642.

Zhou W, Lozano-Torres JL, Blilou I, Zhang X, Zhai Q, Smant G, Li C, Scheres B. 2019. A Jasmonate Signaling Network Activates Root Stem Cells and Promotes Regeneration. *Cell*.

Chapter 2

Exocyst subunit Sec6 is positioned by microtubule overlaps in the moss phragmoplast prior to the arrival of cell plate membrane

Han Tang[1], Jeroen de Keijzer[1,4], Elysa Overdijk[1,2], Els Sweep[1,5], Maikel Steentjes[1,6], Joop E. Vermeer[1,3], Marcel E. Janson[1]* and Tijs Ketelaar[1]*

[1] Laboratory of Cell Biology, Wageningen University, Droevendaalsesteeg 1, 6708 PB Wageningen, The Netherlands
[2] Laboratory of Phytopathology, Wageningen University, Droevendaalsesteeg 1, 6708 PB Wageningen, The Netherlands
[3] Department of Plant and Microbial Biology and Zurich-Basel Plant Science Center, University of Zurich, Zurich, Switzerland
[4] Present address: Department of Crop Genetics, John Innes Centre, Norwich Research Park, Norwich NR4 7UH, UK
[5] Present address: Department of Bionanoscience, Kavli Institute of NanoScience, TU Delft, Van der Maasweg 9, 2629 HZ Delft, The Netherlands
[6] Present address: Laboratory of Phytopathology, Wageningen University

This work is published in Journal of Cell Science 132: jcs222430 (2019)

Abstract

During plant cytokinesis a radially expanding membrane-enclosed *cell plate* is formed from fusing vesicles that compartmentalizes the cell in two. How fusion is spatially restricted to the site of cell plate formation is unknown. Aggregation of cell-plate membrane starts near regions of microtubule overlap within the bipolar phragmoplast apparatus of the moss *Physcomitrella patens*. Since vesicle fusion generally requires coordination of vesicle tethering and subsequent fusion activity we analysed the subcellular localization of several subunits of the exocyst, a tethering complex active during plant cytokinesis. We found that Sec6, but neither Sec3 nor Sec5 subunits localized to microtubule overlap regions in advance of cell plate construction in moss. Moreover, Sec6 exhibited a conserved physical interaction with an orthologue of the Sec1/Munc18 protein KEULE, an important regulator for cell-plate membrane vesicle fusion in Arabidopsis. Recruitment of PpKEULE and vesicles to the early cell plate was delayed upon Sec6 gene silencing. Our findings thus suggest that vesicle-vesicle fusion is in part enabled by a pool of exocyst subunits at microtubule overlaps that is recruited independent of the delivery of vesicles.

Introduction

The physical separation of two daughter cells formed during plant cell division occurs via a transient, disk-shaped membrane compartment that expands radially towards the parental cell wall. This membrane compartment is termed the cell plate and its construction culminates in a new cell wall segment dividing two individual plasma membranes (Drakakaki, 2015; Müller and Jürgens, 2015; Smertenko et al., 2017). Cell plate initiation and radial expansion rely on the fusion of vesicles that are supplied mainly by the secretory pathway (Mcmichael and Bednarek, 2013; Richter et al., 2014; Boruc and Van Damme, 2015). Adaptations of canonical trafficking mechanisms are however required because there is no pre-existing target membrane at the site of cell division to which vesicles can fuse. Instead, membrane deposition is thought to be initiated by 'homotypic' fusion of vesicles (Smertenko et al., 2017). This raises the question of how vesicle fusion is spatially restricted to the site of cell division instead of it occurring spuriously throughout the whole cell. It is proposed that vesicles are transported along polarized microtubules to the centre of the phragmoplast, a cytoskeletal apparatus that supports cell plate assembly. Transport may concentrate vesicles locally to enhance fusion rates but whether transport alone can provide the spatial accuracy required to build a straight and flat cell plate is unknown. Recently we identified short stretches of antiparallel microtubule overlap at the midzone of phragmoplasts in the moss *Physcomitrella patens* as sites where membrane build up is initiated (de Keijzer et al., 2017). It remained however unclear whether there are specific molecules present at overlaps that trigger vesicle fusion locally.

In eukaryotic cells the fusion of transport vesicles with endomembrane compartments and the plasma membrane relies on the combined action of fusion and tethering complexes. The force driving the fusion of a vesicle and its destination membrane is almost universally generated by SNARE (soluble *N*-ethylmaleimide-sensitive factor attachment receptor) complexes that are typically composed of 4 membrane-associated proteins (Söllner et al., 1993; Wickner and Schekman, 2008; Südhof and Rothman, 2009). Tethering – the establishment of the initial physical connection between the two membranes – on the other hand, is orchestrated by a multitude of molecular machinery, often in the form of multimeric protein complexes (Koumandou et al., 2007; Vukašinović and Žárský, 2016). To

enable targeted trafficking among the various distinct membrane compartments in eukaryotic cells, membranes acquire different identities that dictate which membrane fusion reactions are allowed. Although SNARE complex composition bestows some of this specificity (Paumet et al., 2004), other factors including Rab GTPases (Grosshans et al., 2006; Stenmark, 2009) and the various tethering complexes play an important role as well (Yu and Hughson, 2010). Indeed, each of the several tethering complexes typically facilitates the docking of vesicles at a specific target membrane (Vukašinović and Žárský, 2016; Yu and Hughson, 2010).

While work in Arabidopsis has uncovered much about the composition, trafficking and function of the SNARE complexes involved in fusing cell plate vesicles (reviewed in Müller and Jürgens, 2015; Jürgens et al., 2015), comparatively little is known about the functioning of tethering factors involved. In Arabidopsis, both the TRAPPII (Transport Protein Particle II) and exocyst tethering complexes contribute to cell plate biogenesis (Thellmann et al., 2010; Fendrych et al., 2010; Qi et al., 2011; Rybak et al., 2014). Both are multimeric protein complexes that function in post-Golgi membrane trafficking (Drakakaki et al., 2012; Fendrych et al., 2010; reviewed by Vukašinović and Žárský, 2016). Interestingly, while TRAPPII is associated with the cell plate throughout its formation, the exocyst is present on the cell plate during cell plate initiation, whereafter its abundance drops during cell plate expansion and increases again after cell plate attachment (Fendrych et al., 2010; Zhang et al., 2013; Rybak et al., 2014). Nonetheless, the two tethering complexes physically interact and most likely function cooperatively during cytokinesis (Rybak et al., 2014). While functional analysis of the TRAPPII complex is expedited by only single genes encoding the two unique TRAPPII subunits (Thellmann et al., 2010; Qi et al., 2011), the diverse complement of genes encoding exocyst subunits have made dissecting the role of the exocyst comparatively cumbersome. Nonetheless, various exocyst mutants have been identified that harbour cell plate defects (Fendrych et al., 2010; Wu et al., 2013; Rawat et al., 2017).

Here, to understand if the exocyst could be a cell-plate assembly factor active on microtubule overlaps, we monitored the localization of several GFP-tagged exocyst subunits during cytokinesis in the moss *P. patens*. Although this representative of a basal land plant lineage has seen a similar degree of gene amplification of exocyst subunit genes as Arabidopsis, with a notable smaller radiation of Exo70 paralogs (Cvrčková et al., 2012), it features a major haploid phase in its life cycle expediting genetic analysis. Since cell plate assisted cytokinesis is a hallmark of all land plants (Buschmann and Zachgo, 2016) and a comprehensive toolset to study cell division exists for *P. patens* (Yamada et al., 2016), we anticipated that this model plant is particularly useful for studying exocyst functioning in relation to cell plate membrane fusion. We show that exocyst subunit Sec6, and not the subunits Sec3 and Sec5, localizes to microtubule overlaps at the phragmoplast midzone prior to the arrival of membrane vesicles. The localisation of Sec6 is dependent on the presence and size of the microtubule overlaps. Our findings make the case that, in general, spatial control over homotypic vesicle fusion can be achieved by linking tethering activity to a pre-defined, non-membranous subcellular structure.

Results

Exocyst subunit Sec6 arrives at the division apparatus from anaphase onset

The eukaryotic exocyst is best studied for its role in the targeting and fusion of exocytotic vesicles to the plasma membrane. A key step is thought to be the formation of a fully assembled complex between

two subunit subsets at the vesicle and plasma membranes (e.g. Yu and Hughson, 2010; Boyd et al., 2004). How exocyst assembly proceeds in absence of a plasma membrane in the context of homotypic fusion is unknown. To characterize assembly dynamics during cytokinesis in *P. patens*, we generated a time-resolved localization map of selected exocyst subunits in protonemal tip cells that exhibit repetitive cell divisions. Sec6 was included in the screen because it is the only exocyst subunit that is represented by a single gene in the moss *P. patens* (Cvrčková et al., 2012). The protein is therefore expected to be part of all fully assembled exocyst complexes. Moreover, Sec6 from Arabidopsis was shown to interact with vesicle fusion machinery and may thus be an important regulator of cell plate formation (Wu et al., 2013).

To investigate whether exocyst complex assembly occurs in sequential steps we included Sec5 and Sec3 paralogs, which in yeast were proposed to be associated to the vesicle and plasma membrane, respectively (He and Guo, 2009). Sec5 is encoded by 4 genes and Sec3 by 3 genes in *P. patens*. To conduct the screen, a GFP-encoding fragment was integrated at the end of the single Sec6 gene, all three genes encoding Sec3 paralogs, and the three Sec5 paralogs that are expressed in protonemal tissue, either caulonemal and/or chloronemal cells (Ortiz-Ramírez et al., 2016) (Fig. **S1a**). Firstly we analysed the relative abundance of the different isoforms by imaging interphase apical caulonemal cells (Fig. **S1b**). Imaging-based assessment of relative protein abundance followed the gene expression data in Figure **S1a**. All investigated exocyst subunits, except for the low expressing Sec3c, localized to plasma membrane foci as reported previously and some, notably Sec6 and sec5b, were also abundant in the cytoplasm (Fendrych et al., 2013; Zhang et al., 2013; Vukašinović and Žárský, 2016; Bloch et al., 2016; Synek et al., 2017; van Gisbergen et al., 2018). Of the subunits that showed brightest cortical localization: Sec3a, Sec5b, Sec5d and Sec6, fusion proteins were expressed alongside mCherry-α-tubulin such that exocyst localization dynamics could be related to mitotic progression (Fig. **S1**, **1a**). All selected exocyst subunits and additionally an established cell plate membrane marker (SCAMP4; de Keijzer et al. 2017) were imaged throughout cell division. The onset of anaphase was used as temporal reference to aid in the mutual comparison of arrival times to specific cytokinetic structures (Fig. **1a**).

The selected exocyst subunits showed disparate localization patterns during cell division. Sec3a and Sec5b localized to the phragmoplast midzone during cell plate initiation (Fig. **1a**). Unlike the exocyst subunits studied in Arabidopsis (Fendrych et al., 2010; Zhang et al., 2013; Rybak et al., 2014), no sharp drop in intensity occurred during cell plate expansion. However, similar to the observations in Arabidopsis, the amount of Sec3a and Sec5b on the new wall facet transiently increased after cell plate attachment. Sec5d deviated from this localization and was absent from the cell plate until late cytokinesis. Moreover, Sec6 was detected already at the centre of the division apparatus from spindle formation onwards (Fig. **1a**, white arrowhead). Unlike the other studied exocyst subunits, the intensity of Sec6 at the phragmoplast midzone peaked during cell plate initiation and expansion, and dropped after cell plate attachment. Imaging of Sec6 in conjunction with FM4-64, an amphiphilic dye for the endomembrane system, showed that a distinct pattern of bright Sec6 sections was already visible in the phragmoplast midzone already before initial deposits of cell plate membrane appeared about 2 minutes after anaphase onset (Fig. **1c**; De Keijzer et al., 2017).

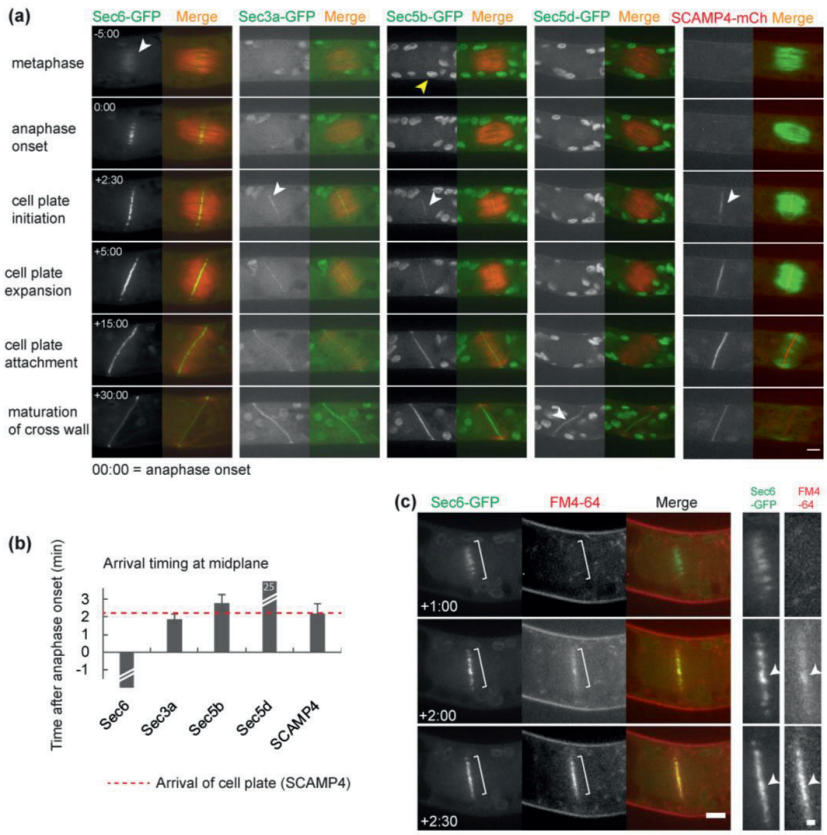

Figure 1. Localization survey of a subset of *Physcomitrella patens* exocyst subunits during cell division.
(a) Localization of exocyst subunits Sec6, Sec3a, Sec5b and Sec5d during cell division visualized in caulonemal apical cells expressing mCherry-α-tubulin (appearing red in the merged image) and a GFP-tagged version of the indicated exocyst subunit. The progression of cell plate and phragmoplast development, visualized with cell plate marker SCAMP4 (de Keijzer et al. 2017) and GFP-α-tubulin, is depicted on the right as a reference. Time after anaphase onset (t=0) is indicated in min:sec. Localization to the phragmoplast midzone is indicated with white arrowheads. A typical autofluorescent chloroplast is indicated by a yellow arrowhead. Images are maximum z-projections of 3 confocal planes spaced 0.5 µm apart. Scalebar, 5 µm.
(b) Bar graph showing the average appearance time of GFP-tagged exocyst subunits at the phragmoplast midzone compared to that of cell plate membrane (SCAMP4-mCherry, dashed line). The cut bar for Sec6 indicates that it appeared on the spindle from prophase onwards, the timing of which was not quantified (see Fig. 1a). Error bars indicate standard deviation. Averages were obtained from n=4 cells (Sec6 and Sec3a), n=5 cells (Sec5b and Sec5d) or n=8 cells (SCAMP4).
(c) Early cell plate membrane accumulation visualized in a dividing cell expressing Sec6-GFP stained with FM4-64 membrane dye. Time with respect to anaphase onset (t=0) is indicated in min:sec. The bracketed areas are shown in detail on the right. Here, arrowheads mark membranous material accumulating at Sec6-labelled sites. Images are maximum z-projections of 3 confocal planes spaced 0.5 µm apart. Scalebar in overview images, 5 µm; Scalebar in zoomed images, 1 µm.

The exocyst subunits arrive at the parental cortex prior to cell plate insertion

Interestingly, all four selected subunits stably associated with the cell cortex already before cell plate attachment at a site where the cell division plane intersected with the parental cell wall (Fig. **2a, 2b**). To our knowledge such a cortical localization pattern has not been observed during cytokinesis for any labelled subunit in Arabidopsis (Fendrych et al., 2010; Zhang et al., 2013; Rybak et al., 2014). The early cortical labelling was punctate, with numerous puncta together making up a 2-3 µm wide band that formed a continuous ring at the cell cortex (Fig. **2a**). The band was mobile on the cortex until cell plate attachment and its movement was synchronous with rotation of the phragmoplast in these cells (Fig. **2b, 2d**).

To further characterize the observed differences in localization, we identified the moments with respect to anaphase onset at which subunits first became visible at the phragmoplast midzone and the cortex (Fig. **1a, 2c**). This analysis showed that all studied subunits arrived at the cortex at around the same time (5-10 minutes post anaphase onset). The average time of arrival at the phragmoplast midzone however diverged for the studied subunits. Sec6 was already visible when the spindle midzone transformed into the phragmoplast midzone at the onset of anaphase. Sec3a and Sec5b, on the other hand, appeared simultaneously with the initial membrane accumulations (Fig. **2**), and Sec5d only appeared approximately 23 minutes later. The more weakly expressing paralogs Sec3b-GFP and Sec5a-GFP also appeared at the midzone at the time of initial membrane accumulation. Thus, while sharing localization at the cortex and late cell plate with the other studied exocyst subunits, Sec6 exhibited localization to the phragmoplast and spindle midzones apparently independent of the other studied exocyst complexes and membrane compartments.

Exocyst subunit Sec6 partially co-localizes with MAP65 on antiparallel microtubule overlaps

The early localization pattern of Sec6 showed strong resemblance to the sites where microtubules from opposite poles form antiparallel overlaps in the spindle and phragmoplast midzone (Ho et al., 2011; Kosetsu et al., 2013; de Keijzer et al., 2017). To investigate their interdependency, we generated a moss line expressing Sec6-mCherry together with a Citrine-tagged version of the antiparallel microtubule bundling protein MAP65 (Kosetsu et al., 2013). Sec6 localization indeed closely followed the distribution of MAP65-citrine labelled regions (Fig. **3**, left panels). Strikingly, this behaviour was even visible during prophase, when no bipolar spindle is yet formed (Fig. **3**, arrowheads). We previously generated cells lacking a regulator of microtubule dynamics, Kin4-Ic, that show delayed shortening of microtubule overlaps at anaphase onset (de Keijzer et al., 2017). In this genetic background a similar strong co-localization of MAP65 and Sec6 was observed during prophase and spindle stages. The width of the Sec6 patches after anaphase onset was larger in Δ*kin4-Ic* cells in accordance with the larger overlaps. As cytokinesis progressed Sec6 increasingly localized to only the central region of MAP65 regions resembling membrane depositions which also gradually become more confined to overlap centres (Fig. **3**, arrows in right panel; de Keijzer et al., 2017). This behaviour was best visible before overlaps shorten in Δ*kin4-Ic* cells approximately 5 minutes after anaphase onset . Thus, Sec6 localizes to MAP65 regions but after cell plate initiation, other factors may additionally affect its localization.

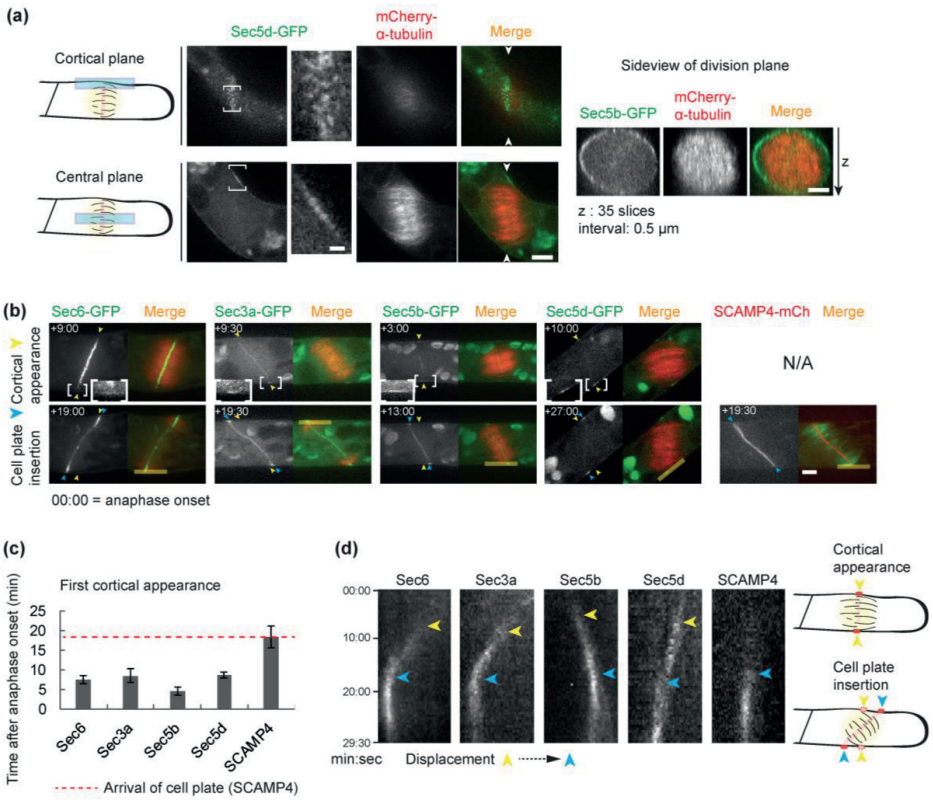

Figure 2. Exocyst subunits arrive to cortical membrane prior to cell plate insertion

(a) Cortical localization of the exocyst during cell division visualized in a cell expressing Sec5d-GFP and mCherry-α-tubulin at a single cortical and a central confocal plane (illustrated on the left). A detailed view of the Sec5d-GFP signal indicated by the brackets is shown. A sideview of the division plane (marked with arrowheads) is depicted on the right. This sideview was generated with 35 z-slices using interpolation to obtain a 1:1 pixel aspect ratio. Scalebar in overview and sideview images, 5 µm; Scalebar in zoomed images, 1 µm.

(b) Snapshots of dividing caulonemal cells expressing exocyst subunit-GFP (Sec6, Sec3a, Sec5b and Sec5d) and membrane marker SCAMP4-mCherry. Microtubules labelled with mCherry-α-tubulin or GFP were used as a temporal reference. Images are maximum z-projections of 3 planes spaced 0.5 µm apart acquired in the central plane. Images were recorded with 30 sec intervals. Time with respect to anaphase onset (t=0) is indicated in min: sec. Scale bar=5 µm. The time point each subunit first appeared at the cortex is indicated by yellow arrowheads in the upper panels, which have been copied to the lower panels. The bracketed areas are shown in detail. The final localization of each subunit in the cortex at the moment of cell plate insertion is indicated by blue arrowheads in the lower panel.

(c) Bar graph showing the average appearance time of GFP-tagged exocyst subunits at the cell cortex compared to that of cell plate membrane (SCAMP4-mCherry, dashed line). Error bars indicate standard deviation. Averages were obtained from n=4 cells (Sec6 and Sec3a), n=5 cells (Sec5b and Sec5d) or n=8 cells (SCAMP4).

(d) Kymograph of exocyst subunits and SCAMP4 generated along the parental plasma membrane as indicated by the yellow lines depicted in B. A region of 0.67 µm perpendicular to the line was used to calculate average intensity. The yellow arrowheads mark the timing of arrival while the blue arrowheads indicate the timing of cell plate attachment. Scalebar, 1 µm.

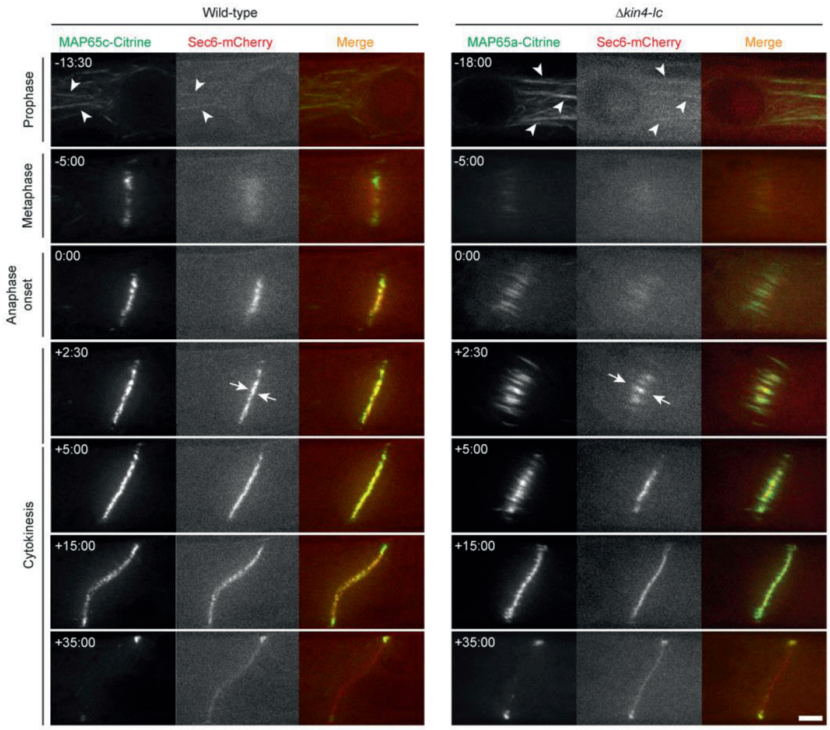

Figure 3. Exocyst subunit Sec6 partially co-localizes with MAP65 on antiparallel microtubule overlaps.
Caulonemal cells expressing citrine labelled MAP65 and Sec6-mCherry in a wild-type and Δ*kin4-Ic* genetic background imaged throughout mitosis. MAP65-labelled microtubule bundles present during prophase that show concomitant Sec6 labelling are marked with arrowheads. Arrows highlight the difference in width of the Sec6-labelled and MAP65-labelled zones during early cytokinesis. Time with respect to anaphase onset (t=0) is indicated in min:sec. Images are maximum z-projections of 3 confocal planes spaced 0.5 µm apart. Scalebar, 5 µm.

The localization of exocyst subunit Sec6 to antiparallel microtubule overlaps depends on overlap length and presence of MAP65

To further understand the extent to which the presence of microtubule overlaps is a prerequisite for the localization of Sec6 during cytokinesis, we silenced the three *MAP65* genes expressed in protonema. Earlier studies have demonstrated that upon knockdown of *MAP65* antiparallel microtubule overlap formation in the phragmoplast is severely compromised, ultimately leading to phragmoplast collapse and cytokinesis failure. Nonetheless, during early cytokinesis cell plate membrane does aggregate and phragmoplast microtubules remain organized as two opposing sets (Kosetsu et al., 2013). While in control cells the Sec6-GFP appeared regularly distributed over the division plane during early cytokinesis, in *MAP65* silenced cells Sec6-GFP formed discontinuous patterns (Fig. **4**). There was no obvious correlation between the appearance of gaps in the Sec6 localization pattern and the presence of microtubules; areas devoid of Sec6 were visible both in regions populated and unpopulated by microtubules (Fig. **4** and **S6**). Localization of Sec6 to the phragmoplast

midzone therefore not just correlates with the presence of bipolar microtubules but requires an ordered array of microtubule overlaps.

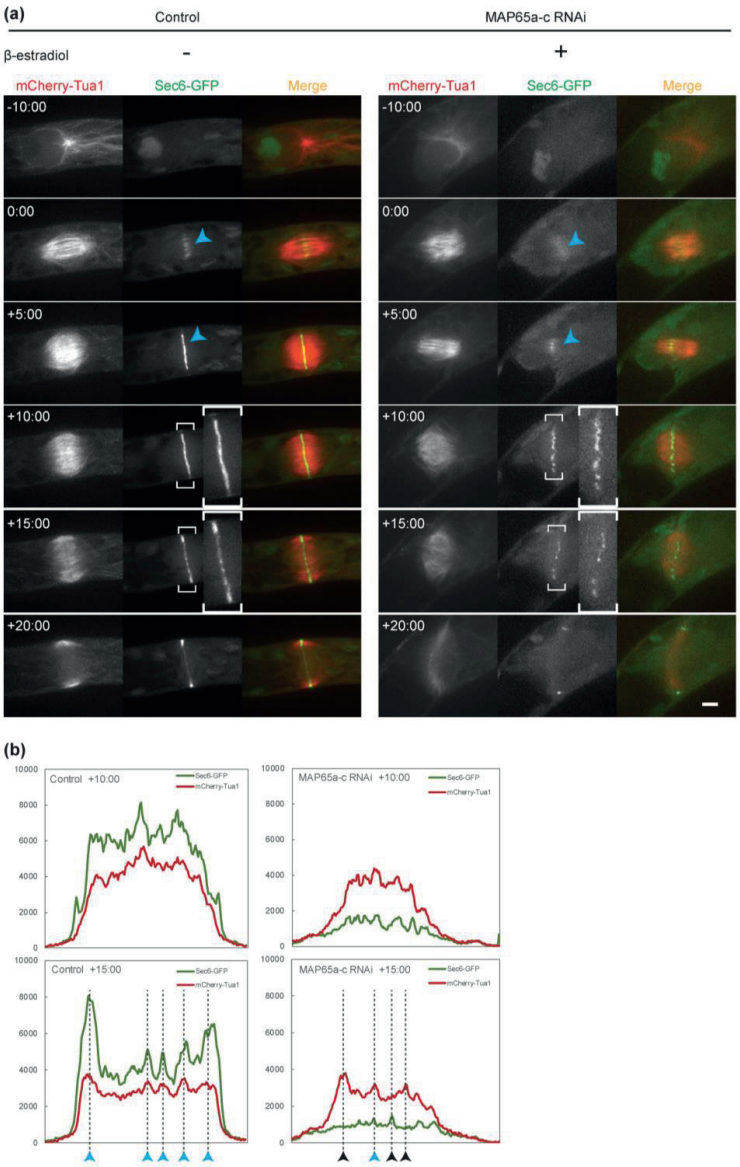

Figure 4. The localization of exocyst subunit Sec6 to antiparallel microtubule overlaps depends on overlap length and presence of MAP65.

(a) Time sequence of dividing caulonemal cells expressing Sec6-GFP and mCherry-α-tubulin with silencing of MAP65a, b and c for non-induced (control) and induced conditions. Arrowheads mark the accumulation of Sec6 to the phragmoplast midzone during early cytokinesis and the bracketed areas delineate the midzone during a later stage of cytokinesis in detail. Time with respect to anaphase onset (t=0) is indicated in min:sec. Images are maximum z-projections of 3 confocal planes spaced 0.5 µm apart. Scalebar, 5 µm.

(b) Fluorescence line plots, 15 pixels in width, of Sec6 and microtubule signals as shown in A parallel to the phragmoplast midzone. Blue arrowheads indicate positions at which both tubulin signals and Sec6 signals have a local maximum. Black arrowheads indicate positions at which only one of the signals has a local maximum. The lack of correlation between signals was especially apparent 15 min after anaphase onset.

Identification of a *P. patens* KEULE orthologue that physically interacts with Sec6 and co-localizes at the phragmoplast midzone during cell plate formation

A physical interaction between Sec6 and Sec1/munc18 (SM) family protein KEULE was proposed to be an important regulatory step in cytokinetic vesicle fusion in Arabidopsis (Wu et al., 2013). KEULE contributes to fusion by preventing the important cytokinetic SNARE-component KNOLLE from refolding into its closed, non-fusion-competent conformation, thereby allowing the formation of fusogenic trans-SNARE complexes among vesicles delivered to the cell plate (Park et al., 2012; Karnahl et al., 2017; Jürgens et al., 2015). Whether the Sec6 interaction regulates this specific activity is presently unknown. Nonetheless, cytokinesis defects were found in Sec6-mutants that resemble these encountered in plants lacking KEULE (Wu et al., 2013; Assaad et al., 1996), hinting that a cooperative Sec6-KEULE interaction regulates cytokinesis. Based on these findings we hypothesized that Sec6 on overlaps in moss may regulate vesicle fusion activity in space through an interaction with KEULE. In search of gene homologous to *KEULE* we identified 7 loci in the *P. patens* genome that are predicted to encode SM family proteins. Of the identified loci, two contained genes with a predicted exon number equal to that of the Arabidopsis *KEULE* gene and their expected gene products exhibited an overall similarity to Arabidopsis *KEULE* at least twice higher than the other predicted SM genes (Fig. **5a**). Analysis of gene expression levels revealed that the gene encoded at locus Pp3c17_24130 was ubiquitously expressed in all moss tissues, while the other gene (Pp3c16_570) was only expressed in rhizoids (Fig. **3a** and **S2**; Ortiz-Ramírez et al., 2016). We therefore focussed on the former gene and tentatively named it PpKEULE. Since the position of introns in genes contains information on the evolutionary trajectory of the gene family they belong to (e.g. Rogozin et al., 2003; Garcia-España et al., 2009; Javelle et al., 2011), we compared the intron-exon structure between Arabidopsis *KEULE* and *PpKEULE*. The intron positions were highly similar for both species (Fig. **5b**). Introns in the *PpKEULE* gene were slightly longer, however this is in line with average intron length being bigger in moss compared to Arabidopsis (Rensing et al., 2005). The concurrent intron-exon structure of the genes of both species shows that *PpKEULE* is a likely ortholog of *AtKEULE*.

In Arabidopsis, the interaction domain of KEULE with Sec6 was narrowed to a C-terminal portion of the protein designated C1 (Wu et al., 2013). The high degree of sequence conservation allowed us to delineate the same domain in PpKEULE and test it for its ability to interact with Sec6. In a reciprocal yeast 2-hybrid assay with *P. patens* Sec6, KEULE and the KEULE-C1 domain, we found a strong interaction between Sec6 and both PpKEULE and PpKEULE-C1 when Sec6 was fused to the activation domain of the Gal4 transcription factor. When Sec6 was fused to the DNA-binding domain of Gal4 only a weak interaction with the PpKEULE-C1 domain was found (Fig. **5c**). Possibly, in this case, the binding partners are in a less favourable configuration for reconstituting Gal4 function since a similar result was reported for the interaction of Arabidopsis proteins (Wu et al., 2013). Because PpKEULE interacts with Sec6 in a fashion indistinguishable from its orthologue in Arabidopsis, the two proteins could form a conserved module regulating cell plate membrane fusion. To investigate where and when in *P. patens* Sec6 and PpKEULE may interact, we visualized Sec6-mCherry together with endogenous PpKEULE tagged with GFP (Fig. **S3**). We chose to fuse GFP to the C-terminal end, since this yielded a functional

fusion protein for Arabidopsis KEULE (Steiner et al., 2016). While absent from Sec6-labelled regions during prophase and metaphase, PpKEULE-GFP became rapidly enriched at the site of Sec6-mCherry at the onset of cytokinesis around the time that localized membrane deposition is first observed at overlaps (Fig. **5d**). During radial expansion of the phragmoplast, appearing sites of Sec6 localization at the leading zone, likely corresponding with newly formed microtubule overlaps with yet little accumulated vesicles (de Keijzer et al., 2017), had low PpKEULE-GFP signal associated (Fig. **5d**, arrowheads). At the cortical zone marked by the labelled exocyst subunit no corresponding PpKEULE signal was found (Fig. **5d**, arrow). Taken together, the co-localization pattern suggested that physical association between Sec6 and PpKEULE in a cytokinetic context is both spatially and temporally regulated.

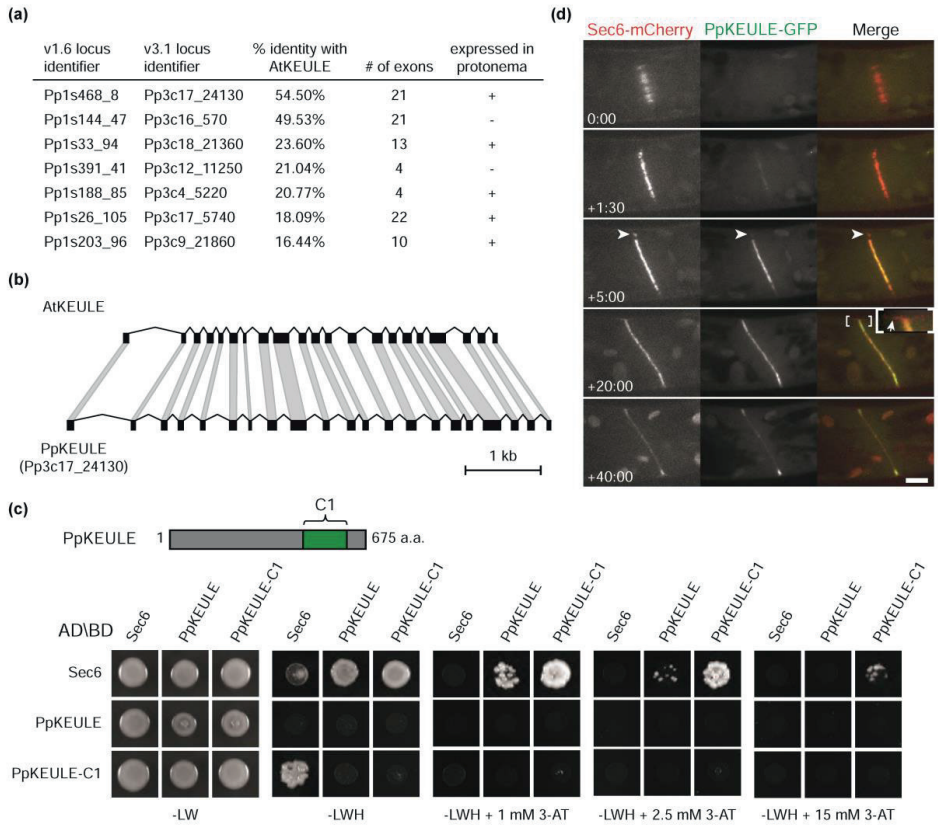

Figure 5. Identification of a *P. patens* KEULE orthologue that physically interacts with Sec6 and co-localizes at the phragmoplast midzone during cell plate formation.

(a) Table summarizing loci putatively encoding Sec1/munc18-like (SM) family proteins and their identity to the cytokinetic Sec1 protein KEULE of Arabidopsis at the protein level. The locus identifiers for two versions of the *P. patens* genome assembly are given. For each predicted gene the number of exons and the presence of indicators of gene expression in protonemal tissue are given.

(b) Comparison between the exon (black boxes) and intron (connecting chevrons) structure of the gene encoding Arabidopsis KEULE and the putative *P. patens* orthologue expressed in protonema.

(c) Yeast-two-hybrid interaction assay between Sec6, PpKEULE, and the PpKEULE C1 domain (illustrated at the top). Proteins were fused with the Gal4 activation domain (AD) and binding domain (BD) and their different

combinations were co-expressed in yeast strains that were tested for growth on reporter media lacking histidine in combination with increasing amounts of the competitive inhibitor 3-AT.
(d) Sec6 and PpKEULE co-visualized throughout cell division in a cell expressing Sec6-mCherry and PpKEULE-GFP. The arrowheads indicate Sec6-labelled regions at the expanding edge of the phragmoplast showing less associated KEULE-GFP compared to the central regions. An enlarged view of the bracketed area is depicted in the inset where the arrow points to Sec6 located at the cortex without associated PpKEULE-GFP signal. Images are maximum z-projections of 3 confocal planes spaced 0.5 µm apart. Scalebar, 5 µm.

To investigate the functional importance of Sec6 for correct KEULE localization and cell plate assembly in general we sought ways to reduce or abolish cellular Sec6 levels. We failed to isolate a Sec6 knock-out mutant, suggesting that Sec6 is an essential protein for cell proliferation, as was reported for RNAi studies by van Gisbergen et al. (2018). We therefore introduced inducible Sec6 RNAi in cells expressing either the cell plate membrane marker SCAMP4-mCherry or PpKEULE-GFP. Induction of Sec6 RNAi caused an approximately 5-fold reduction of moss colony expansion over a 5-day growth period and an absence of caulonemal cells (Fig. **S4a - S4c**). Continuation of colony expansion suggested that some functional exocyst complexes remained present after induction of RNAi. This was in agreement with an incomplete, approximately three-fold, reduction of transcript levels after RNAi (Fig. **S5b**). Chloronemal cells with induced RNAi targeting different regions of the *Sec6* gene reproducibly showed a more bulbous tip shape suggesting that exocyst functioning in polarized tip growth was severely disrupted but not completely abolished (Fig. **S4c and S6**). Three days after induction of RNAi knockdown, finalized cell walls separating two daughter cells showed various morphological defects (Fig. **S4d**). Incomplete cytokinesis could however not be concluded without ultrastructural analysis of the formed cell plates.

Initial recruitment of membrane materials and PpKEULE is reduced upon Sec6 silencing

To understand whether defects arose due to exocyst malfunctioning during cell plate initiation and expansion we observed cells expressing SCAMP4-mCherry as a membrane marker throughout cytokinesis (Fig. **6a**). Although the time of initial membrane appearance remained similar (Fig. **6c**), the rate at which membrane material accumulated was delayed after RNAi induction (Fig. **6b**). RNAi experiments thus suggested that reduction of Sec6 functioning at the midzone decreased membrane build up during early cytokinesis, a time at which Sec6 levels peaked in unperturbed cells (Fig. **1a**). Surprisingly, the velocity of cell plate expansions appeared similar for both induced and non-induced conditions (Fig. **6d**). To test whether silencing of Sec6 affected KEULE levels at the phragmoplast midzone we imaged PpKeule-GFP after RNAi induction. A delay in the recruitment of PpKEULE-GFP to the midzone was observed after induction with similar dynamics as SCAMP4-mCherry (Fig. **6e,f**). This suggested that KEULE accumulation to the phragmoplast midzone was at least partly dependent on Sec6 in agreement with the observed interaction between KEULE and Sec6 (Fig. **5**).

Discussion

Our cytokinesis-oriented localization screen of exocyst subunits in moss revealed two localization patterns that have not been previously described in plants. Firstly, exocyst subunits localized to MAP65-labeled regions in the midzones of the spindle and phragmoplast. Secondly, they formed a cortical ring prior to cell plate attachment. Interestingly, the two localization patterns overlapped in time yet differed in subunit composition. In the midzone, Sec6 arrival preceded Sec5 and Sec3

homologues whilst this was not evident for the cortical localization. The systematic design of the conducted screen thus provides some of the clearest evidence for sequential assembly of the exocyst complex to date. So although biochemical purification and live cell data show that the eight exocyst subunits in yeast form a stable complex, our work shows that subunits can have individual localization patterns as well (Hála et al., 2008; Heider et al., 2016; Picco et al., 2017).

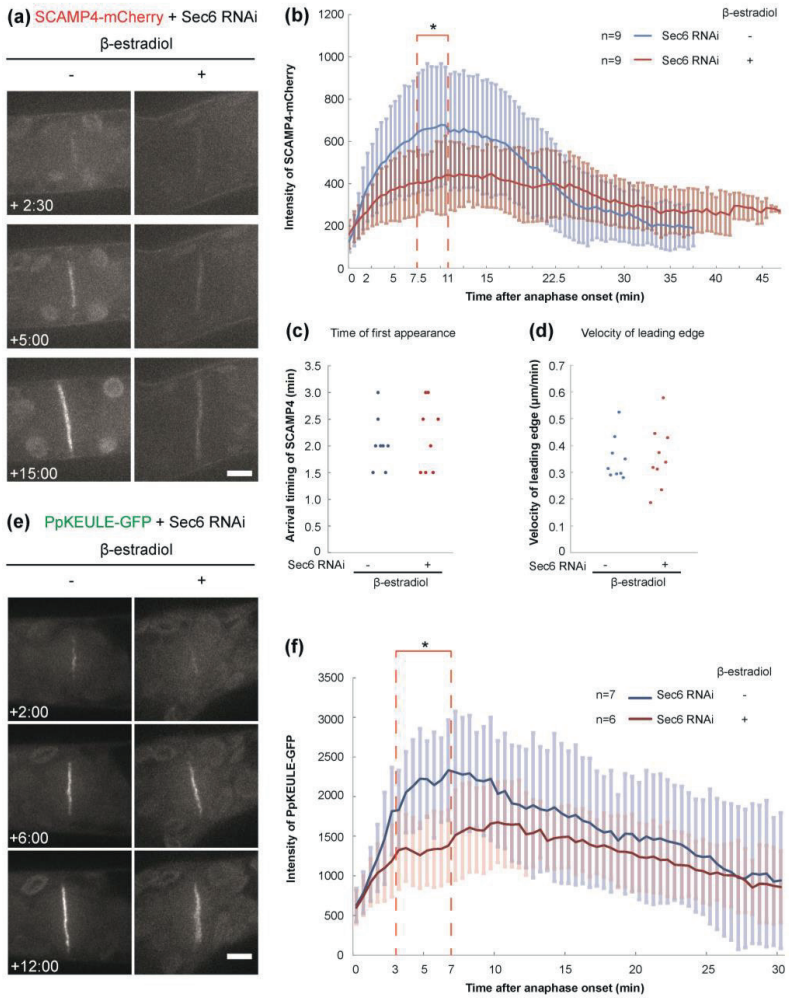

Figure 6. Initial recruitment of membrane materials and PpKEULE is reduced upon Sec6 silencing.
(a) Snapshots of dividing cell with membrane marker SCAMP4-mCherry in Sec6 RNAi without or with RNAi induction by β–estradiol treatment. The intensity of SCAMP4-mCherry is depicted with the same contrast settings. Time with respect to anaphase onset (t=0) is indicated in min:sec. Images are maximum z-projections of 3 planes spaced 0.5 µm apart acquired in the central plane. Scale bar =5 µm.
(b) Average intensity of SCAMP4-mCherry quantified throughout cytokinesis. The error bars represent SD of each time point. * indicates the significant difference ($P < 0.05$) between control and Sec6 RNAi from 7.5 to 11 min in Student's two-tailed t-tests.

(c) The onset of membrane arrival in Sec6 RNAi background with or without induction. Anaphase onset is set up as t=0. n=8 for both treatments.
(d) The expansion rate of the cell plate in Sec6 RNAi background with or without induction. n=8 for both control and Sec6 RNAi.
(e) The Localization of PpKEULE-GFP in Sec6 RNAi background. Representative snapshots are shown in the early, middle, and late phase of cytokinesis. Images are maximum z-projections of 3 planes spaced 0.5 µm apart acquired in the central plane. KEULE-GFP is depicted using identical contrast settings among RNAi and control cells. Scale bar =5 µm.
(f) Average PpKEULE-GFP intensity throughout cytokinesis. The error bars represent SD of each time point. * indicates the significant difference ($P < 0.05$) between control and Sec6 RNAi from 3 to 7 min in Student's two-tailed t-tests.

In most plant cells a cortical ring of microtubules, the preprophase band (PPB), is thought to demarcate a functionalized section of the cortex, called the cortical division zone (CDZ), to which cell plate expansion is directed during cytokinesis (van Damme, 2009; Müller et al., 2009; Stöckle et al., 2016). Known components of the CDZ do however assemble into ring-like structures in mutants that are unable to form a PPB (Schaeffer and Bouchez, 2010). Other cells, including moss protonemal cells, lack a PPB altogether but cytokinesis does involve the formation of a cortical band with established CDZ components, including myosins and kinesins, prior to cell plate attachment (Schmiedel et al., 1981; Doonan et al., 1985; Otegui and Staehelin, 2000; Hiwatashi et al., 2008; Wu et al., 2011; Nakaoka et al., 2012; Miki et al., 2014; Wu and Bezanilla, 2014; Lipka et al., 2014; Schaefer et al. 2017; Kosetsu et al., 2017). Given the early cortical localization of the exocyst observed in moss, it will be interesting to find out if the exocyst and vesicle trafficking have a role in the establishment or maintenance of the CDZ in absence of a PPB, or whether its function is limited to attachment of the cell plate. Analogies may be present with fission yeast cytokinesis where exocyst localization and vesicle fusion to the division site appear to precede cleavage furrow ingression (Wang et al., 2016). It is surprising that no exocyst subunits have been reported as components of the CDZ in higher plants (Vukašinović and Žárský, 2016; Borucand van Damme, 2015). Characterization of exocyst localization in plants is however impeded by the large number of subunits homologues, particularly of the Exo70 subunit.

Local accumulations of exocyst subunits were first described for their role in polarized exocytosis at the plasma membrane (TerBush and Novick 1995; Hazuka et al., 1999). However, exocyst subunits also localize to internal membrane compartments to assist in autophagosome formation (Kulich et al., 2013; Bodemann et al., 2011). Moreover, in budding and fission yeast it was demonstrated that the deliberate targeting of exocyst subunits to mitochondria reroutes cellular trafficking towards these organelles (Luo et al., 2014; Wang et al., 2016). These observations lead us to propose that a local pool of exocyst subunits on microtubule overlaps in moss may stimulate the immobilization and fusion of vesicles to initiate cell plate assembly. However, in all mentioned examples local pools of exocyst subunits are bound to membranes whereas Sec6 in our studies localized to non-membranous microtubule overlaps. It is therefore not self-evident how Sec6 on overlaps may initiate membrane-membrane interactions for homotypic vesicle fusion even when it seeds the assembly of a complete exocyst complex. Possibly, vesicles arrive at the phragmoplast midzone in a fusion-incompetent state and formation of enabled SNARE complexes involves interactions between SNAREs, KEULE and exocyst subunits. In fact, Sec6 appears to be at the centre of an interaction network since SEC6-homologues in diverse systems interact with both SNARE- and SM proteins apart from other exocyst subunits (Hong and Lev, 2014; Hashizume et al., 2009; Morgera et al., 2012; Dubuke et al., 2015; Siviram et al., 2005,

2006). Cytosolic levels of Sec6 may be insufficient to establish these regulatory molecular interactions on vesicles whilst concentrated Sec6 on overlaps could generate a local pool of fusion-competent vesicles near overlaps. Our finding thus suggests how vesicle fusion activity may be regulated in space, an aspect that so far remained unresolved. Interestingly, *Pp*KEULE does not localize to cortical exocyst subunits prior to cell plate attachment. It may thus be exclusively required to regulate vesicle fusion activity in the phragmoplast midzone during cytokinesis.

Unique about Sec6 during moss cytokinesis was its initial localization to the phragmoplast midzone in complete absence of membranes. Possibly, other exocyst subunits share this localization pattern but not Sec5 and Sec3 which arrived later, around the time of initial membrane accumulation. Colocalization of MAP65 and Sec6 at a stage in which MAP65 is localized to visible regions of microtubule overlap in the phragmoplast midzone (Fig. **3**; Kosetsu et al., 2013) demonstrated that Sec6 first associates along microtubule overlaps. Observations in mammalian cells suggest that microtubule overlaps may have a more common role in controlling vesicular transport. Through an interaction with centralspindlin, the protein MICAL3 first localizes to the spindle midzone starting in anaphase and later targets Rab8a positive vesicles to the midbody (Liu et al., 2016). Centralspindlin does however transfer from microtubule overlaps to an adjacent exocyst-containing ring-shaped bulge (Hu et al., 2012; Gromley et al., 2005). It is therefore not clear how intimate the spatial association between microtubule overlaps and vesicles is in these cells (Green et al., 2013). Moss was not shown to have centralspindlin but MAP65 itself, or other midzone associated proteins, may have a function in Sec6 recruitment to microtubule overlaps. Physical interactions between cytoskeletal regulators and exocyst subunits were reported in various other systems (van Gisbergen et al., 2018; Gromley et al., 2005; Zuo et al., 2006; Oda et al., 2015). MAP65 silencing and Δ*kin4-Ic* experiments clearly showed that the length and presence of microtubule overlaps affected Sec6 localization. Sec6 was however also present in the phragmoplast midzone independent from MAP65 during later stages of cytokinesis and Sec6 localized predominantly to the centre of long MAP65 regions in Δ*kin4-Ic* cells (Fig. **1a**). We therefore hypothesize that Sec6 and possibly other proteins on overlaps are gradually incorporated in a structure that also drives membrane accumulation away from overlaps. This structure may represent the Cell Plate Assembly Matrix (CPAM) that is visible in EM micrographs and from which microtubule overlaps are excluded (Seguí-Simarro et al., 2004). Cell plate dimensioning and assembly defects in cells lacking Kin4 do however show that overlap length is important for templating cell plate initials, likely in part through patterning of the exocyst complex (de Keijzer et al., 2017).

Our findings provide the first indication that molecules driving membrane fusion processes are at least temporarily associated with microtubule overlaps during plant cytokinesis. The formation of intracellular septa in general is a complex task that requires spatial control over vesicle fusion to make a *de novo* plasma membrane. The involvement of multiple tethering complexes has been reported in various eukaryotes (see Neto and Gould, 2011; Wang et al., 2016; Rybeck et al., 2014). These complexes may however act redundantly, which hinders their functional characterization. It will be interesting to learn how positioning tethering complexes may fine tune cell plate formation at the ultrastructural level. Differential localization of TRAPPII and exocyst complexes was reported during fission yeast cytokinesis and the two complexes in Arabidopsis where present sequentially at the developing cell plate (Wang et al., 2016; Rybak et al., 2014). The molecular and light microscopic tools available in the moss, together with the identification of overlaps as sites of vesicle accumulation, will help to resolve how multiple tethering complexes together shape the cell plate.

Materials and methods

Plasmids and cloning procedures

All plasmids used throughout this study are listed in Supplemental table 2. For construction of GFP/mCherry tagging constructs for Sec6, Sec3a, Sec3b, Sec3c, Sec5a, Sec5b, Sec5d, and PpKEULE, regions of approximately 1 kb before and after the stop codon of the encoding gene were amplified by PCR using primers listed in Supplemental table 1. The PCR fragments were digested with restriction enzymes indicated in supplemental table 1and ligated into correspondingly digested peGFP-NPTII or pmCherry-LoxP-BsdR vector (de Keijzer et al., 2017).

For β-estradiol inducible RNAi, targeting Sec6 transcript, we used the system published by Nakaoka et al. (2012). A ~500 bp fragment of the coding sequence of Sec6 (Fig. **S5**) was amplified by PCR from a cDNA library derived from protonemal tissue and cloned into gateway entry plasmid pENTR-D-TOPO. The fragment was subsequently introduced into silencing vector pGG626 via a Gateway LR reaction.

To generate the expression constructs used for yeast-two-hybrid assays, first the coding sequences of Sec6, PpKEULE, and the PpKEULE-C1 domain were PCR-amplified from a *P. patens* cDNA library derived from protonemal tissue. The PCR products were then introduced into the pENTR-D-TOPO vector and subsequently subcloned into destination plasmids pDEST22 and pDEST32 (Invitrogen) via Gateway LR reactions.

For transient RNAi constructs, the region used for induced silencing as described above and regions located at the 5'-untranslated region and the 3'-end of the coding sequence were amplified and cloned into pENTR-D-TOPO. The fragments were then introduced into the RNAi vector pUGGi (Bezanilla et al., 2005) via a Gateway LR reaction.

P. patens growth conditions and transformation

P. patens tissues were routinely grown on BCDAT plates under continuous light. Plasmids were linearized and introduced into the *P. patens* genome by homologous recombination using PEG-mediated protoplast transformation (Nishiyama et al., 2000). Correct insertion events were characterised by PCR (Fig. **S3**). Knock-down in RNAi lines upon induction was verified by quantitative RT-PCR 3 days after induction with β-estradiol (Fig. **S5**). Characteristics of generated moss lines and their use throughout the study are summarized in Supplemental table 3. For imaging, protonemal tissue was grown for 5 to 7 days on BCD medium in glass bottom dishes (Yamada et al., 2016).

For transient RNAi silencing, RNAi constructs were transformed into the SNAP-TM-mCherry moss line expressing nuclear targeted GFP-GUS (Van Gisbergen et al., 2018). The nuclear GFP signal was used as a visual marker to identify silenced tissues. Filaments with decreased GFP intensity were selected for analysis (Fig. **S6**).

Identification of *P. patens* Sec1 homologues

Proteins of the Sec1/Munc18 family were identified by BLAST using the Arabidopsis KEULE protein sequence as input against the predicted proteins of *P. patens* genome assemblies version 1.6 and 3.1 and by keyword search in the Phytozome 10.3 browser (www.phytozome.org). Expression in protonema was assessed by verifying the presence of ESTs derived from protonemal tissue and using the *Physcomitrella* eFP browser (Ortiz-Ramírez et al., 2016).

Yeast two-hybrid assay

Yeast 2-hybrid assays were performed with a split Gal4 transcription factor system using the His3 gene as reporter (James et al., 1996). For this, pDEST22/32-based constructs (supplemental table 2) were transformed into yeast strain PJ69-4a or PJ69-4α by PEG-mediated transformation. Positive transformants with minimal background reporter activity were selected on double dropout medium (–Leu–His or –Trp–His) with different concentrations of 3-amino-1,2,4-triazole (3-AT) present to increase histidine-dependent growth stringency. Selected clones were then allowed to mate and resulting diploids were selected on –Leu–Trp plates. With surviving of the cells a yeast 2-hybrid assay was then performed on triple dropout medium (–Leu–Trp–His) with increasing amounts of 3-AT present.

Fluorescence microscopy and staining

All live cell imaging was performed on a Roper spinning disk microscope system composed of a Nikon Ti eclipse body, Yokogawa CSU-X1 spinning disc head and Photometrics Evolve 512 camera or Prime 95B camera. All imaging was conducted with a 100x Plan Apo VC oil immersion objective (NA 1.40), using a 1.2x post-magnification fitted before the camera. The GFP and citrine probes were exited using 491 nm light generated by a Cobolt Calypso50 laser and their emitted light was bandpass filtered at 497-557 nm. For FM4-64 and mCherry 561 nm excitation light generated by a Cobolt Jive50 laser was used in combination with bandpass filtering at 570-620 nm. During image digitization a camera electron multiplication gain of 300 was employed and typical exposures were 800-1000 ms for GFP, citrine and FM4-64, except for Movie S8 and S9, where we used 3000 ms exposure times. For the mCherry probeexposure times of 1000-2000 ms were used. FM4-64 was dissolved in dH_2O at a final concentration of 10 µM and added to cells at the moment of nuclear envelope breakdown as described (Kosetsu et al., 2013).

Image analysis

FIJI (Schindelin et al., 2012) was used for all image analysis and processing. Figures were prepared in Adobe Illustrator CC 2015. The arrival time of labelled exocyst subunits to the phragmoplast midzone (Fig. **1b**) was taken as the time at which structural features with a residence time of more than one timeframe first appeared in the generated maximum projections of three image planes. The appearance was abrupt and synchronously over the full length of the midzone. The arrival time of labelled exocyst subunits to a cortical band (Fig. **2c**) was defined as the time at which stable cortical patches, visible for more than one timeframe, first became visible in the region where the division plane intersected the parental cell wall. These patches were distinctly less dynamic compared to cortical localizations of the exocyst elsewhere in the cell.

Analysis of Sec6 RNAi mutant phenotype

To quantify the accumulation of cell plate membrane material and PpKEULE upon Sec6 RNAi silencing, we imaged SCAMP4-mCherry and PpKEULE-GFP throughout cytokinesis at a 30 second intervals. Images were taken in the central plane of the dividing cell at 3 confocal planes spaced 0.5 µm apart. Maximum projections made along the z-axis were then used to measure the average intensity of SCAMP4-mCherry and KEULE-GFP using a 5-pixel wide line manually drawn along the division plane for each time point. Simultaneously, the mean level of cytosolic background fluorescence was recorded in an area right next to the cell division site. For each time point, the background fluorescence level was subtracted from the obtained level of fluorescence at the division plane. The expansion rate of the cell plate (Fig. **6d**) was calculated as described by de Keijzer et al. (2017).

Acknowledgements

We would like to thank Henk Kieft for technical assistance, Richard Immink and Marco Busscher (WUR-Bioscience) for assistance with Y2H experiments and Magdalena Bezanilla (Darthmouth College, USA) for the kind gift of the pUGGi plasmid.

Author Contributions

H.T. and J.K. planned and designed the research. H.T. and E.O. generated experimental materials. H.T., E.S., and M.S. performed experiments. H.T. conducted data analysis. J.K., H.T., J.V., M.J., and T.K. wrote the manuscript.

Supplemental Information

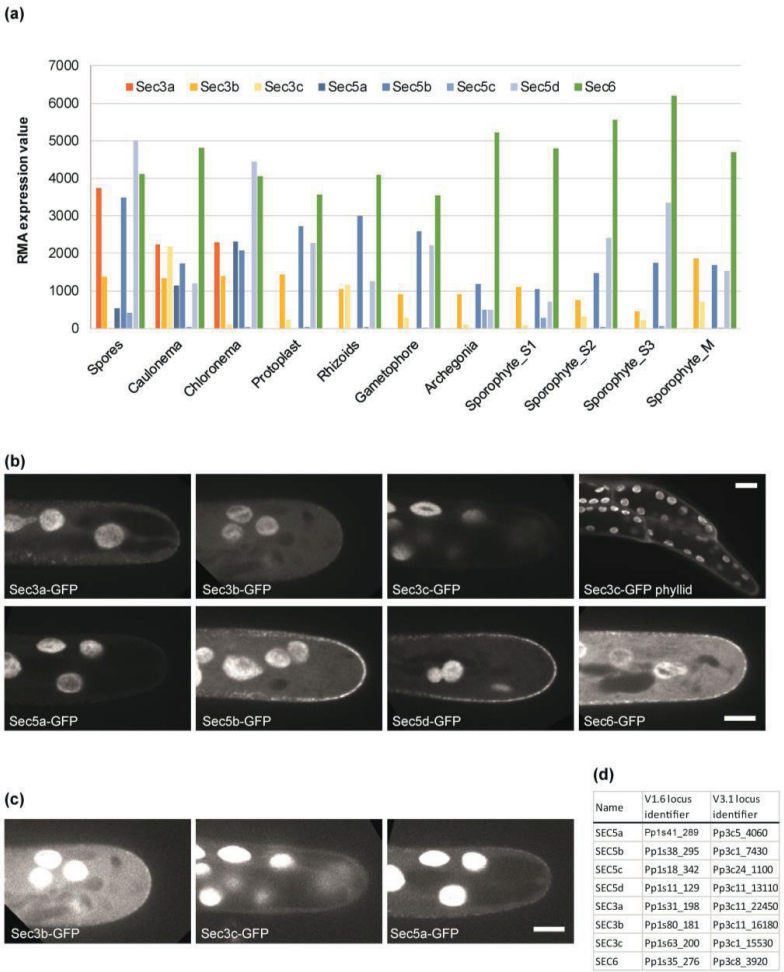

(d)

Name	V1.6 locus identifier	V3.1 locus identifier
SEC5a	Pp1s41_289	Pp3c5_4060
SEC5b	Pp1s38_295	Pp3c1_7430
SEC5c	Pp1s18_342	Pp3c24_1100
SEC5d	Pp1s11_129	Pp3c11_13110
SEC3a	Pp1s31_198	Pp3c11_22450
SEC3b	Pp1s80_181	Pp3c11_16180
SEC3c	Pp1s63_200	Pp3c1_15530
SEC6	Pp1s35_276	Pp3c8_3920

Figure S1. Expression analysis of *P. patens* exocyst subunits Sec3, Sec5, and Sec6.

(a) The robust multi-array average (RMA) expression values of the Sec3 and Sec5 gene families, and the single Sec6 gene are plotted for various moss tissues/life cycle stages. The locus identifiers of the genes are given in Figure S1D.Expression data was obtained from the publically available *Physcomitrella* transcriptome atlas (Ortiz-Ramírez et al. 2016).

(b) The localization s of GFP-tagged exocyst subunits in the tip of protonemal cells, and Sec3c-GFP in phyllids.

(c) Images with enhanced contrast settings show the localization of the weakly expressing genes Sec5a-GFP, Sec3b-GFP, and Sec3c-GFP in the tip of a protonemal cell. Due to oversaturation of the chloroplast autofluorescence in these images, chloroplasts are visible as white areas.

(d) The locus identifiers of the genes encoding exocyst subunits, Sec3, Sec5 and Sec6 in *P. patens* from the *Physcomitrella* genome assembly (version 1.6 and 3.1).

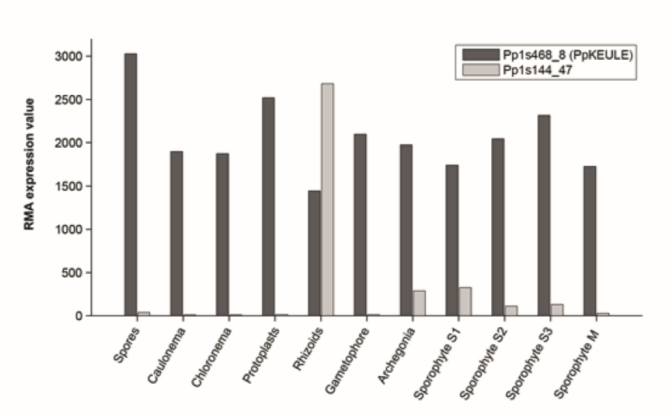

Figure S2. Expression analysis of the two *P. patens* genes encoding Sec1/munc18 family proteins similar to Arabidopsis KEULE.

The robust multi-array average (RMA) expression values of two genes encoding KEULE homologs are plotted for various moss tissues/life cycle stages. The locus identifiers in version 1.6 of the *Physcomitrella* genome assembly of these genes are given in the legend. Expression data were obtained from the publically available *Physcomitrella* transcriptome atlas (Ortiz-Ramírez et al. 2016).

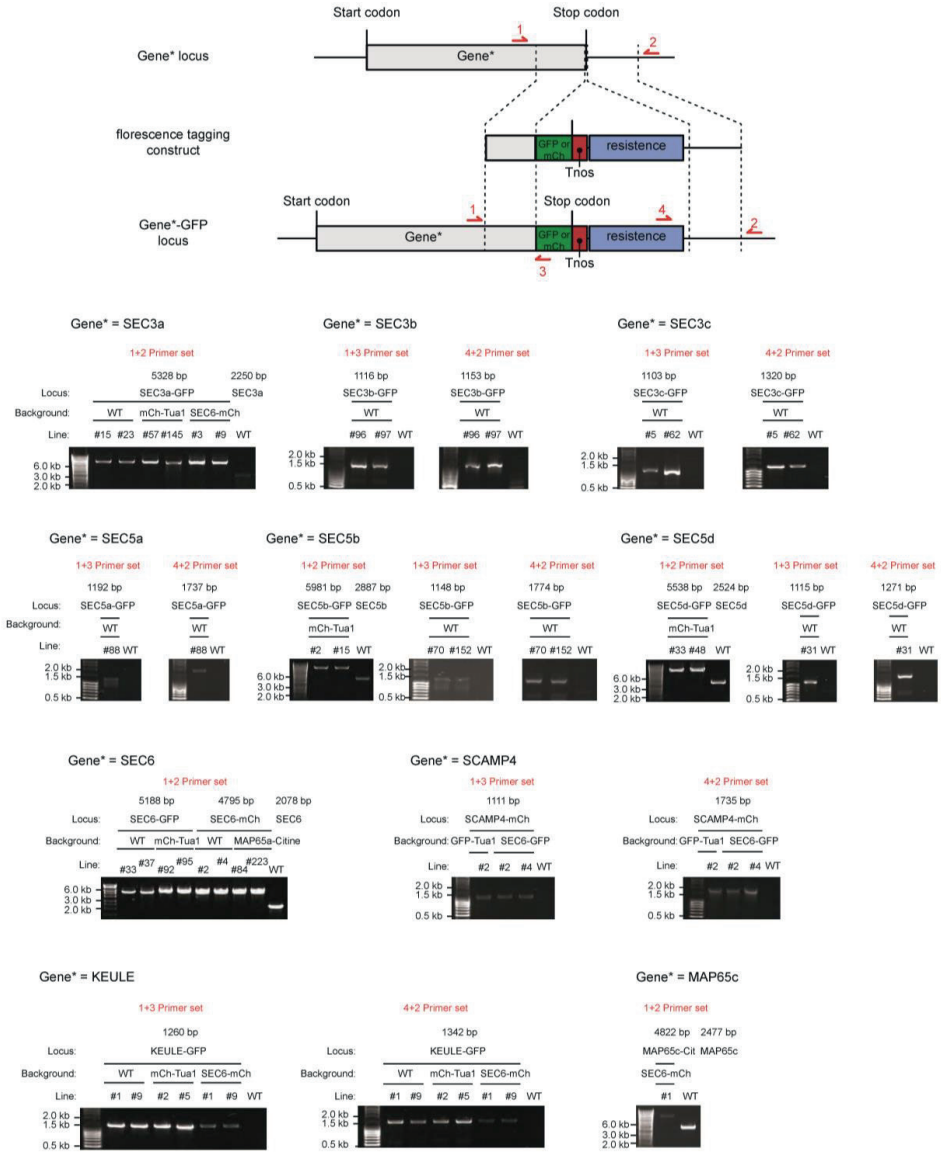

Figure S3. Generation and verification of fluorophore tagged versions of Sec3a, Sec5b, Sec5d, Sec6 and PpKEULE.

Schematic representation of a typical genetic locus and the construct used for C-terminal GFP/citrine/mCherry tagging via homologous recombination (dashed lines; not drawn to scale). In labelled lines, the original stop codon is replaced with a fragment containing a fluorophore encoding sequence (orange box), the nopaline synthase terminator (red box) and a cassette conferring G418 or blasticidin resistance (blue box). Red arrows denote primer binding sites used for confirmation of the obtained lines by PCR. For each indicated gene with a knocked-in construct for fluorescent labelling the product obtained after PCR reaction and its predicted size are given. The line numbers of independent transformants and their genetic background are given above the gel images.

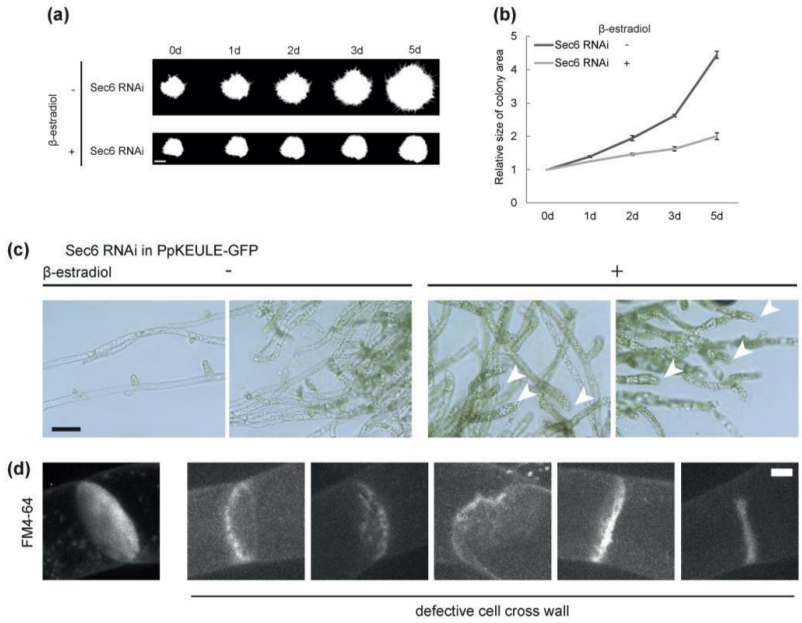

Figure S4. Growth and cell cross wall defects in Sec6 silencing.

(a) Colony growth of uninduced and induced Sec6 RNAi moss plants, scale bar is 1mm.

(b) The average colony expansion rates of uninduced and induced Sec6 RNAi moss plants (n=3).

(c) Protonemal cells of uninduced and induced Sec6 RNAi moss plants, 3 days after induction. The arrowheads indicate swollen chloronema cell tips. Scale bar is 50 µm.

(d) Cross wall defects in induced Sec6 RNAi moss plants. The left panel displays a representative cross wall in an uninduced line. The right panels display a variety of cross wall defects that were observed during Sec6 silencing, including punctuate, irregular and ring-shaped signal and incomplete cross walls. Cross walls were visualized by FM4-64 staining after 3 days induction. Images are maximum z-projections of 3 planes spaced 0.5 µm apart acquired in the cortical area. Scale bar is 5 µm.

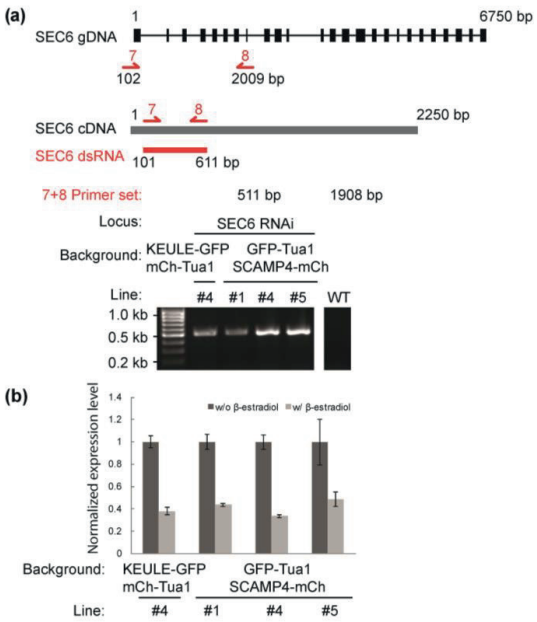

Figure S5. Characterization of Sec6 RNAi lines by genotyping analysis and quantitative RT-PCR.
(a) Schematic representation of genomic DNA, cDNA, and the range of RNAi target sequence (SEC6 dsRNA) in the Sec6 locus. Red arrows denote primer binding sites used for confirmation of the obtained lines by PCR. The product obtained after PCR reaction and its predicted size are given. The line numbers of transformants and their genetic background are given above the gel images.
(b) The expressional level of Sec6 in indicated backgrounds in the absent or presence of β–estradiol treatment verified by quantitative reverse-transcription PCR.

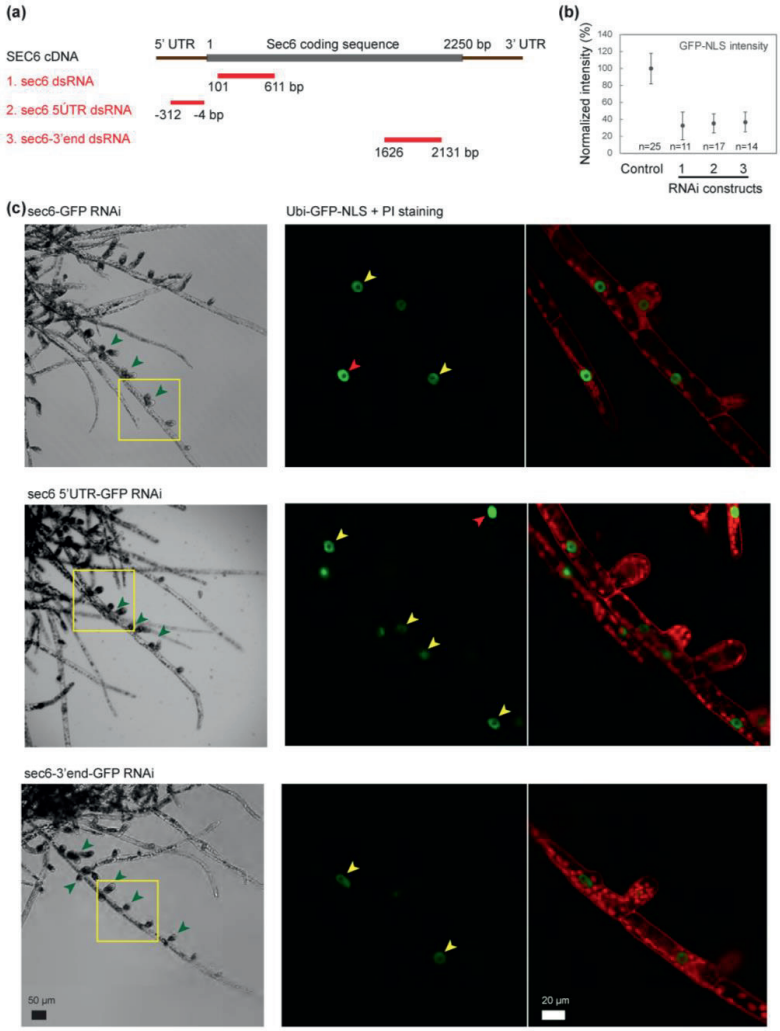

Figure S6. Three independent silencing constructs targeted against different parts of the Sec6 gene show similar defects.

Simultaneous targeting of RNAi against Sec6 and GFP allows using the nuclear GFP signal as a visual marker to assess silencing efficiency. We failed to obtain fully silenced plants, as previously reported by Van Gisbergen et al. (2018). However, in partially silenced tissues, all three Sec6-directed RNAi fragments cause excessive branching and defects in the polar growth of newly formed branches. The defects in polar growth partially resemble the defects observed in the inducible Sec6 RNAi line (Fig. S4).

(a) Schematic representation of the RNAi target sites in the Sec6 locus.

(b) Quantification of the NLS-GFP signal in partially silenced Sec6 RNAi tissue fragments. The numbers of the RNAi constructs correspond to the numbers in a.

(c) Partially silenced fragments of all three RNAi lines show excessive branching and swollen branch cells (green arrowheads). The yellow square is enlarged in the right panels. Yellow arrowheads indicated nuclei in which the NLS-GFP signal was partially silenced and red arrowheads indicate nuclei where silencing was absent.

Supplemental Tables

Table S1 – Primers used in this study

Primer	Use	Sequence (5' > 3')	RE site
HT23	Cloning of SEC6 left targeting arm	CGG GGTACC CCGACTTCTTACCCAGGTTTG	*KpnI*
HT24	Cloning of SEC6 left targeting arm	ACCG CTCGAG CTTCCTTCCTGGCCTGTATTTTGC	*XhoI*
HT03	Cloning of SEC6 right targeting arm	AAAACTAGTCGAGAGAAGGAAATAGTGTTATGAC	*SpeI*
HT04	Cloning of SEC6 right targeting arm	AAAGCGGCCGCGATGACTACAGAATCCCGATTAGC	*NotI*
HT11	Cloning of SEC3a left targeting arm	ACCG CTCGAG GTGCTGAAGTCAAATTTGCTGATTG	*XhoI*
HT12	Cloning of SEC3a left targeting arm	AAA GATATC GAAAATGAAGTTCTTGAAGATTTCTTTCATCTC	*EcoRV*
HT13	Cloning of SEC3a right targeting arm	ACG GGATCC GGGGTAGGTTGTAGAATGATGGTC	*BamHI*
HT14	Cloning of SEC3a right targeting arm	AGAA GCGGCCGC GGTTGACTTAATACAAAGAGTCTACATCCC	*NotI*
EO9	Cloning of SEC5b left targeting arm	TCTGGTACCGGCCATCAAATCTCTCGTGGAAGC	*KpnI*
EO10	Cloning of SEC5b left targeting arm	TGCGGGCCCTCTCAAGTCATCGTTATCTACATAGGCG	*ApaI*
EO11	Cloning of SEC5b right targeting arm	TCGACCGGTTTTAGTGCGACGCCGTGCG	*AgeI*
EO12	Cloning of SEC5b right targeting arm	TCCCGAGCGGCCGCCACAAGGCATGTGGGCCAAGC	*NotI*
EO1	Cloning of SEC5d left targeting arm	TCAGGTACCTGCCGATTGTGTGGTTGCTTTG	*KpnI*
EO2	Cloning of SEC5d left targeting arm	CGCCGTATCGATTCTCAACTCATCGTTATCTACATAAAT TTGAGGG	*ClaI*
EO3	Cloning of SEC5d right targeting arm	TCTACCGGTCAAGAATTGAAGGCCTCACAGGG	*AgeI*
EO4	Cloning of SEC5d right targeting arm	GGACCCGGGCCGGTGCATCCGACTTTGCTG	*SmaI*
JK277	Cloning of KEULE left targeting arm	ACGCGGGCCCTGTAGGTTGCAGTTACGATGTGG	*ApaI*
JK278	Cloning of KEULE left targeting arm	ACGCGTCGACAAAGTCGTCCATCTCTAATTTGCC	*SalI*
JK279	Cloning of KEULE right targeting arm	CGGGATCCGAAGGAGCACGAAGGAATTTTTGG	*BamHI*
JK280	Cloning of KEULE right targeting arm	CGCGAGCTCGTAAATTGACACTCGGGCAAGTGC	*SacI*
HT98	Cloning of SEC6 RNAi fragment/RNAi genotyping	CACC CAGATCTGACTACGCCTTGC	
HT88	Cloning of SEC6 RNAi fragment/RNAi genotyping	CTATCTTTGGCGAGGTGGAA	
HT120	Cloning of KEULE RNAi fragment/RNAi genotyping	CACC CAGCTAGCGAAGTTGAGTGAT	
HT121	Cloning of KEULE RNAi fragment/RNAi genotyping	TCA ATCACTGACGGCATGCCTC	
HT122	Cloning of SEC6 coding sequence for Y2H	CACC ATGATGATGCATGATGCTGGC	
HT123	Cloning of SEC6 coding sequence for Y2H	TCA CTTCCTTCCTGGCCTG	
HT118	Cloning of KEULE coding sequence for Y2H	CACC ATGGATTCCTCGCACGGTTC	
HT119	Cloning of KEULE coding sequence for Y2H	TCA AAAGTCGTCCATCTCTAATT	
HT120	Cloning of KEULE-C1 coding sequence for Y2H	CACC CAGCTAGCGAAGTTGAGTGAT	
HT121	Cloning of KEULE-C1 coding sequence for Y2H	TCA ATCACTGACGGCATGCCTC	
HT124	Cloning of SMAP65a coding sequence for Y2H	CACC ATGGGCCAGCAACCTGGA	
HT125	Cloning of SMAP65a coding sequence for Y2H	TTA CGCGTCGATACAGGGAAC	
HT126	Cloning of MAP65c coding sequence for Y2H	CACC ATGGGTCAGCAACCTGTTGTC	
HT127	Cloning of MAP65c coding sequence for Y2H	TCA GCTGTTCATGCTTTTCCA	

HT57	SEC6 GFP/mCherry tagging genotyping	GCAGGTATGTGGAAGAGAGA	
HT86	SEC6 GFP/mCherry tagging genotyping	CTCTTTACGAGAGGCGACAA	
HT69	SEC3a GFP tagging genotyping	GGCTCGCTACTATCAACAAGCTAG	
HT70	SEC3a GFP tagging genotyping	CCCATTACTCATTGAAATTCAAATCAAAAACTG	
HT71	SEC3b GFP tagging genotyping	tgttggcaaagaacgacgcc	
HT72	SEC3b GFP tagging genotyping	TCTTGTGGGTGGAAATTGGAGGG	
HT73	SEC3c GFP tagging genotyping	tgaattaggataaacttcctccaaggag	
HT74	SEC3c GFP tagging genotyping	cttcaacatgccacctctaatgattattaacc	
HT61	SEC5a GFP tagging genotyping	TAGGGCATACGAGGAGCAGT	
HT62	SEC5a GFP tagging genotyping	GCGAACTGTGTTCAGCATGT	
HT63	SEC5b GFP tagging genotyping	CACTCATGCGGAGGTTAGCA	
HT64	SEC5b GFP tagging genotyping	CTCAGTGGTTGGTCCTTGTT	
HT67	SEC5d GFP tagging genotyping	TGTGCGTCTTTTGGCGGATT	
HT68	SEC5d GFP tagging genotyping	GAATGCTATGTGCAAGCGGA	
JK164	MAP65c Citrine tagging genotyping	ACTCCTTGACCGCTTGCTTCC	
JK202	MAP65c Citrine tagging genotyping	CGTCCAAACGCTGGCTACAAGG	
HT163	KEULE GFP tagging genotyping left arm_Forward	CACGATCAGGCTAAACGAC	
HT164	KEULE GFP tagging genotyping right arm_Reverse	ACTTTTTTCTCATGCGTAC	
JK219	SCAMP4 mCherry tagging genotyping left arm_Forward	TAGCGTTCTGAGGTTCGGGTGG	
JK220	SCAMP4 mCherry tagging genotyping_right arm_Reverse	GTGATCAACGTGGGATTAAAGAAGTCAC	
JK129	mCherry upstream_Reverse (primer_5 in S3)	CCCTTGGTCACCTTCAGCTTGG	
JK112	GFP upstream_Reverse (primer_3 in S3)	GCCGGACACGCTGAACTTGTG	
JK114	Downstream of resistance cassette_Forward (primer_4 and 6 in S3)	ACTCAAGAGGATAAAACCTCACC	
HT159	SEC6 5'UTR qPCR_Forward	CTCTCTCTCGGTGCAAACTATTC	
HT160	SEC6 5'UTR qPCR_Reverse	CCGATCAAATTTCCAACGCATC	
HT161	KEULE 5'UTR qPCR_Forward	GTCTCTGGATCCACAACATCTG	
HT162	KEULE 5'UTR qPCR_Reverse	GACCTCGTTACACTGCCTTAAA	
HT213	Sec6_cds3'_RNAi_F	CACC GCCCTGTCGCAGGCCG	
HT214	Sec6_cds3'_RNAi_R	CTTCTTTGGCGTCTTTCTTTGGGATATC	
HT209	Sec6_5'UTR_RNAi_F	CACC CTCTCTCTCGGTGCAAACTATTCTG	
HT212	Sec6_5'UTR_RNAi_R2	GCTCCGAACTGCTCACACACC	

Table S2 – Plasmids used in this study

Plasmid	Usage
SEC6-GFP	C-terminal GFP tagging of SEC6
SEC3a-GFP	C-terminal GFP tagging of SEC3a
SEC3b-GFP	C-terminal GFP tagging of SEC3b
SEC3c-GFP	C-terminal GFP tagging of SEC3c
SEC5a-GFP	C-terminal GFP tagging of SEC5a
SEC5b-GFP	C-terminal GFP tagging of SEC5b
SEC5d-GFP	C-terminal GFP tagging of SEC5d
SEC6-mCherry	C-terminal mCherry tagging of SEC6
SCAMP4-mCmerry	C-terminal mCherry tagging of SCAMP4
MAP65c-Citrine	C-terminal Citrine tagging of MAP65c
SEC6 RNAi	Inducible knock down of SEC6
MAP65 RNAi	Inducible knock down of MAP65
pDEST22-SEC6	Yeast-2-Hybrid
pDEST22-KEULE	Yeast-2-Hybrid
pDEST22-KEULE-C1	Yeast-2-Hybrid
pDEST32-SEC6	Yeast-2-Hybrid
pDEST32-KEULE	Yeast-2-Hybrid
pDEST32-KEULE-C1	Yeast-2-Hybrid
KEULE-GFP	C-terminal GFP tagging of KEULE
pUGGi_sec6_RNAi	transient knockdkwon of SEC6
pUGGi_sec6_3'end_RNAi	transient knockdkwon of SEC6
pUGGi_sec6_5'UTR_RNAi	transient knockdkwon of SEC6

Table S3 – Summary of *P. patens* strains and their usage throughout this study

Name	Experimental use	Main clone	Background strain	Plasmid transformed	Figures	Video	Reference
SEC6-GFP	Exocyst/FM4-64 colocalization	#37	WT	SEC6-GFP	1		This study
SEC3a-GFP	Exocyst/FM4-64 colocalization	#15	WT	SEC3a-GFP	S1		This study
SEC3b-GFP	Exocyst/FM4-64 colocalization	#96	WT	SEC3b-GFP	S1		This study
SEC3c-GFP	Exocyst on tip cell	#5	WT	SEC3c-GFP	S1		This study
SEC5a-GFP	Exocyst/FM4-64 colocalization	#88	WT	SEC5a-GFP	S1		This study
SEC5b-GFP	Exocyst on tip cell	#70	WT	SEC5b-GFP	S1		This study
SEC5d-GFP	Exocyst on tip cell	#31	WT	SEC5d-GFP	S1		This study
KEULE-GFP	Exocyst/FM4-64 colocalization	#1	WT	KEULE-GFP	6		This study
SEC6-mCherry	background line for double labeling	#2	WT	SEC6-mCherry	5		This study
SEC6-GFP / mCherry-Tua1	Exocyst/phragmoplast colocalization	#92	EF1-mCherry-Tua1	SEC6-GFP	1,2,4		K. Kosetsu
SEC3a-GFP/mCherry-Tua1	Exocyst/phragmoplast colocalization	#57	EF1-mCherry-Tua1	SEC3a-GFP	1,2		K. Kosetsu
SEC5b-GFP/mCherry-Tua1	Exocyst/phragmoplast colocalization	#2	EF1-mCherry-Tua1	SEC5b-GFP	1,2		K. Kosetsu
SEC5d-GFP/mCherry-Tua1	Exocyst/phragmoplast colocalization	#48	EF1-mCherry-Tua1	SEC5d-GFP	1,2		K. Kosetsu
KEULE-GFP/mCherry-Tua1	SM/phragmoplast colocalization	#2	EF1-mCherry-Tua1	KEULE-GFP	1,2		K. Kosetsu
SEC6-mCherry/KEULE-GFP	SM/exocyst colocalization	#9	SEC6-mCherry	KEULE-GFP	5		This study
SEC6-mCherry/SEC3a-GFP	SEC6/SEC3a colocalization	#9	SEC6-mCherry	SEC3a-GFP	/		This study
Sec6-GFP/SCAMP4-mCherry	background line for RNAi anaylsis	#2	SEC6-GFP	SCAMP4-mCherry	/		This study
GFP-tua1/SCAMP4-mCherry	Phragmoplast/cell plate membrane colocalization	#2	GFP-Tua1	SCAMP4-mCherry	1,2		(Hiwatashi et al., 2008)
SEC6-mCherry/MAP65c-Citrine	SEC6/overlap colocalization	#1	SEC6-mCherry	MAP65c-Citrine	3		This study
SEC6-mCherry/MAP65a-Citrine/Kif4-Ic-KO	SEC6/overlap colocalization in Kif4-Ic-KO	#223	KIF4-Ic-KO/ MAP65a-Citrine	SEC6-mCherry	3		This study
SEC6 RNAi/KEULE-GFP/mCherry-Tua1	Intensity analysis of KEULE-GFP in SEC6 RNAi	#4	KEULE-GFP/mCherry-Tua1	SEC6 RNAi	6		This study
SEC6 RNAi/GFP-tua1/SCAMP4-mCherry	Intensity analysis of SCAMP4-mCherry in SEC6 RNAi	#1	GFP-tua1/SCAMP4-mCherry	SEC6 RNAi	6		This study
SEC6 RNAi/SEC6-GFP/SCAMP4-mCherry	Phenotypic analysis of SEC6 RNAi	#6	SEC6-GFP/SCAMP4-mCherry	SEC6 RNAi	6		This study
MAP65 RNAi/SEC6-GFP/mCherry-Tua1	SEC6 localization in MAP65 RNAi	#15	SEC6-GFP/mCherry-Tua1	MAP65 RNAi	4		This study
SEC6 RNAi/Ubi-GFP-NLS4/SNAP-mCherry	transient tranformation of sec6 RNAi	N/A	Ubi-GFP-NLS4 /SNAP-mCherry	SEC6 RNAi	S6		This study

References

Assaad, F.F., Mayer, U., Wanner, G. and Jürgens, G. (1996). The KEULE gene is involved in cytokinesis in Arabidopsis. *Molecular & General Genetics*, 253, 267–277.

Bloch, D., Pleskot, R., Pejchar, P., Potocký, M., Trpkošová, P., Cwiklik, L., Vukašinović, N., Sternberg, H., Yalovsky, S. and Žárský, V. (2016). Exocyst SEC3 and phosphoinositides define sites of exocytosis in pollen tube initiation and growth. *Plant Physiol.* **172**, 980-1002.

Boruc, J. and Van Damme, D. (2015). Endomembrane trafficking overarching cell plate formation. *Current Opinion in Plant Biology*, **28**, 92–98.

Bodemann, B.O., Orvedahl, A., Cheng, T., Ram, R.R., Ou, Y.-H., Formstecher, E., Maiti, M., Hazelett, C.C., Wauson, E.M., Balakireva, M., Camonis, J.H., Yeaman, C., Levine, B. and White, M.A. (2011). RalB and the exocyst mediate the cellular starvation response by direct activation of autophagosome assembly. *Cell* **144**, 253–267.

Boyd, C., Hughes, T., Pypaert, M. and Novick, P. (2004). Vesicles carry most exocyst subunits to exocytic sites marked by the remaining two subunits, Sec3p and Exo70p. *J Cell Biol.* **167**, 889-901.

Buschmann, H. and Zachgo, S. (2016). The evolution of cell division: From streptophytealgae to land plants. *Trends in Plant Science* 21, 872–883.

Cvrčková, F., Grunt, M., Bezvoda, R., Hála, M., Kulich, I., Rawat, A. and Zárský, V. (2012). Evolution of the land plant exocyst complexes. *Frontiers in Plant Science* **3**, 159.

Van Damme, D. (2009). Division plane determination during plant somatic cytokinesis. *Current Opinion in Plant Biology* **12**, 745–751.

Drakakaki, G., van de Ven, W., Pan, S., Miao, Y., Wang, J., Keinath, N.F., Weatherly, B., Jiang, L., Schumacher, K., Hicks, G. and Raikhel, N. (2012). Isolation and proteomic analysis of the SYP61 compartment reveal its role in exocytic trafficking in Arabidopsis. *Cell Research* **22**, 413–424.

Drakakaki, G. (2015). Polysaccharide deposition during cytokinesis: Challenges and future perspectives. *Plant Science* **236**, 177–184.

Dubuke, M.L., Maniatis, S., Shaffer, S.A. and Munson, M. (2015). The exocyst subunit Sec6 interacts with assembled exocytic SNARE complexes. *Journal of Biological Chemistry* **290**, 28245–28256.

Fendrych, M., Synek, L., Pecenková, T., Toupalová, H., Cole, R., Drdová, E., Nebesárová, J., Sedinová, M., Hála, M., Fowler, J.E. and Zársky, V. (2010). The Arabidopsis exocyst complex is involved in cytokinesis and cell plate maturation. *The Plant Cell*, **22**, 3053–3065.

Fendrych, M., Synek, L., Pecenková, T., Drdová, E.J., Sekeres, J., de Rycke, R., Nowack, M.K. and Zársky, V. (2013). Visualization of the exocyst complex dynamics at the plasma membrane of Arabidopsis thaliana. *Mol Biol Cell.* **24**, 510-520.

Garcia-España, A., Mares, R., Sun, T.T. and Desalle, R. (2009). Intron evolution: Testing hypotheses of intron evolution using the phylogenomics of tetraspanins. *PLoS one* **4**, e4680.

Grosshans, B.L., Ortiz, D. and Novick, P. (2006). Rabs and their effectors: achieving specificity in membrane traffic. *Proceedings of the National Academy of Sciences of the United States of America* **103**, 11821–11827.

Gromley, A., Yeaman, C., Rosa, J., Redick, S., Chen, C.T., Mirabelle, S., Guha, M., Sillibourne, J. and Doxsey, S.J. (2005). Centriolin anchoring of exocyst and SNARE complexes at the midbody is required for secretory-vesicle-mediated abscission. *Cell* **123**, 75-87.

Hála, M., Cole, R., Synek, L., Drdová, E., Pecenková, T., Nordheim, A., Lamkemeyer, T., Madlung, J., Hochholdinger, F., Fowler, J.E. and Zárský, V. (2008). An exocyst complex functions in plant cell growth in Arabidopsis and tobacco. *Plant Cell* **20**, 1330–1345.

Hashizume, K., Cheng, Y.S., Hutton, J.L., Chiu, C.H. and Carr, C.M. (2009). Yeast Sec1p functions before and after vesicle docking. *Molecular Biology of the Cell* **20**, 4673–4685.

Hazuka, C.D., Foletti, D.L., Hsu, S.C., Kee, Y., Hopf, F.W. and Scheller, R.H. (1999). The sec6/8 complex is located at neurite outgrowth and axonal synapse-assembly domains. *J. Neurosci.* **19,** 1324–1334.

He, B. and Guo, W. (2009). The exocyst complex in polarized exocytosis. *Curr. Opin.Cell Biol.* **21**, 537–542.

Heider, M.R., Gu, M., Duffy, C.M., Mirza, A.M., Marcotte, L.L., Walls, A.C., Farrall, N., Hakhverdyan, Z., Field, M.C., Rout, M.P., Frost, A. and Munson, M. (2016). Subunit connectivity, assembly determinants and architecture of the yeast exocyst complex. *Nature Structural & Molecular Biology*, **23**, 59–66.

Hiwatashi, Y., Obara, M., Sato, Y., Fujita, T., Murata, T. and Hasebe, M. (2008). Kinesins are indispensable for interdigitation of phragmoplast microtubules in the moss *Physcomitrella patens*. *The Plant Cell* **20**, 3094–3106.

Ho, C.M., Hotta, T., Guo, F., Roberson, R.W., Lee, Y.R. and Liu, B. (2011). Interaction of antiparallel microtubules in the phragmoplast is mediated by the microtubule-associated protein MAP65-3 in Arabidopsis. *Plant Cell* **23**, 2909–2923.

Hong, W. and Lev, S., 2014. Tethering the assembly of SNARE complexes. *Trends in Cell Biology*, 24(1), pp.35–43.

Hu, C.K., Coughlin, M., and Mitchison, T.J. (2012). Midbody assembly and its regulation during cytokinesis. *Molecular biology of the cell* **23**, 1024-1034.

James, P., Halladay, J. and Craig, E.A. (1996). Genomic libraries and a host strain designed for highly efficient two-hybrid selection in yeast. *Genetics* **144**, 1425–1436.

Javelle, M., Klein-Cosson, C., Vernoud, V., Boltz, V., Maher, C., Timmermans, M., Depège-Fargeix, N. and Rogowsky, P.M. (2011). Genome-wide characterization of the HD-ZIP IV transcription factor family in maize: Preferential expression in the epidermis. *Plant Physiology* **157**, 790–803.

Jürgens, G., Park, M., Richter, S., Touihri, S., Krause, C., El Kasmi, F. and Mayer, U. (2015). Plant cytokinesis: a tale of membrane traffic and fusion. *Biochemical Society Transactions* **43**, 73–78.

Karnahl, M., Park, M., Mayer, U., Hiller, U. and Jürgens, G. (2017). ER assembly of SNARE complexes mediating formation of partitioning membrane in Arabidopsis cytokinesis. *eLife* **6**, e25327.

de Keijzer, J. Kieft, H., Ketelaar, T., Goshima, G. and Janson, M.E. (2017). Shortening of microtubule overlap regions defines membrane delivery sites during plant cytokinesis. *Current Biology* **27**, 514–520.

Kosetsu, K., de Keijzer, J., Janson, M.E. and Goshima, G. (2013). MICROTUBULE-ASSOCIATED PROTEIN65 is essential for maintenance of phragmoplast bipolarity and formation of the cell plate in *Physcomitrella patens*. *Plant Cell* **25**, 4479–4492.

Koumandou, V.L., Dacks, J.B., Coulson, R.M. and Field, M.C. (2007). Control systems for membrane fusion in the ancestral eukaryote; evolution of tethering complexes and SM proteins. *BMC Evolutionary Biology* **7**, 29.

Kulich, I., Pečenková, T., Sekereš, J., Smetana, O., Fendrych, M., Foissner, I., Höftberger, M. and

Zárský, V. (2013). Arabidopsis Exocyst Subcomplex Containing Subunit EXO70B1 Is Involved in Autophagy-Related Transport to the Vacuole. *Traffic* **14**, 1155-1165.

Liu, Q., Liu, F., Yu, K.L., Tas, R., Grigoriev, I., Remmelzwaal, S., Serra-Marques, A., Kapitein, L. C., Heck, A. J. R. and Akhmanova, A. (2016). MICAL3 flavoprotein monooxygenase forms a complex with centralspindlin and regulates cytokinesis. *J. Biol. Chem.* **291**, 20617-20629.

Luo, G., Zhang, J., and Guo, W. (2014). The role of Sec3p in secretory vesicle targeting and exocyst complex assembly. *Molecular Biology of the Cell* 25, 3813-3822.

Mcmichael, C.M. and Bednarek, S.Y. (2013). Cytoskeletal and membrane dynamics during higher plant cytokinesis. *New Phytologist* **197**, 1039–1057.

Morgera, F., Sallah, M.R., Dubuke, M.L., Gandhi, P., Brewer, D.N., Carr, C.M. and Munson, M. (2012). Regulation of exocytosis by the exocyst subunit Sec6 and the SM protein Sec1. *Molecular Biology of the Cell* **23**, 337–346.

Müller, S. and Jürgens, G. (2015). Plant cytokinesis - No ring, no constriction but centrifugal construction of the partitioning membrane. *Seminars in Cell and Developmental Biology* **53**, 10–18.

Müller, S., Wright, A.J. and Smith, L.G. (2009). Division plane control in plants: new players in the band. *Trends in Cell Biology*, 19(4), pp.180–188.

Nakaoka, Y., Miki, T., Fujioka, R., Uehara, R., Tomioka, A., Obuse, C., Kubo, M., Hiwatashi, Y. and Goshima, G. (2012). An inducible RNA interference system in *Physcomitrella patens* reveals a dominant role of augmin in phragmoplast microtubule generation. *Plant Cell* **24**, 1478-1493.

Neto, H. and Gould, G.W. (2011). The regulation of abscission by multi-protein complexes. *J Cell Sci* **124**, 3199-3207.

Nishiyama, T., Hiwatashi, Y., Sakakibara, I., Kato, M. and Hasebe, M. (2000). Tagged mutagenesis and gene-trap in the moss, *Physcomitrella patens* by shuttle mutagenesis. *DNA Research* **7**, 9–17.

Oda, Y., Iida, Y., Nagashima, Y., Sugiyama, Y. and Fukuda, H. (2015). Novel coiled-coil proteins regulate exocyst association with cortical microtubules in xylem cells via the conserved oligomeric golgi-complex 2 protein. *Plant Cell Physiol.* **56**, 277-286

Ortiz-Ramírez, C., Hernandez-Coronado, M., Thamm, A., Catarino, B., Wang, M., Dolan, L., Feijó, J.A. and Becker, J.D. (2016). A transcriptome atlas of *Physcomitrella patens* provides insights into the evolution and development of land plants. *Molecular Plant* **9**, 205–220.

Park, M., Touihri, S., Müller, I., Mayer, U. and Jürgens, G. (2012). Sec1/Munc18 protein stabilizes fusion-competent syntaxin for membrane fusion in Arabidopsis cytokinesis. *Developmental Cell* **22**, 989–1000.

Paumet, F., Rahimian, V. and Rothman, J.E. (2004). The specificity of SNARE-dependent fusion is encoded in the SNARE motif. *Proceedings of the National Academy of Sciences of the United States of America Sciences* **101**, 3376–3380.

Picco, A., Irastorza-Azcarate, I., Specht, T., Böke, D., Pazos, I., Rivier-Cordey, A.-S., Devos, D.P., Kaksonen, M., and Gallego, O. (2017) The in vivo architecture of the exocyst provides structural basis for exocytosis. *Cell* **168**, 400–412.

Qi, X., Kaneda, M., Chen, J., Geitmann, A. and Zheng, H. (2011). A specific role for Arabidopsis TRAPPII in post-Golgi trafficking that is crucial for cytokinesis and cell polarity. *The Plant Journal* **68**, 234–248.

Rawat, A., Brejšková, L., Hála, M., Cvrčková, F. and Žárský, V. (2017). The *Physcomitrella patens*

exocyst subunit EXO70.3d has distinct roles in growth and development, and is essential for completion of the moss life cycle. *New Phytologist* **216**, 438-454.

Rensing, S.A. Fritzowsky, D., Lang, D., Reski, R. (2005). Protein encoding genes in an ancient plant: analysis of codon usage, retained genes and splice sites in a moss, *Physcomitrella patens*. *BMC Genomics* **6**, 43.

Richter, S., Kientz, M., Brumm, S., Nielsen, M.E., Park, M., Gavidia, R., Krause, C., Voss, U., Beckmann, H., Mayer, U., Stierhof, Y.D. and Jürgens, G. (2014). Delivery of endocytosed proteins to the cell-division plane requires change of pathway from recycling to secretion. *eLife* B, e02131.

Rogozin, I.B., Wolf, Y.I., Sorokin, A.V., Mirkin, B.G. and Koonin, E.V. (2003). Remarkable interkingdom conservation of intron positions and massive, lineage-specific intron loss and gain in eukaryotic evolution. *Current Biology* **13**, 1512–1517.

Rybak, K., Steiner, A., Synek, L., Klaeger, S., Kulich, I., Facher, E., Wanner, G., Kuster, B., Žárský, V., Persson, S. and Assaad, F.F. (2014). Plant cytokinesis is orchestrated by the sequential action of the TRAPPII and exocyst tethering complexes. *Developmental Cell* **29**, 607–620.

Schaefer, E., Belcram, K., Uyttewaal, M., Duroc, Y., Goussot, M., Legland, D., Laruelle. E., de Tauzia-Moreau, M.L., Pastuglia, M. and Bouchez, D. (2017). The preprophase band of microtubules controls the robustness of division orientation in plants. *Science* **356,** 186-189.

Schindelin, J., Arganda-Carreras, I., Frise, E., Kaynig, V., Longair, M., Pietzsch, T., Preibisch, S., Rueden, C., Saalfeld, S., Schmid, B., Tinevez, J.Y., White, D.J., Hartenstein, V., Eliceiri, K., Tomancak, P. and Cardona, A. (2012). Fiji: an open-source platform for biological-image analysis. *Nature Methods* **9**, 676-682.

Schmiedel, G., Reiss, H.D. and Schnepf, E. (1981). Associations between membranes and microtubules during mitosis and cytokinesis in caulonema tip cells of the moss Funaria hygrometrica. *Protoplasma* **108**, 173–190.

Seguí-Simarro, J.M., Austin, J.R. 2nd, White, E.A. and Staehelin, L.A. (2004). Electron tomographic analysis of somatic cell plate formation in meristematic cells of Arabidopsis preserved by high-pressure freezing. *Plant Cell* **16**, 836-856

Sivaram, M.V.S., Saporita, J.A., Furgason, M.L., Boettcher, A.J. and Munson, M. (2005). Dimerization of the exocyst protein Sec6p and its interaction with the t-SNARE Sec9p. *Biochemistry* **44**, 6302–6211.

Sivaram, M.V.S., Furgason, M.L., Brewer, D.N. and Munson, M. (2006). The structure of the exocyst subunit Sec6p defines a conserved architecture with diverse roles. *Nature Structural & Molecular Biology* **13**, 555–556.

Smertenko, A., Assaad, F., Baluška, F., Bezanilla, M., Buschmann, H., Drakakaki, G., Hauser, M.T., Janson, M., Mineyuki, Y., Moore, I., Müller, S., Murata, T., Otegui, M.S., Panteris, E., Rasmussen, C., Schmit, A.C., Šamaj, J., Samuels, L., Staehelin, L.A., van Damme, D., Wasteneys, G. and Žárský, V. (2017). Plant cytokinesis: terminology for structures and processes. *Trends in cell biology* **27,** 885-894

Söllner, T., Whiteheart, S.W., Brunner, M., Erdjument-Bromage, H., Geromanos, S., Tempst, P. and Rothman, J.E. (1993). SNAP receptors implicated in vesicle targeting and fusion. *Nature* **362**, 318–324.

Steiner, A., Müller, L., Rybak, K., Vodermaier, V., Facher, E., Thellmann, M., Ravikumar, R., Wanner, G., Hauser, M.T. and Assaad, F.F. (2016). The membrane-associated Sec1/Munc18 KEULE is required for phragmoplast microtubule reorganization during cytokinesis in

Arabidopsis. *Molecular Plant* **9**, 528–540.

Stenmark, H. (2009). Rab GTPases as coordinators of vesicle traffic. *Nature Reviews: Molecular Cell Biology* **10**, 513–525.

Stöckle, D., Herrmann, A., Lipka, E., Lauster, T., Gavidia, R., Zimmermann, S. and Müller, S. (2016). Putative RopGAPs impact division plane selection and interact with kinesin-12 POK1. *Nature Plants* 2, 16120.

Südhof, T.C. and Rothman, J.E. (2009). Membrane fusion: grappling with SNARE and SM proteins. *Science* **323**, 474–477.

Synek, L., Vukašinović, N., Kulich,I., Hála, M., Aldorfová, K., Fendrych, M. and Žárský, V. (2017). EXO70C2 Is a Key Regulatory Factor for Optimal Tip Growth of Pollen. *Plant Physiology* **174**, 223-240.

TerBush, D.R. and Novick, P. (1995). Sec6, Sec8, and Sec15 are components of a multisubunit complex which localizes to small bud tips in Saccharomyces cerevisiae. *J. Cell Biol* **130,** 299–312.

Thellmann, M., Rybak, K., Thiele, K., Wanner, G. and Assaad, F.F. (2010). Tethering factors required for cytokinesis in Arabidopsis.*Plant Physiology* **154**, 720–732.

Vukašinović, N. and Žárský, V. (2016). Tethering complexes in the Arabidopsis endomembrane system. *Frontiers in Cell and Developmental Biology* 4, 46.

van Gisbergen, P.A., Wu, S.Z., Chang, M., Pattavina, K.A., Bartlett, M.E., and Bezanilla, M. (2018). An ancient Sec10–formin fusion provides insights into actin-mediated regulation of exocytosis. *J Cell Biol* 217, 945-957.

Wang, N., Lee, I.J., Rask, G., and Wu, J.Q. (2016). Roles of the TRAPP-II complex and the exocyst in membrane deposition during fission yeast cytokinesis. *PLoS biology* **14**, e1002437.

Wickner, W. and Schekman, R. (2008). Membrane fusion. *Nature Structural & Molecular Biology* **15**, 658–664.

Wu, J., Tan, X., Wu, C., Cao,K., Li, Y. and Bao, Y. (2013). Regulation of cytokinesis by exocyst subunit SEC6 and KEULE in Arabidopsis thaliana. *Molecular Plant* **6**, 1863–1876.

Wu, S.Z., Ritchie, J.A., Pan, A.H., Quatrano, R.S., and Bezanilla, M. (2011). Myosin VIII regulates protonemal patterning and developmental timing in the moss *Physcomitrella patens*. *Molecular plant* **4**, 909-921.

Yamada, M., Miki, T. and Goshima, G. (2016). Imaging mitosis in the moss *Physcomitrella patens*. In P. Chang & R. Ohi, eds. *Methods in Molecular Biology (Clifton, N.J.)*. New York, NY, United States: Springer New York, pp. 263–282.

Yu, I.-M. and Hughson, F.M. (2010). Tethering factors as organizers of intracellular vesicular traffic. *Annual Review of Cell and Developmental Biology* 26, 137–156.

Zhang, Y., Immink, R., Liu, C.M., Emons, A.M. and Ketelaar, T. (2013). The Arabidopsis exocyst subunit SEC3A is essential for embryo development and accumulates in transient puncta at the plasma membrane. *New Phytologist* 199, 74–88.

Zuo, X., Zhang, J., Zhang, Y., Hsu, S.C., Zhou, D. and Guo, W. (2006). Exo70 interacts with the Arp2/3 complex and regulates cell migration. *Nat Cell Biol.* **8**, 1383-1388.

Chapter 3

Geometric cues forecast the switch from 2D-to-3D growth in *Physcomitrella patens*

Han Tang[1,2], Kilian Duijts[2], Magdalena Bezanilla[4], Ben Scheres[1], Joop E.M. Vermeer[3,5], and Viola Willemsen[1]*

[1] Laboratory of Plant Developmental Biology, Wageningen University & Research, Wageningen, The Netherlands
[2] Laboratory of Cell Biology, Wageningen University & Research, Wageningen, The Netherlands
[3] Plant Cell Biology, Department of Plant and Microbial Biology and Zurich-Basel Plant Science Center, University of Zürich, 8008 Zürich, Switzerland
[4] Biological Sciences Department, Dartmouth College, Hanover, NH, USA
[5] Present address: Laboratory of Cell and Molecular Biology, Institute of Biology, University of Neuchâtel, 2000 Neuchâtel, Switzerland

This work is accepted in New Phytologist (2019), in press

Abstract

During land colonization plants acquired a range of body plan adaptations, of which the innovation of three-dimensional (3D) tissues increased organismal complexity and reproductivity. In the moss, *Physcomitrella patens*, a 3D leafy gametophore originates from filamentous cells that grow in a two-dimensional (2D) plane through a series of asymmetric cell divisions. Asymmetric cell divisions that coincide with different cell division planes and growth directions enable the developmental switch from 2D to 3D, but insights into the underlying mechanisms coordinating this switch are still incomplete. Using 2D-, 3D-imaging and image segmentation, we characterized two geometric cues, the width of the initial cell and the angle of the transition division plane, which sufficiently distinguished a gametophore initial cell from a branch initial cell. These identified cues were further confirmed in gametophore formation mutants. The identification of a fluorescent marker allowed us to successfully predict the gametophore initial cell with more than 90% accuracy before morphological changes, supporting our hypothesis that, before the transition division, parental cells of the gametophore initials possess different properties compared to branch initials. Our results suggest that the cell fate decision of the initial cell is determined in the parental cell, prior to the transition division.

Introduction

During plant evolution, the transition to land coincided with the innovation of 3D growth (Graham *et al.*, 2000; Whitewoods *et al.*, 2018), suggesting that the 'escape' from planar growth was a significant step in the colonization of land. The early land plant lineage developed shooting systems that allow them to grow upward and to evolve radially positioned organs, which increase the degree of productivity and complexity. These shooting systems depended on a novel stem cell function that was capable of rotating cell division planes (Harrison *et al.*, 2009). Conversely, the algal sister groups of land plants generally grow as 2D filaments.

In the moss, *Physcomitrella patens*, the main growing tissue is composed of 2D filamentous protonemata cells, from which a 3D gametophore tissue can be formed through a series of asymmetric cell divisions. In the protonema stage, cells grow by tip growth along with the emergence of branches. The transition from 2D to 3D growth is initiated from one asymmetric cell division that generates a new gametophore initial cell from its parental filament at the branching site (Harrison *et al.*, 2009), hereafter referred to as the "transition division" (Fig. **1a**). The branch initial cell elongates by tip cell growth and divides in a horizontal plane, whereas the gametophore initial cell swells and executes a first oblique division. 3D growth commences after this oblique division, which gives rise to one apical stem cell and one basal cell. Two following divisions that occur roughly perpendicular to the oblique division plane result in a tetrahedral apical stem cell, from which a gametophore is established (Whitewoods *et al.*, 2018). Cell swelling and the oblique division are therefore two visible morphological markers of the 3D growth initiation. Approximately 5% of protonema side branches develop into gametophore initial cells (Cove & Knight, 1993; Kofuji & Hasebe, 2014). The coordination of division plane orientations and gametophore cell identity thus plays a vital role during the 2D-to-3D transition. A central question is at what stage the cell fate of gametophore initial instead of side branch initial is determined.

Two plant hormones, auxin and cytokinin, induce the transition from 2D filament to 3D gametophore development (Ashton *et al.*, 1979; Cove *et al.*, 2006). Exogenous application of cytokinin increases the number of emerging early gametophores, while auxin stimulates the formation of early gametophore

in a cytokinin-dependent manner. (Ashton *et al.*, 1979; Prigge & Bezanilla, 2010; Aoyama *et al.*, 2012). Homologs of master regulators of stem cell specification in angiosperms, APETALA2-type transcription factors *PpAPBs*, are indispensable for gametophore formation (Aoyama *et al.*, 2012). Since the orthologous genes to *PpAPBs* in Arabidopsis are essential in stem cell niche formation, cell proliferation and embryogenesis (Elliott *et al.*, 1996; Boutilier *et al.*, 2002; Aida *et al.*, 2004; Galinha *et al.*, 2007), it has been proposed that *PpAPBs* specify gametophore initial cell identity (Aoyama *et al.*, 2012). Persistent APB activity marks the gametophore initial cell, whereas *APB* expression rapidly diminishes in branch protonemal cells. Additionally, mutations in the *NO GAMETOPHORE 1-REFERENCE (Ppnog1-R)* gene causes defects in early gametophore formation (Moody *et al.*, 2018). Deletion of another gene, *DEFECTIVE KERNEL 1 (DEK1),* causes multiple early gametophore initiation events followed by aberrant gametophore development. In addition, it was recently reported that also CLAVATA (CLV) signalling is essential for gametophore initiation, orientation of the first oblique division, development of mature gametophores, and cell proliferation in the gametophore base of *Physcomitrella* (Whitewoods *et al.*, 2018). The cytoskeleton has been reported to play a key role to orient spindle angles during swelling of the gametophore initial cell that ultimately results in the oblique division (Kosetsu *et al.*, 2017). How hormones, regulatory genes such as *PpAPB*s and *CLV*, and the cytoskeleton co-ordinately control asymmetric cell divisions and morphological changes has remained unknown.

In the model plant Arabidopsis multiple early embryonic cells acquire new identities with various cell shapes via a series of asymmetric cell divisions (Scheres *et al.*, 1994; Yoshida *et al.*, 2014). Computational simulation at the early embryo stage indicated that cell shape, cortical microtubules, and auxin effects can be sufficient to predict the orientation of division planes (Chakrabortty *et al.*, 2018). Accumulating evidence implicates regulatory genes, the cytoskeleton and hormones in this process (Boyer & Simon, 2015; Pillitteri *et al.*, 2016), but it is still a challenge to study this process in mechanistic detail in seed plants.

Here, we used the moss *Physcomitrella patens* as a system to investigate the regulation of asymmetric cell divisions. In a previous study, the identity of the gametophore fate was confirmed by the appearance of cell swelling and the oblique division (Harrison *et al.*, 2009). Until now most studies of the transitions from 2D-to-3D growth in moss have focused on the oblique division during gametophore initiation, which occurs well after the transition division (Fig. **1a**). Although it has been proposed that the transition from filamentous to gametophore fate occurs prior to the swelling and oblique division for about a decade (Harrison *et al.*, 2009), no differences between gametophore and branch initial cells before swelling and the oblique division have been reported yet. Here, we performed 2D-imaging and 3D geometric analysis to examine if a gametophore initial cell reveals detectable morphological differences from a branch initial cell within the small time window between the transition division and swelling. Our analysis reveals that a gametophore initial cell possesses significant geometric differences from a branch initial cell, sufficient to predict the gametophore fate with a ~90% accuracy. To verify the gametophore fate prediction, a fluorescent marker was introduced that predicts gametophore cell fate at the initial stage. This feature allowed us to predict the cell fate of the gametophore initial cell before notable swelling with a ~90% accuracy. The high prediction accuracy suggests that the parent cell of a gametophore initial cell possesses different properties from that of a branch initial cell and provides a new tool for mechanistic investigation of the transition from 2D- to 3D-growth in moss.

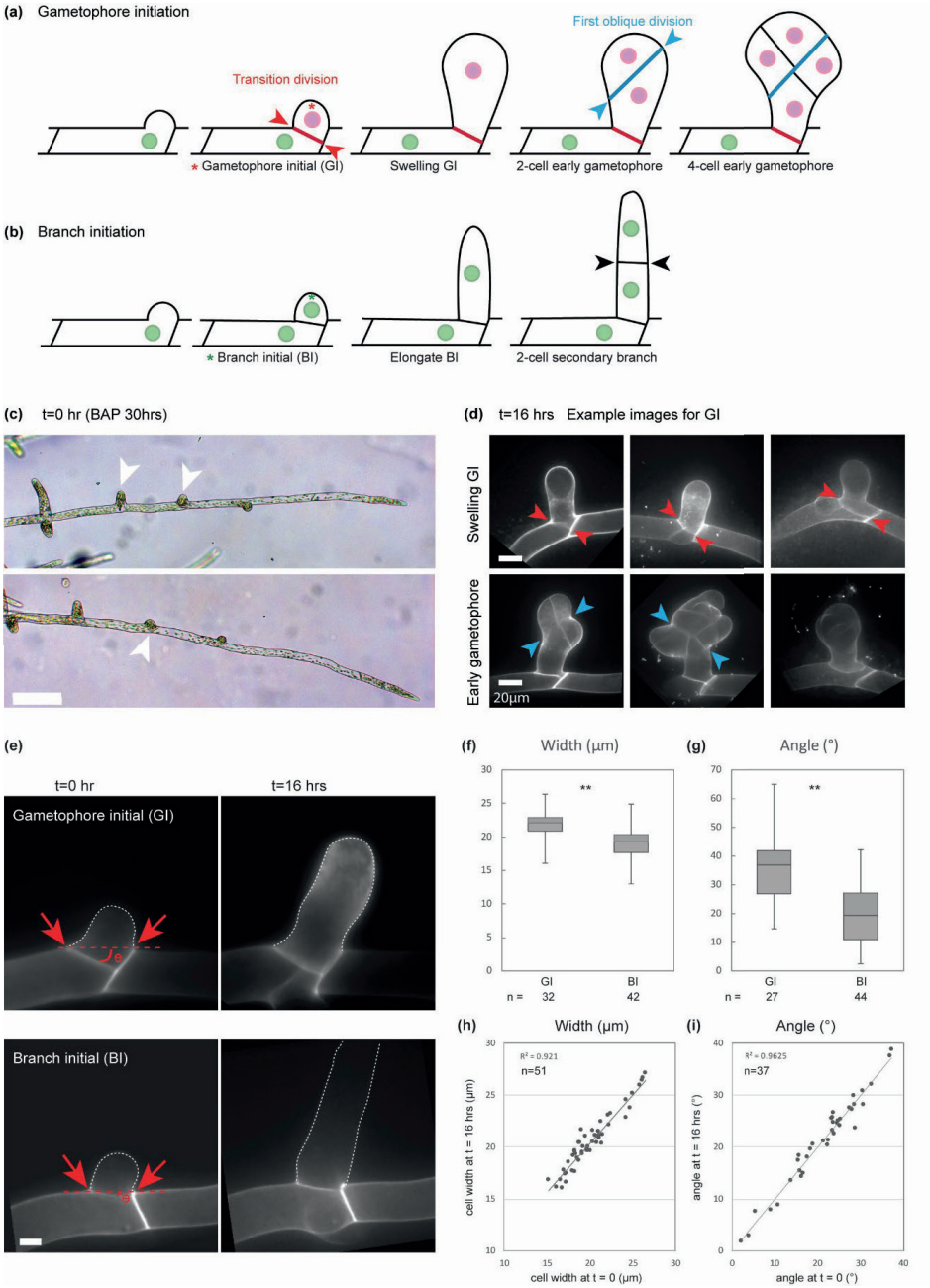

Figure 1. Prior to swelling gametophore initial cells are geometrically distinct from branch initial cells.
(a) Schematic representation of gametophore initiation. The transition division that cleaves a gametophore initial cell and its parental cell is depicted by a red line and red arrowheads; the first oblique division in a swelling gametophore initial cell is shown by a blue line and blue arrowheads. Nucleus of parental cells are indicated in green and for different gametophore stages in pink. The early gametophore is defined from 2-cell until the stage with visible leafy structures.

(b) Schematic representation of branch initiation. The orientation of cell division is perpendicular to cell growth axis as indicated by black arrowheads. Nucleus of parental cells and secondary branch filaments are indicated in green.
(c) Tissue was cultured in imaging dish for 6d, and treated with BAP for 30 hrs to induce gametophore formation. Potential gametophore initial cells were indicated by white arrowheads. Scale bar = 0.1 mm.
(d) Example images of swelling gametophore initials and early gametophores with multiple divisions. The images were captured at t=16 hrs, when cells were treated with BAP for total 46 hrs. The transition division are depicted by red arrowheads; and the first oblique divisions are depicted by blue arrowheads. Scale bar = 20 µm.
(e) Representative images of gametophore and branch initial cells and their future fate after 16 hours. The initial cells were stained with propidium iodide and observed at t=0 by spinning disk microscopy; the same target cells were revisited after 16 hours to confirm their cell fates by cell swelling or elongation.
The projected images were re-orientated such that the parental cell membrane was horizontal. The red arrowheads indicate cell length measured; angle (θ) was measured between horizontal axis depicted by the red dashed lines and the division plane. Scale bar = 10 µm.
(f) and (g) The measurement of the cell width and the angle of division plane as indicated in (a). The number of gametophores and branches collected from three independent experiments was indicated (N=3). The horizontal line in the box denotes the median value of all collected individual cells. ** represents a significant difference (p<0.01) between three means of gametophore and branch datasets using Student's two-tailed t-tests.
(h) The correlation coefficient of cell width and the angle of division plane between time = 0 hr and 16 hrs.

Results

Geometric cues that predict cell fate are visible before transition division

To identify differences between gametophore and branch initial cells before visible swelling, we observed early initial cells right after the transition division (Fig. **1a**). These initial cells were imaged in the presence of the cell outline staining dye propidium iodide (PI), and their ultimate cell fates were examined after overnight recovery in the incubator and tracked by pre-marked positions in the microscope (Fig. **1c,d**). Cell fates were identified by either cell swelling or the oblique division for gametophore initials or tip cell elongation with perpendicular division for branch initials (Fig. **1a,b,d,e**). To investigate whether these observed swollen cells ultimately developed into early gametophores or rather arrest or reverse back to filaments, we tracked swollen initial cells and confirmed their outgrowth into early gametophores with multiple divisions (Fig. **S1a**). We considered a gametophore after the oblique division but before any leafy structure can be seen as an early gametophore (Fig. **1a**). 90-95% swollen gametophore initial cells continually developed into early gametophores with apparent divisions and morphological changes under two growth conditions used in this study (Fig. **S1b**).

Cell fates of gametophore initial cells were confirmed after 16 hrs, which showed that 25% cells displayed swelling characteristic and 75% revealed the oblique division, while none of them exhibited filamentous features (n=32). The width of analysed initial cells and the division plane angle of the transition division often revealed different patterns between gametophore and branch initials. Gametophore initial cells have a wider cell width and a larger division plane angle compared to branch initial cells (Fig. **1f,g**). We quantified these two parameters, and found that gametophore initials have, on average, a cell width of 21.9 µm (sd=0.45, n=32) and division angle of 34.6 degrees (sd=5.0, n=27), the latter ranging from 15 degrees to 65 degrees in our observation. While branch initials revealed an average cell width of 19.7 µm, (sd=0.59, n=42) and an average division angle of 17.7 degrees (sd=1.24, n=44,) (Fig. **1f,g**). Taken together, gametophore and branch initial cells significantly differ with respect to cell width and division angle.

To examine if cell width and division angle change during growth, we measured and compared these two parameters in all initial cells, including gametophore and branch initials, and their descendants by tracking the same cell after overnight recovery. We found that once the initial cell emerged from its parental cell, the cell width and the division angle were almost fixed. We observed an average cell width of 20.2 μm at the early stage and 20.6 μm (n=51) after growing for overnight. The division angles also did not change once the division was completed, since we observed an average division angle of 21.49 degrees before and 21.51 degrees (n=37) after overnight growth (Fig. **1h**), demonstrating that gametophore initials and branch initials are geometrically distinct prior to visible swelling.

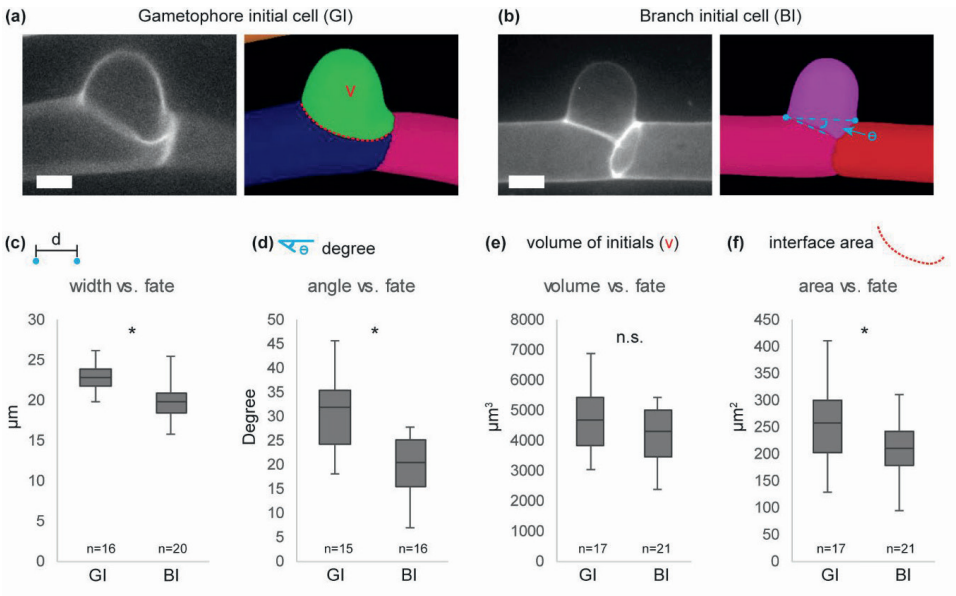

Figure 2. Gametophore and branch initial cells exhibit differences in 3D geometry.
(a) and (b) Representative images of gametophore (a) and branch (b) initial cells and corresponding segmented images obtained from MorphoGraphX. Initial cells were stained with propidium iodide and observed by spinning disk microscopy. Blue dots in (b) indicate the length that was measured; angle (θ) was measured between the horizontal axis and division plane as depicted by blue dashed lines. The red v in (a) stands for volume indication in (e); the red dotted line in (a) demonstrates the interface area for the indication in (f).
(c) to (f) Geometric analysis of gametophore and branch initial cells. Cell fates were verified by revisiting the same cell after 16 hours and confirmed by cell swelling for the gametophore or elongation for the branch.
Cell width between the protruding site of initial cells (c); orientation angle of division plane (d); volume measurement of initial cells (e); the size of interface area (f). The number of gametophore and branch initials collected from three independent experiments was indicated. The horizontal line in the box denotes the median value of all collected individual cells. * represents a significant difference (p<0.05) between three means of gametophore and branch datasets using Student's two-tailed t-tests. GI: gametophore initial cells; BI: branch initial cells.

Gametophore and branch initial cells exhibit differences in 3D geometry

Using 2D imaging, we identified two geometric cues that differ in initial cells that fated either to early gametophore or branch. To confirm that these subtle differences were not an artifact caused by image orientation, we analysed image stacks of initial cells with MorphographX to perform segmentation and volumetric analysis. The future fate confirmation of targeted initial cells was carried out as described above, which showed that after 16 hrs, 24% of gametophore initial cells swollen and 76% cells presented the oblique division, while none of them exhibited filamentous features (n=17). The 3D-reconstructed shape information of initial cells can be viewed from any angle, which allowed us to visualize and measure the cell width and division angle very precisely (Fig. **2a,b**). Measurements acquired from 3D segmented images confirmed the 2D data, and they consistently showed that the base of gametophore initial cells had an average cell width of 22.7 µm (sd=1.69, n=16) and an average division angle of 31.4 degrees (sd=8.46, n=15), while branch initial cells had an average cell width of 19.9 µm (sd=2.23, n=20) and an average division angle of 19.8 degrees (sd=6.65, n=16) (Fig. **2c,d**).

To examine whether initial cells fated to become gametophores or branches exhibited differences in cell volume or the area of the division plane connecting to the parental cell, we obtained volumetric information and quantified the interface area from the 3D analysis. To avoid variation in volume due to cell length of chosen cells, all the images of initial cells were taken 30hrs after BAP induction, which was used to synchronize gametophore induction. Secondly, only initial cells with longitudinal lengths between 15 to 30 µm were chosen. No visible differences in cell length between chosen initial cells of early gametophores and branches were detected as shown in Fig. **S2**, indicating that the comparisons of the cell volumes were unbiased between gametophore and branch initial cells. While, the cell volumes of gametophore initials were on average 4697.2 μm^3 (n=17) and branch initials on average 4159.4 μm^3 (n=21) and did not show a significant difference, the average size of the interface area in branch initials was about 211.3 μm^2, which is significantly smaller than the average 259.4 μm^2 observed in gametophore initial cells (n=17/21 for gametophore/branch, p=0.02, 2-tailed t-test) (Fig. **2e,f**). The larger size of the interface area in gametophore initial cells likely results from the aforementioned wider cell width and greater division angle.

Geometric cues in gametophore initial cells are independent of exogenously supplied cytokinin and consistent in gametophore mutants

Under standard growth conditions it is challenging to investigate fate transitions since only ~5% of emerging branching cells ultimately commit to gametophore fate. Therefore, similar to other studies focused on gametophore development (Ashton *et al.*, 1979; Aoyama *et al.*, 2012; Moody *et al.*, 2018), we supplemented the liquid medium with exogenous cytokinin, BAP, to induce gametophore initiation. To investigate whether the observed differences in cell width and division plane were influenced by exogenous cytokinin treatment, we compared the width and angle of the division plane in the absence and presence of the synthetic cytokinin BAP (Fig. **3a**). We observed the same geometric patterns in terms of width and angle in gametophore and branch initial cells (Fig. **3b,c**), suggesting that the differences are not due to additional cytokinin supply.

Next, we asked whether the geometric cues predicting cell fate persist in mutants that possess gametophore development phenotypes. In Δ*dek1* and *Ppnog1-R* mutants, gametophore initiation is induced or repressed, respectively (Perroud *et al.*, 2014; Moody *et al.*, 2018). To inhibit branching and therefore synchronize gametophore induction, plant tissues were cultured under unilateral red-light

for two weeks, where the Δ*dek1* mutant showed a growth phenotype with bulbous filamentous cells (Fig. **3d**). While under white light condition, the Δ*dek1* mutant exhibited undistinguishable filamentous cell growth as wild-type (Perroud *et al.*, 2014). Although the growth of protonema cells in the Δ*dek1* mutant is affected by red-light illumination, induction of gametophore formation by BAP treatment is comparable to wild-type. Conversely, induction of gametophores failed in the *Ppnog1-R* mutant, in which >99% of emerging initial cells developed to branch cells instead (Fig. **3d,** arrowhead is early gametophore; arrow is branch). To test whether the differences in the width and division angle between gametophore and branch initial cells can be observed in these two mutants, we measured the width and angle of division plane in all developing cells after 40 hours of BAP treatment.

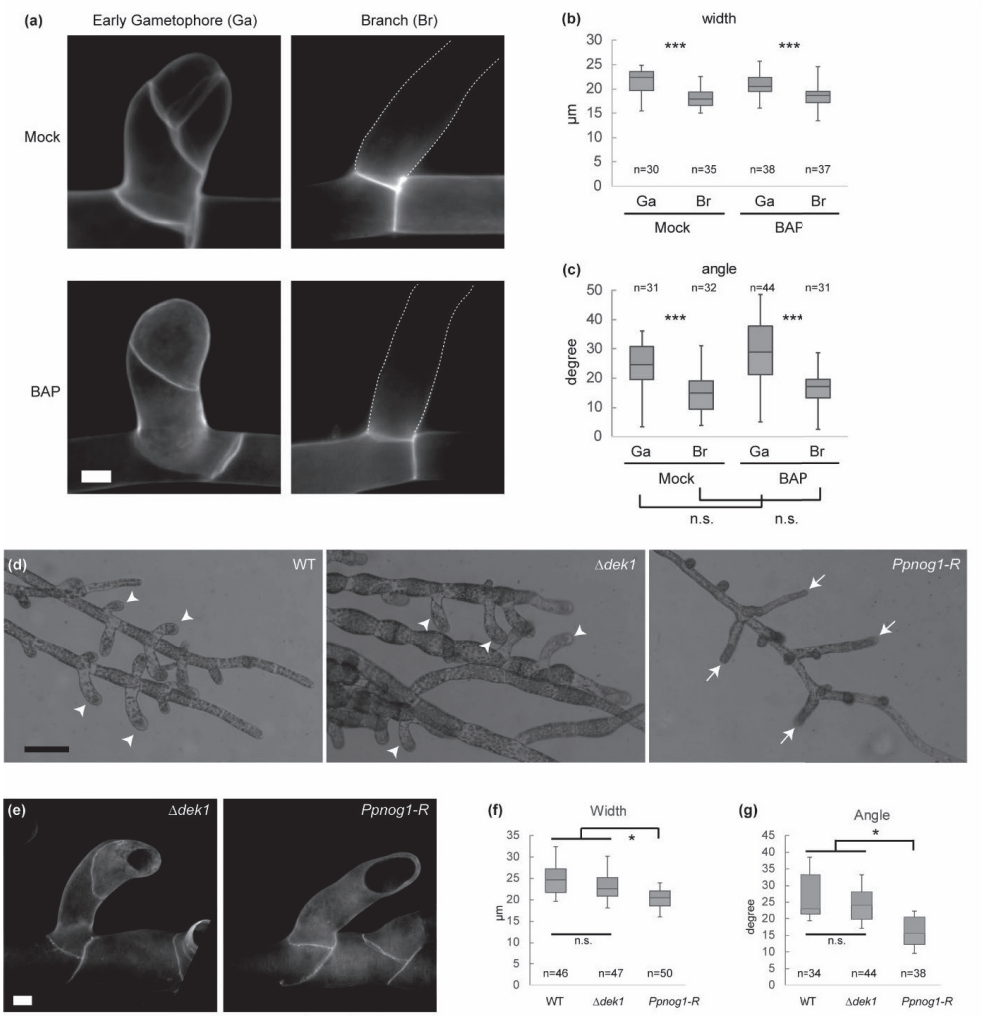

Figure 3. Geometric cues in gametophore initials are independent of exogenously supplied cytokinin and consistent in gametophore mutants.

(a) Representative images of early gametophore and branch in presence and absence of BAP treatment as indicated. The early gametophores and branches were stained with propidium iodide and imaged by spinning disk confocal microscopy. Cell outlines of branches are marked by white dotted lines. Scale bar = 10 µm.
(b) and (c) The measurement of the cell width and the angle of the divisional plane. The number of gametophores and branches collected from three independent experiments was indicated with *** representing significant difference with $p<0.001$ by Mann-Whitney U test. The dataset of gametophore and branch initials obtained with BAP treatment was compared to the same initial cell type without BAP treatment, which neither in gametophore nor in branch initials revealed significant differences.
(d) Overview of gametophore induction in wild-type (WT), *Δdek1*, and *Ppnog1-R*. Plants were cultured under unilateral red-light for two weeks, followed by BAP treatment with continuous white light illumination for 40 hours. Early gametophores were induced in WT and *Δdek1* (arrowheads), but *Ppnog1-R* only formed branches under the same growth condition (arrows). Scale bar = 1 mm.
(e) Examples of early gametophore and branch cells in *Δdek1 and Ppnog1-R* were stained with SCRI Renaissance 2200 and imaged by confocal microscopy. Scale bar = 10 µm.
(f) and (g) The measurement of the cell width and the angle of the divisional plane. * represents significant difference with $p<0.05$ between three means of gametophore and branch datasets using Student's two-tailed t-tests.

The measurement of all emerging initial cells in *Δdek1* mutants, in which >90% initial cells developed into early gametophore, presented an average cell width/division angle of 24.2 µm/23.0 degrees (n=47 for width; n=44 for angle) compared to the 23.7 µm/25.4 degrees in wild-type (n=46 for width; n=34 for angle), showing that the mutant and wild-type had similar cell width and angle. In contrast, the *Ppnog1-R* mutant exhibited similar patterns to wild-type branch initial cells with an average cell width of 20.3 µm (n=50) and average division angle of 16.2 degrees (n=38) (Fig. **3e,f,g**). To exclude the possibility that the cell shape of filamentous cells causes a wider cell width or a larger divisional angle in *Δdek1* mutants, the cell width and division angle were measured in the presence of unidirectional red light, but in the absence of BAP. Initial cells of *Δdek1* mutants developed into branches that were indistinguishable to wild-type branches in terms of cell width and division angle with an average cell width of 17.4 and 20.1 µm, and division angle of 13.8 and 16.5 degrees in wild-type and *Δdek1* mutants (n=17 for wild-type; n=12 for *Δdek1)* without any statistical significance (Fig. **S3**). These results indicate that the geometric parameters measured in *Δdek1* mutants in the presence of BAP were due to the formation of gametophore initials.

The gametophore or branching cell fate can be robustly predicted using geometric cues

We identified two geometric cues, the cell width and the division angle, that differed from gametophore to branch initial cells. To test if these two parameters are good indicators to accurately predict the cell fate of emerging initial cells, the same imaging tracking strategy was used with an additional criterion. Based on our previous results, we set the threshold to predict a gametophore initial cell to 20 µm cell width, and 30 degrees for the division plane angle (Fig. **1f,g**). Once a candidate initial cell reached the threshold for either cell width or divisional angle, it was predicted to become a gametophore initial. The predicted result was then compared to the confirmed cell fate in order to evaluate the prediction accuracy. After 16 hrs, cell fates of gametophore initial cells were confirmed by either swelling (26%) or the oblique division (74%, n=39). The prediction accuracy was the success rate of cells with correct prediction, which was calculated by dividing the number of cells with confirmed cell fate to their predicted cell fate. Our prediction accuracy of around 90% (n=39 for gametophores; n=24 for branches) with statistical significance reinforced that gametophore initial cells

exhibit geometric differences compared to branch initial cells, and that these cues are sufficient to distinguish their future cell fate at the initial stage and can be used as an early predictive tool (Fig. **4**). Moreover, we propose that the observed differences in divisional planes are controlled in the parental cell, suggesting that prior to the transition division and thus prior to the swelling, the cell fate of the gametophore initial cell is already determined.

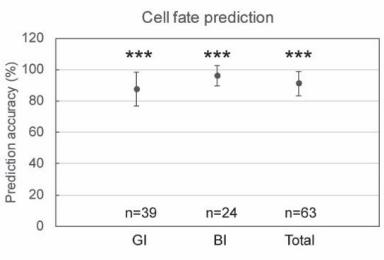

Figure 4. Geometric cues forecast the fates of emerging initial cells. Based on the criteria in width > 20 µm and divisional angle > 30°, fates of initial cells were predicted. If the initial cell passes one of the criteria, the cell was predicted to become a gametophore. The prediction accuracy was calculated as a ratio between predicted and verified cell fates for gametophore, branch, and all observed samples as shown in total. The prediction assay was performed in three biological replicates with a total indicated number of examined cells. *** indicates statistic significant with $p<0.001$ using exact binomial test. GI: gametophore initial cells; BI: branch initial cells.

Identification of a fluorescent marker that predicts the cell fate of the emerging initial cell

To verify that the cell fate of an initial cell is predictable at an early stage of initiation, we used an alternative strategy. We used a reporter line that carries a nuclear-localized GFP-GUS reporter driven by a 2X35S promoter with a synthetic plasma membrane marker (SNAP-TM-mCherry) driven by maize ubiquitin promoter (hereafter referred as NLS4-GFP-GUS). We found that the GFP intensity was dramatically decreased in gametophore tissues at early stage. Reduction of the nuclear GFP was already recognizable in gametophore initial cells at swelling or 2-cell stage in comparison to persistently bright signal in branch filaments (Fig. **5a**).

We performed time-lapse imaging to record the reduction of nuclear GFP, which showed that the GFP intensity remained high in initial cells right after the transition division, while the signal gradually decreased along with the growth and swelling of a gametophore initial cell.

To test the predictive potential of the NLS4-GFP-GUS marker line, we first quantified the differences of GFP intensity in both gametophore and branch initial cells. Because the GFP intensity on parental filaments and branch initials located on different focal planes as shown in Fig. **5a** may result in inaccurate quantification. To overcome this, the median plane of the nucleus, recognized by the unstained area of the nucleolus, was imaged as a standard focal plane in both parental cells and initial cells. The ratio of the GFP intensity in a gametophore initial cell relative to its own parental cell was ~20% (n=28 for pairs of gametophore initials and parental cells) with an average intensity in gametophore initials of 347 arbitrary units (AU) and their parental cells of 2003 AU (Fig. **S4**); while branch initials remained about 80% relative to their parental cells with an average intensity in branch initials of 1798 AU and their parental cells of 2294 AU (n=27 for pairs of branch initials and parental cells, Fig. **S4**). Since the decrease in GFP intensity is obvious prior to swelling of a gametophore initial, we were able to successfully predict cell fate up to 90% (Fig. **5b,c**), at which we confirmed the gametophore cell fate by cell swelling (39%) or the oblique division (61%, n=28). This result is consistent with previous results predicted by cell width and division angle.

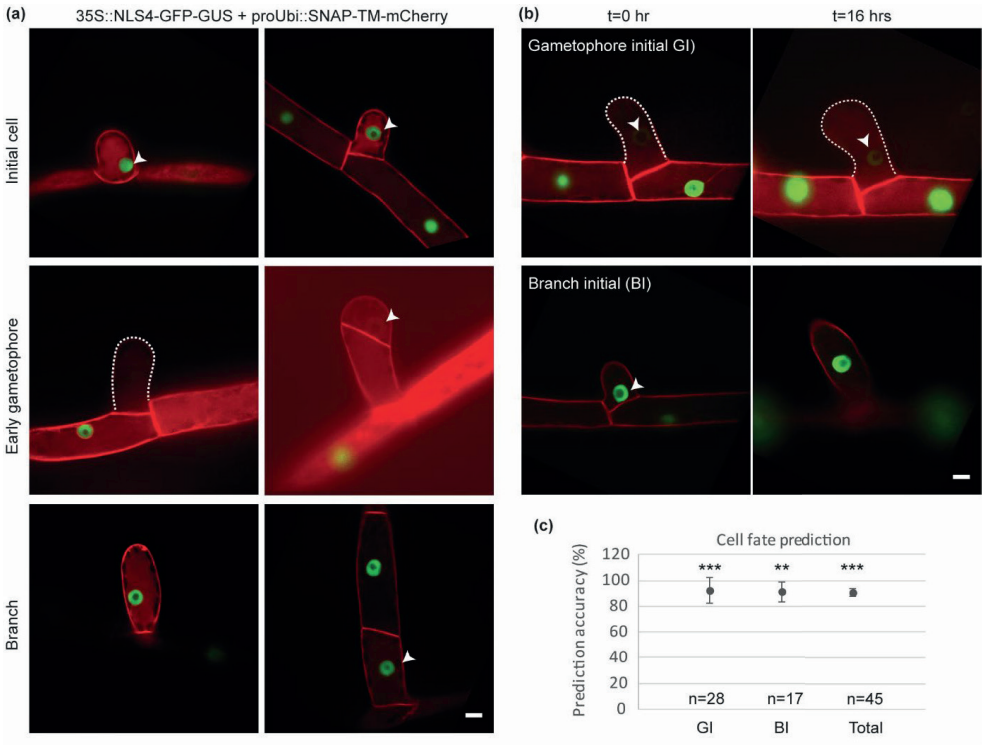

Figure 5. Identification of a fluorescent marker to predict the cell fate of emerging initial cells.
(a) Example images of undetermined initial cells, early gametophores, and branch cells with a green fluorescent labeled nucleus (NLS4-GFP-GUS) and mCherry labeled plasma membrane (SNAP-TM-mCherry) as indicated. Arrowheads depict the nucleus with the unstained nucleolus. Scale bar = 10 µm.
(b) Based on nuclear GFP intensity, the cell fated to gametophore or branch was predicted as indicated in t=0 hr panels. Cell fates of target initial cells were confirmed after 16 hours by GFP intensity and cell morphology.
(c) Prediction accuracy was calculated as a ratio between predicted and verified cell fates for gametophore, branch, and all observed samples as shown in total. The prediction assay was performed in three biological replicates with a total indicated number of examined cells. *** indicates statistic significant with $p<0.001$; ** = $p<0.01$ using exact binomial test.

Discussion

Here, we used for the first time the MorphoGraphX software for 3D image processing to accurately quantify the geometric differences between gametophore and branch initials in the moss *Physcomitrella*. Upon emergence of initial cells right after the transition division, we identified two morphological features, cell width and division angle, which distinguish gametophore and branch initial cells. Additionally, we revealed that the fluorescent reporter NLS4-GFP-GUS presented a dramatically lower nuclear GFP signal in gametophore tissues than protonema cells. Both identified geometrical cues and the fluorescent marker allowed us to accurately predict the gametophore initial cell identity prior to visible swelling. In sum, we presented early markers for 2D-to-3D transition,

implying that the gametophore cell fate decision occurs within a specified microenvironment in the parental cell of the initial.

The transition division is executed and regulated by the parental cell, suggesting that the decision for the transition to 3D growth has been made in the parental cell prior to the transition division. A parental cell can be transcriptionally specified as a founder cell and/or be the source of a specific molecular microenvironment to induce the 3D growth transition. In some cases a filamentous parental cell gives rise to a second emerging initial cell, this requires the parental cell to re-enter the cell cycle, which is likely mediated through transcriptional control (Polyn *et al.*, 2015). Thus, the specification of a parental cell giving rise to a gametophore initial is conceivable to take place in parallel with the transcriptional activation of a new cell cycle. Previous reports (Harrison *et al.*, 2009) as well as our own observations (*unpublished results*) show that a gametophore and a branch can develop from the same parental cell, suggesting the trigger for 3D transition is mediated through a transient and local specification of a parental cell. The filamentous parental cell might trigger gametophore formation via different, not mutually exclusive, regulatory mechanisms such as transient polarity changes, cytoskeletal reorganization, and re-distribution of determinants.

Our newly identified geometric markers allow early, rapid and straightforward identification of a cell transitioning into a gametophore compared to previous studies and provides a powerful tool to investigate the central question of how gametophore formation is initiated. For example, it is now possible to investigate the transition division by recognizing and isolating the gametophore initial cell and its parental cell at early stages and perform comprehensive transcriptome analysis. A transcriptomic analysis has been performed with 4-cell early gametophore samples (Frank & Scanlon, 2015), and an extension of these data can provide important information on crucial initial steps of the 3D growth transition.

Material and Methods

Plant material and growth conditions

Wild type *Physcomitrella patens* (Gransden strain) (Ashton & Cove, 1977) was used as a standard line for the observation of gametophore initiation. Moss tissues were routinely grown on BCDAT plates under continuous light at 25°C as described before (Nishiyama *et al.*, 2000). A marker line possessing the nuclear marker 2X35S::NLS4-GFP-GUS with a synthetic plasma membrane marker SNAP-TM-mCherry driven by the maize ubiquitin promoter was used for intensiometric analysis during gametophore initiation (Bezanilla *et al.*, 2003; van Gisbergen *et al.*, 2018). Imaging of early gametophore formation was induced with 1µM 6-Benzylaminopurine (BAP) treatment, besides the mock treatment described in Figure 3. For general imaging, protonema tissue was grown on BCD medium in glass bottom dishes (Yamada *et al.*, 2016) for 3 days under continuous white light, then moved to red light (light transmission with wavelength > 600 nm) for another 3 days. After 3 days of growth under red light the dish was moved back to white light and supplied with ½ liquid BCD medium containing 1µM BAP. Gametophore initiation was recorded between 30 to 54 hrs after BAP induction. For cell fate prediction, the imaging dish was moved back to the incubator after image acquirement for recovery overnight.

Fluorescence microscopy and staining

Live cell imaging was performed on a Roper spinning disk microscope system composed of a Nikon Ti eclipse body, Yokogawa CSU-X1 spinning disc head and Photometrics Evolve 512 camera. Imaging was conducted with a Nikon 60x Plan Apo VC oil immersion objective (NA 1.40), using a 1.2x post-magnification lens fitted before the camera. GFP and probes were excited using 491 nm light from a Cobolt Calypso50 laser and emitted light was bandpass filtered at 497-557 nm. For PI staining and mCherry 561 nm excitation, a Cobolt Jive50 laser light, was used in combination with bandpass filtering at 570-620 nm. During image digitization, a camera electron multiplication gain of 300 was employed and typical exposures were 200 ms for both GFP and mCherry probes. Propidium iodine was dissolved in dH_2O at a final concentration of 10 µg/ml and added to cells right before imaging. For cell fate prediction, the memory function was used to track back positions when moving the dish back after recovery. For computational geometry analysis, cell outlines were stained and fixed with SCRI Renaissance 2200 solution (0.1% (v/v) SR2200, 1% (v/v) DMSO, 0.05% (w/v) Triton-X 100, 5% (w/v) glycerol, 3.75% (w/v) para-formaldehyde in PBS buffer (pH 7.4), (Kerstens *et al*., in press) and recorded using a laser scanning confocal microscope (Zeiss LSM510) with a 40x magnification lens at 0.4 µm z-stack intervals using 405nm excitation and detection at 450-560 nm.

Cell segmentation and volume extraction

Segmentation and volume extractions were carried out using the MorphoGraphX software (http://www.MorphoGraphX.org) designed for analysis of 3D images (de Reuille *et al.*, 2015). Acquired images of early gametophores were directly imported without modification and smoothed by 3D Gaussian filter blur function. The autoseeded watershed function was used to segment cells. After trimming unwanted tissues and correcting segments by deletion or merge functions, the marching cube algorithm with a cube size of 1 µm was used to create a 3D mesh and extract geometric information (Kerstens *et al*., in press). For cell width and angle measurement of the segmented initial cells, the segmented mesh was first rotated to orient the parental cell in a horizontal orientation. Images were then imported in Fiji (Schindelin *et al.*, 2012) and cell width and angle were measured using the Fiji line- and angle-drawing functions.

Cell fate prediction analysis

After PI staining, raw images were acquired in about 50 z-stacks with 0.5 µm intervals and projected by the max intensity in Fiji. All images were then re-oriented such that the filamentous parental cell was horizontal. The width of the initial cell was measured by manual usage of the line-drawing tool in which the line was drawn along the horizontal parental membrane that connects the neck of protruding initial cells. The angle of the cell division plane that separates an initial cell and its parental cell was measured in relation to the horizontal line along with parental cell by the angle tool in Fiji. The samples with unclear division plane were discarded from the dataset to avoid miscalculation.

Statistical analysis

For statistical analysis of geometric properties, two different statistical tests have been used, 2-tailed student t-tests and Mann-Whitney U test. The used tests are indicated in the figure legends. The selected methods is depending on the distribution of each dataset. For cell fate prediction analysis, binomial tests were carried out in Excel under the assumptions that each initial cell is independent of another, and the probability of each initial cell to become a gametophore or a branch is p=0.5. Gametophore, branch, and total (gametophore plus branch) cells obtained from three independent

experiments were collectively analysed as shown in Figure 4. Additionally, every dataset of gametophore, branch, and total of the three experiments was also separately tested. Only one gametophore and one branch dataset did not reveal statistical significance, but all other 7 tested samples passed the binomial test with *p* ranging 0.018 to 1.04308E-07.

Acknowledgements

We thank Tijs Ketelaar and Marcel Janson in Cell Biology group for support and discussions, Laura Moody and Viktor Demco for sharing of published material and Peter van Gisbergen for critical reading of the manuscript. This work was supported by the Earth and Life Sciences Council (ALW) of the Netherlands Organization for Scientific Research (NWO; ALW-VIDI 864.13.008 to J.E.M.V.).

Author Contributions

H.T. and V.W. planned and designed the research. H.T. performed experiments. H.T., K.D., and V.W. conducted data analysis. M.B. contributed important materials. H.T., M.B., B.S., J.V., and V.W. wrote the manuscript.

Supplemental Information

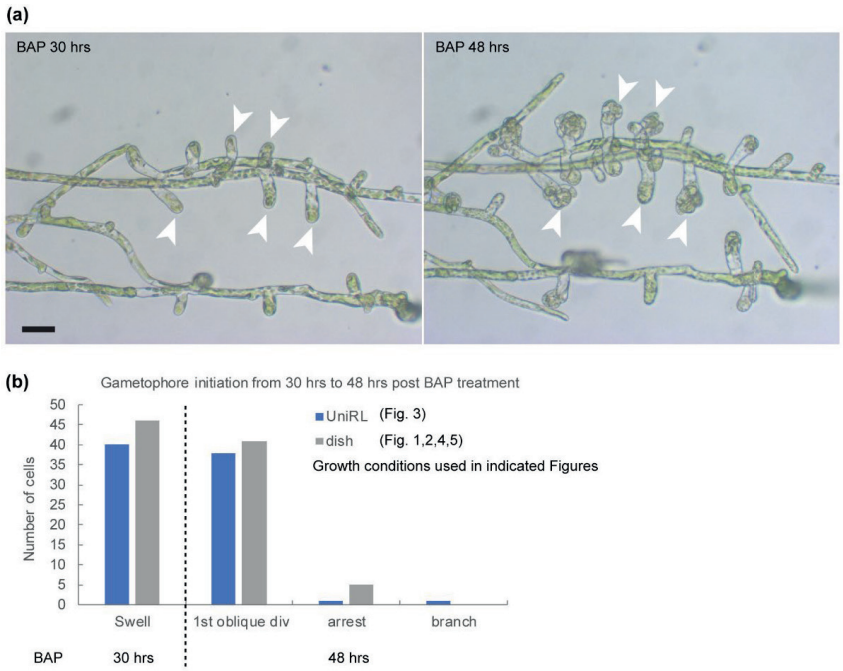

Figure S1. Swelling gametophore initial cells develop into early gametophores.
(a) Wild-type tissues grew in UniRL condition and supplied with BAP for 30 hrs. Initial cells with apparent swelling but not undergoes the first oblique division were targeted and indicated by white arrowheads. Most of swelling gametophore initial cells develop into early gametophores with multiple divisions. scale=1mm.
(b) Swollen gametophore initial cells were tracked at the first time point (BAP 30hrs) and most of them (38/40 in uni-RL; 40/45 in dish) continually develop into gametophores at second time point (BAP 48 hrs) with at least the first oblique division in indicated conditions.

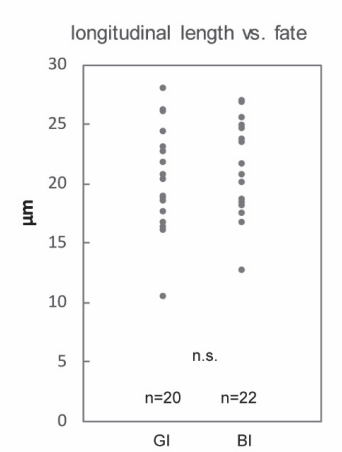

Figure S2. The longitudinal cell length in gametophore or branch initial cells for MGX analysis do not show differences.

All examined initial cells were rotated to orient the cell axis towards the top side. The height, or the longitudinal cell length, thus can be measured automatically by MorphoGraphX software.

GI: gametophore initial cells; BI: branch initial cells.

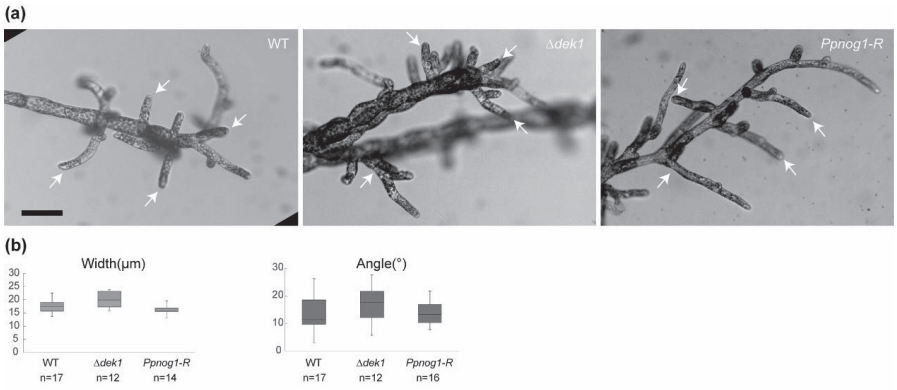

Figure S3. The width of branch initial cells in *Δdek1* is similar to the width of wildtype branch initial cells.
Protonemal tissues were cultured under uni-lateral red-light for two weeks and released to white light with supplied liquid ½ BCD medium for 48 hrs.
The development of secondary branches was indicated by white arrows in (a), scale bar = 1 mm.
The width and angle of all emerged branching cells were quantified as (b) shown.

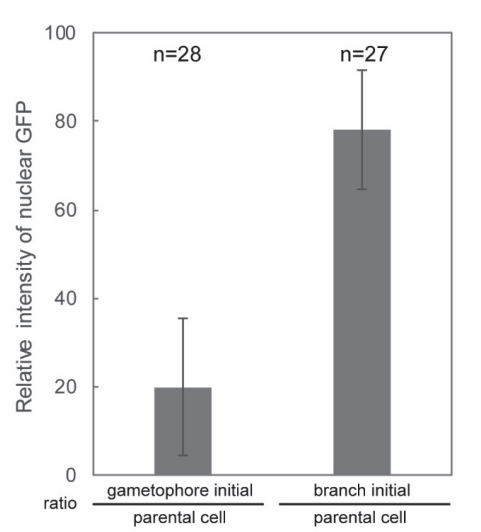

Figure S4. Quantification of nuclear GFP intensity in gametophore and branch initials relative to their parental cells.

References

Aida M, Beis D, Heidstra R, Willemsen V, Blilou I, Galinha C, Nussaume L, Noh Y-S, Amasino R, Scheres B. 2004. The PLETHORA genes mediate patterning of the Arabidopsis root stem cell niche. *Cell* **119**(1): 109-120.

Aoyama T, Hiwatashi Y, Shigyo M, Kofuji R, Kubo M, Ito M, Hasebe M. 2012. AP2-type transcription factors determine stem cell identity in the moss Physcomitrella patens. *Development* **139**(17): 3120-3129.

Ashton N, Cove D. 1977. The isolation and preliminary characterisation of auxotrophic and analogue resistant mutants of the moss, Physcomitrella patens. *Molecular and General Genetics MGG* **154**(1): 87-95.

Ashton NW, Grimsley NH, Cove DJ. 1979. Analysis of gametophytic development in the moss, Physcomitrella patens, using auxin and cytokinin resistant mutants. *Planta* **144**(5): 427-435.

Bezanilla M, Pan A, Quatrano RS. 2003. RNA interference in the moss Physcomitrella patens. *Plant Physiol* **133**(2): 470-474.

Boutilier K, Offringa R, Sharma VK, Kieft H, Ouellet T, Zhang L, Hattori J, Liu C-M, van Lammeren AA, Miki BL. 2002. Ectopic expression of BABY BOOM triggers a conversion from vegetative to embryonic growth. *The Plant Cell* **14**(8): 1737-1749.

Boyer F, Simon R. 2015. Asymmetric cell divisions constructing Arabidopsis stem cell niches: the emerging role of protein phosphatases. *Plant Biol (Stuttg)* **17**(5): 935-945.

Chakrabortty B, Willemsen V, Zeeuw Td, Liao C-Y, Weijers D, Mulder B, Scheres B. 2018. A microtubule-based mechanism predicts cell division orientation in plant embryogenesis. *bioRxiv*.

Cove D, Bezanilla M, Harries P, Quatrano R. 2006. Mosses as model systems for the study of metabolism and development. *Annu. Rev. Plant Biol.* **57**: 497-520.

Cove DJ, Knight CD. 1993. The moss Physcomitrella patens, a model system with potential for the study of plant reproduction. *The Plant Cell* **5**(10): 1483.

de Reuille PB, Routier-Kierzkowska A-L, Kierzkowski D, Bassel GW, Schüpbach T, Tauriello G, Bajpai N, Strauss S, Weber A, Kiss A. 2015. MorphoGraphX: A platform for quantifying morphogenesis in 4D. *Elife* **4**: e05864.

Elliott RC, Betzner AS, Huttner E, Oakes MP, Tucker W, Gerentes D, Perez P, Smyth DR. 1996. AINTEGUMENTA, an APETALA2-like gene of Arabidopsis with pleiotropic roles in ovule development and floral organ growth. *The Plant Cell* **8**(2): 155-168.

Frank MH, Scanlon MJ. 2015. Cell-specific transcriptomic analyses of three-dimensional shoot development in the moss Physcomitrella patens. *Plant J* **83**(4): 743-751.

Galinha C, Hofhuis H, Luijten M, Willemsen V, Blilou I, Heidstra R, Scheres B. 2007. PLETHORA proteins as dose-dependent master regulators of Arabidopsis root development. *Nature* **449**(7165): 1053.

Graham LE, Cook ME, Busse JS. 2000. The origin of plants: body plan changes contributing to a major evolutionary radiation. *Proceedings of the National Academy of Sciences* **97**(9): 4535-4540.

Harrison CJ, Roeder AH, Meyerowitz EM, Langdale JA. 2009. Local cues and asymmetric cell divisions underpin body plan transitions in the moss Physcomitrella patens. *Curr Biol* **19**(6): 461-471.

Kofuji R, Hasebe M. 2014. Eight types of stem cells in the life cycle of the moss Physcomitrella patens. *Curr Opin Plant Biol* **17**: 13-21.

Kosetsu K, Murata T, Yamada M, Nishina M, Boruc J, Hasebe M, Van Damme D, Goshima G. 2017. Cytoplasmic MTOCs control spindle orientation for asymmetric cell division in plants. *Proc Natl Acad Sci U S A* **114**(42): E8847-E8854.

Kerstens M, Strauss S, Smith R, Willemsen V. 2019. From stained plant tissues to quantitative cell segmentation analysis with MorphoGraphX. *Methods Mol Biol*. in press

Moody LA, Kelly S, Rabbinowitsch E, Langdale JA. 2018. Genetic Regulation of the 2D to 3D Growth Transition in the Moss Physcomitrella patens. *Curr Biol* **28**(3): 473-478 e475.

Nishiyama T, Hiwatashi Y, Sakakibara K, Kato M, Hasebe M. 2000. Tagged Mutagenesis and Gene-trap in the Moss, Physcomitrella patens by Shuttle Mutagenesis. *DNA Research* **7**(1): 9-17.

Perroud PF, Demko V, Johansen W, Wilson RC, Olsen OA, Quatrano RS. 2014. Defective Kernel 1 (DEK1) is required for three-dimensional growth in Physcomitrella patens. *New Phytol* **203**(3): 794-804.

Pillitteri LJ, Guo X, Dong J. 2016. Asymmetric cell division in plants: mechanisms of symmetry breaking and cell fate determination. *Cell Mol Life Sci* **73**(22): 4213-4229.

Polyn S, Willems A, De Veylder L. 2015. Cell cycle entry, maintenance, and exit during plant development. *Curr Opin Plant Biol* **23**: 1-7.

Prigge MJ, Bezanilla M. 2010. Evolutionary crossroads in developmental biology: Physcomitrella patens. *Development* **137**(21): 3535-3543.

Scheres B, Wolkenfelt H, Willemsen V, Terlouw M, Lawson E, Dean C, Weisbeek P. 1994. Embryonic origin of the Arabidopsis primary root and root meristem initials. *Development* **120**(9): 2475-2487.

Schindelin J, Arganda-Carreras I, Frise E, Kaynig V, Longair M, Pietzsch T, Preibisch S, Rueden C, Saalfeld S, Schmid B. 2012. Fiji: an open-source platform for biological-image analysis. *Nature methods* **9**(7): 676.

van Gisbergen PA, Wu S-Z, Chang M, Pattavina KA, Bartlett ME, Bezanilla M. 2018. An ancient Sec10–formin fusion provides insights into actin-mediated regulation of exocytosis. *J Cell Biol*: jcb. 201705084.

Whitewoods CD, Cammarata J, Nemec Venza Z, Sang S, Crook AD, Aoyama T, Wang XY, Waller M, Kamisugi Y, Cuming AC, et al. 2018. CLAVATA Was a Genetic Novelty for the Morphological Innovation of 3D Growth in Land Plants. *Curr Biol*.

Yamada M, Miki T, Goshima G 2016. Imaging mitosis in the moss Physcomitrella patens. *The Mitotic Spindle*: Springer, 263-282.

Yoshida S, Barbier de Reuille P, Lane B, Bassel GW, Prusinkiewicz P, Smith RS, Weijers D. 2014. Genetic control of plant development by overriding a geometric division rule. *Dev Cell* **29**(1): 75-87.

Chapter 4

The roles of ROP2 and RIC in *Physcomitrella patens* gametophore formation

Han Tang[1,2,] *, Alejandra Freire Rios[1,2,]*, Tijs Ketelaar[2], Ben Scheres[1], Joop E.M. Vermeer[3,4] and Viola Willemsen[1]

[1] Laboratory of Plant Developmental Biology, Wageningen University & Research, Wageningen, The Netherlands
[2] Laboratory of Cell Biology, Wageningen University & Research, Wageningen, The Netherlands
[3] Plant Cell Biology, Department of Plant and Microbial Biology and Zurich-Basel Plant Science Center, University of Zürich, 8008 Zürich, Switzerland
[4] Present address: Laboratory of Cell and Molecular Biology, Institute of Biology, University of Neuchâtel, 2000 Neuchâtel, Switzerland

*Equal contributions.

Abstract

In eukaryotes, small Rho-GTPases have important roles in regulating multiple cellular responses, including local cell growth, cell shape change, and asymmetric cell division. These proteins are evolutionarily conserved across kingdoms and in plants known as Rho of plants (ROPs). Active GTP-bound ROPs localize to the plasma membrane where they interact with specific effectors e.g. RICs (Rho-interactive CRIB motif-containing proteins) and thereby trigger various signalling pathways. In this study, we used the model moss *Physcomitrella patens* to investigate the role of ROP signalling in the developmental transition from filamentous to gametophytic phase. We address this by characterizing protein localization and phenotyping loss-of-function mutants. In *Physcomitrella,* ROP1 to ROP4 localized at the plasma membrane of tip growing cells, while this apical enrichment was dispersed to the lateral sides of gametophore initial cells. Mutation of *ROP2*, but not other *ROPs*, resulted in defective gametophore initiation and development, which was rescued by mutating the ROP effector RIC, encoded by a single gene copy in moss, in the *rop2* knockout background. In contrast, *rop2* mutant revealed impaired chloronema-caulonema transition in a RIC-independent manner. Transcriptional analysis supported that tissue-specific ROP2-RIC module might operate in early gametophores but not in filaments. Taken together, our results indicate that ROP2 has different essential roles in two developmental transitions.

Introduction

The Rho family of small GTPases controls a wide range of cellular processes in all eukaryotic cells, including cell division, polarization, and morphogenesis. Animals and yeast have evolved subfamilies of Rho-GTPase such as Cdc42, Rac, and Rho; whereas plants possess a single family called Rho of plants (ROPs) (Yang, 2002; Etienne-Manneville, 2004). ROP GTPases are plant-specific small GTPases, that are versatile molecular switches in regulating certain aspects of cell polarity and development (Fu *et al.*, 2005; Lee *et al.*, 2008). ROPs achieve their diverse functions via conformational changes in response to GTP binding and hydrolysis (Yang & Fu, 2007). The active GTP-bound form of ROPs resides on the plasma membrane and transiently interacts with specific effectors to modulate distinct cellular processes, while the inactive GDP-bound form of ROPs is removed from the plasma membrane and sequestered in the cytoplasm (Yalovsky *et al.*, 2008; Feiguelman *et al.*, 2018). The active status and binding to specific effector proteins result in a flexible machinery regulating diverse functions in response to different cellular stimuli.

In *Arabidopsis thaliana* (*Arabidopsis*), 11 members of ROPs have been identified displaying different expression patterns and functions in diverse tissues (Yang, 2002). For polarized tip growth in pollen tubes and root hairs, tip-localized activated AtROP1 is a major contributor to facilitate exocytotic vesicles to be targeted to the plasma membrane of the cell apex (Molendijk *et al.*, 2001; Lee *et al.*, 2008). To coordinate tip cell growth, 11 effectors termed RICs (Rho-interactive CRIB motif-containing proteins) have been identified to differently interact with AtROP1 and perform various functions during pollen tube growth (Wu *et al.*, 2001). In *Arabidopsis*, pollen tube elongation is faster in a *ric1* null mutant compared to the wildtype, while overexpression of RIC1 inhibits tip growth. RIC1 has been demonstrated to directly bind and severe F-actin to regulate pollen tube growth (Fu *et al.*, 2001; Zhou *et al.*, 2015). Besides RIC1, AtROP1 regulates F-actin dynamics by activating two other RICs, RIC3 and RIC4, respectively. RIC4 promotes F-actin assembly, while RIC3 promotes F-actin disassembly through its regulation in tip-focused Ca^{2+} gradients (Gu *et al.*, 2005). Overexpression of

fluorescently-tagged RICs in the absence or presence of AtROP1 reveals different localization patterns in pollen tubes, where RIC4 and RIC6 are localized at the plasma membrane as well as the cytoplasm without AtROP1, but exclusively accumulated at the apical plasma membrane when co-expressed with AtROP1. In addition, variable levels of RIC transcripts are found in mature pollen, where RIC1, RIC3, and RIC7 are detected at higher levels and RIC4 and RIC6 are detectable in lower amounts (Wu *et al.*, 2001). These results suggest that ROP-RIC interaction, localization, and gene expression may contribute to the coordination of ROP-dependent signalling pathways.

In addition to polarized growth, ROPs have been reported to play a pivotal role in diffuse growth by controlling cell shapes. In leaf pavement cells of *Arabidopsis*, auxin-triggered activation of AtROP2 localizes at lobes where it promotes lobe outgrowth via actin assembly while AtROP6 suppresses lobe outgrowth but promotes indention formation via microtubule rearrangements (Fu *et al.*, 2009; Xu *et al.*, 2010; Craddock *et al.*, 2012). The modulation of cytoskeleton organization by ROPs relies on their interaction with specific RICs. For instance, AtROP2 promotes actin assembly via interacting with RIC4 for promoting lobe outgrowth, while AtROP6 suppresses lobe outgrowth by activating RIC1 that promotes microtubule ordering (Fu *et al.*, 2005; Fu *et al.*, 2009). Additionally, extracellular localized auxin activates ROP proteins at the lobe tip (Xu *et al.*, 2010). Auxin triggers the activation of ROP2 that inhibits the endocytosis of auxin transporter PINFORMED1 (PIN1), which exports auxin at the lobe tip and thus form a positive feedback loop (Nagawa *et al.*, 2012). This Rho GTPase-based regulation of vesicle trafficking may promote the formation of interdigitated lobes and indentations (Chen & Friml, 2014; Xu *et al.*, 2014).

Although the function of ROPs in cell growth and morphogenesis have extensively been studied in flowering plants, and roles in plant defence have been revealed (Craddock *et al.*, 2012; Lin *et al.*, 2015; Feiguelman *et al.*, 2018), roles of ROPs in asymmetric divisions and developmental programs still remain elusive. One obstacle to investigating roles of ROPs in asymmetric divisions throughout *Arabidopsis* development is the presence of multiple ROP and RIC paralogs, each with different expression patterns and diverse functions in specific tissues. The combination of functional redundancy, tissue complexity, and downstream effectors makes it difficult to identify which specific developmental programs are regulated by specific ROPs and their interacting effectors.

ROPs are evolutionary conserved in land plants, while relatively few members of the *ROP* gene family and their effectors are identified in early land plant lineages. In the moss *Physcomitrella patens*, four *ROP* genes and single putative *RIC* effector gene have been identified (Eklund *et al.*, 2010). In moss filaments, termed protonemata cells, functional analysis of six-day-old moss plants have revealed that ROPs are essential for tip cell growth, cell wall deposition, cell adhesion, and actin dynamics showing a high functional redundancy (Burkart *et al.*, 2015). The transcription of individual ROP genes is tightly controlled since in single *rop* deletion mutants the expression of the remaining ROP genes appears to be down-regulated (Burkart *et al.*, 2015). Knockdown of RIC through RNA silencing results in plants that grow slightly faster compared to control RNAi plants, suggesting that RIC may inhibit tip cell growth in moss (Bascom *et al.*, 2019).

A moss protonemal filament grows by polar growth along with regular cell divisions and the emergence of new branches. Protonemata are composed of two types of cells: chloronema cells gradually transit to caulonema cells, which exhibit different morphology and characteristics (Vidali & Bezanilla, 2012). Chloronemata are shorter and possess more chloroplasts and transverse cell

division planes; whereas caulonemata are longer and contain less and smaller chloroplasts and have oblique cross walls (Ashton et al., 1979). At the mature stage, a shoot-like gametophore equipped with leafy structures and sexual organs is produced from the filaments. A gametophore is initiated from a transition division that reveals an increased width and a greater division angle when comparing a gametophore initial cell to a branch initial cell (Chapter 4), which marks the 2D-to-3D growth transition of *Physcomitrella* (Moody, 2019). After this first division, a branch initial cell elongates and divides perpendicularly, whereas a gametophore initial cell swells and executes an oblique asymmetric cell division (Harrison *et al.*, 2009). This is followed by two rounds of cell division roughly perpendicular to the oblique division plane and results in a tetrahedral apical stem cell. This apical stem cell executes asymmetric self-renewing divisions to establish new lateral domains in a spiral pattern and this process marks the onset of gametophore development (Harrison *et al.*, 2009).

Although ROPs in *Physcomitrella* have been linked to polar growth, their roles in developmental transitions remain unexplored. Here, we investigated the localization patterns of each ROP and performed loss-of-function phenotyping analyses to characterise roles of ROPs and RIC during the transition from planar to 3D growth. In contrast to other *rop* mutants, knockout of *rop2* (*Δrop2)* lead to a significantly reduced amount of gametophores resulting from a suppression of gametophore initiation and impaired gametophore maturation. Moreover, the transition from chloronema to caulonema was also altered in *Δrop2*. The defective gametophore development of *Δrop2* was complemented when deleting the single effector *ric (Δrop2Δric)*. The double mutant did however not restore the alteration of chloronema-caulonema transition observed in *Δrop2,* which suggests that ROP2 and RIC interact in a tissue-specific manner. Transcriptional analysis of *ROPs* and *RIC* in filaments and early gametophores indicated that *ROP2* and *RIC* are up-regulated in early gametophores while *RIC* is almost undetectable in filaments, suggesting a tissue-specific functional interaction of ROP2 and RIC during gametophore development.

Results

ROPs display dynamic localization during gametophore initiation

In order to test a potential involvement of ROP proteins in the transition from 2D to 3D growth in *Physcomitrella patens*, we first characterized the localization pattern of the ROPs during gametophore initiation (up to the 4-cell early gametophore stage). Since ROP proteins anchor to the membrane via their C-terminal domain, the four ROP homologs were tagged with super Yellow Fluorescent Protein (sYFP) (Kremers *et al.*, 2006) at their N-termini to avoid interference with their proper localization and function. We also used this strategy to tag the single identified canonical ROP effector RIC, but we could not detect any fluorescent signal, indicating low expression levels or instability of the protein. In *Physcomitrella*, ROPs have been reported to localize at the plasma membrane and to accumulate at the apex of tip growing cells (Burkart *et al.*, 2015), which was confirmed in this study (Fig. **1a**). In emerging gametophore initial cells, all four ROPs showed similar apical-localization patterns as previously shown in filamentous tip cells (Fig. **1b**, Initial panel). However, during the swelling of gametophore initial cells, the plasma membrane-localized ROPs reveal a broader expression domain at the apex and are dispersed laterally along the plasma membrane of the swelling cell (Fig. **1b**, Swell panel, yellow arrowheads). In the 2-cell stage, all four ROPs were maintained at the plasma membrane as well at the newly formed oblique division plane (Fig. **1b**). After the 4-cell stage, ROP2 to ROP4 localized at the plasma membrane, division planes, and

cytoplasm in all cells. However, ROP1 revealed a prominent accumulation at the plasma membrane as well as cytoplasm of the apical stem cell (Fig **1b**, 4-cell panel, red arrowhead). This enrichment of ROP1 persisted in subsequent stages after more divisions.

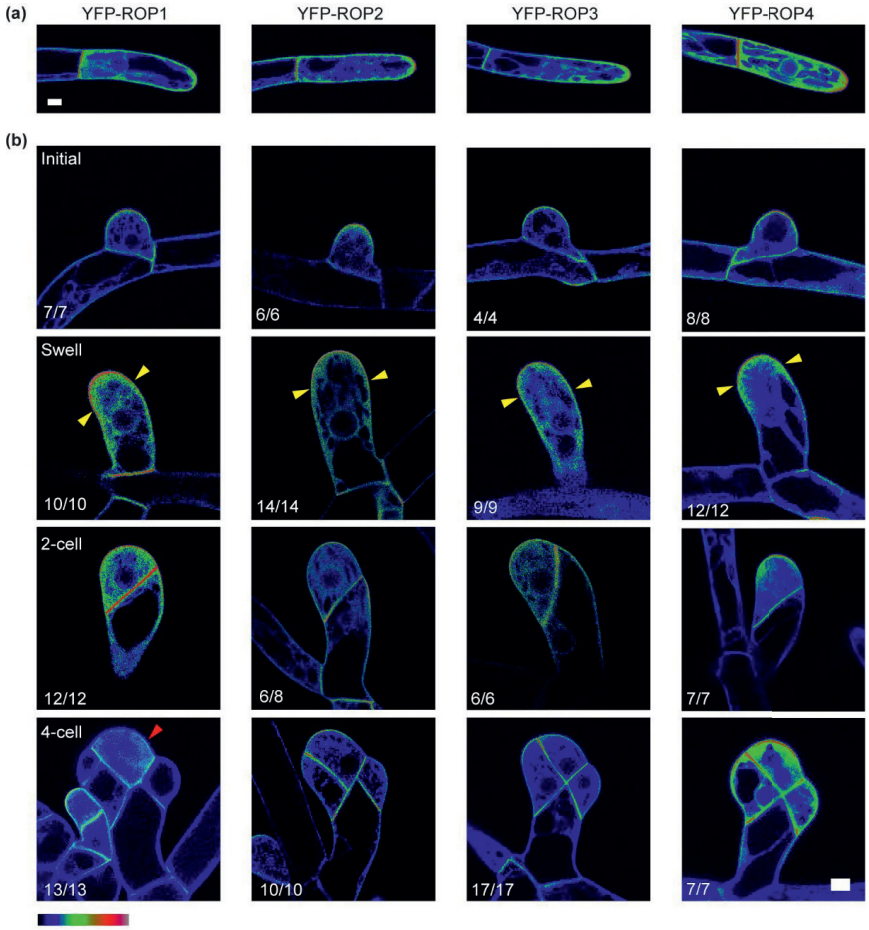

Figure 1. ROPs localization patterns during gametophore initiation.

(a) Representative images of ROPs tagged with N-terminal-fused sYFP in protonema cells were selected to present. sYFP-ROPs signals polarly localized at the apex of tip growing cells. Scale bar = 10 µm.

(b) Early gametophores were imaged at different stages of gametophore initiation from initial, swell, 2-cell, to 4-cell stages. Representative images of ROPs tagged with N-terminal-fused sYFP in each stage were selected. Gametophore initial cells were imaged and the same target cells were revisited after recovery to confirm their fates by cell swelling and oblique division. The pixel values ranged from 0 to 255 is represented by rainbow colouring as indicated. The yellow arrowheads depict the dispersed signal of sYFP-ROPs on the dome side of the swollen cells, and the red arrowhead indicates the accumulation of sYFP-ROP1 in the apical stem cell. The n/N shown at lower left = number of images displayed typical distribution/images obtained. Scale bar = 10 µm.

Deletion of *rop2* reduces gametophore number

Our localization analysis revealed the presence of all four ROPs in early stage gametophores, which could indicate a functional role during this process. Since a gametophore initial cell eventually develops into a mature leafy gametophore, the number of leafy gametophores in a colony provides a first proxy for gametophore initiation. We therefore compared the number of leafy gametophores of wildtype and all four single *ROP* deletion mutants (*Δrop1, Δrop2, Δrop3, and Δrop4*). Colonies of *Δrop2* were compact, probably due to reduced filament growth, and showed an obvious reduction of gametophores (Fig. **2a**). *Δrop2* colonies developed 16±7 gametophores (n=3 colonies for all examined lines), while wildtype colonies formed 87±12 gametophores (Fig. **2b**). Although colonies from other *Δrop* lines also revealed reduced numbers of gametophores (67±12 in *Δrop1*, 53±16 in *Δrop3*, 70±4 in *Δrop4*), the phenotypes were not as severe as seen in *Δrop2*. This result demonstrated that the gametophore formation is severely suppressed in *Δrop2*, whereas other ROP proteins have only small contributions. Therefore, we focused on the *Δrop2* mutant to unravel the role of Rho GTPases during the establishment of gametophore development.

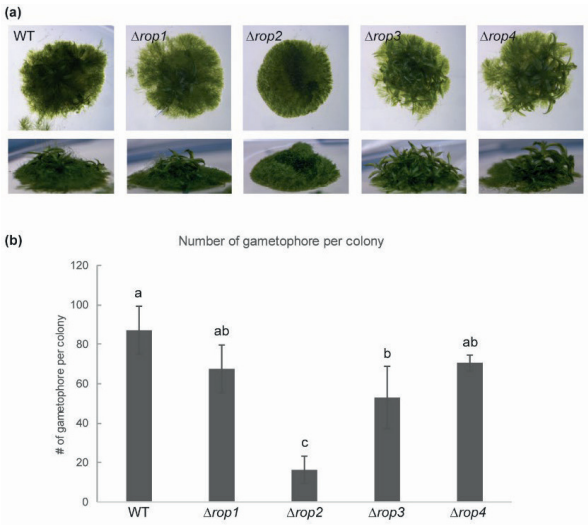

Figure 2. Deletion of *rop2* reveals a reduced amount of gametophores.

(a) 21-day-old moss colonies in indicated genetic backgrounds. All colonies were grown on the same BCDAT plates under continuous white light for three weeks. Side view of colonies shows the lower number of gametophores in *Δrop2* mutant.

(b) The average number of gametophores with at least one clear leaf per colony were counted under a stereomicroscope. N = 3 colonies for each genetic background. Error bars represent SD. The letter above the bars represents statistic groups with $p<0.05$ using ANOVA and Tukey's HSD test.

ROP2 deletion mediated suppression of gametophore initiation is restored by also deleting RIC

Gametophore initiation can be induced by cytokinin (BAP) as previously described (Harrison *et al.*, 2009; Aoyama *et al.*, 2012). We used this method to induce gametophore formation. Because in angiosperms, ROPs interact with effector RICs to drive polarized growth in root hairs and pollen tubes (Molendijk *et al.*, 2001; Gu *et al.*, 2003; Lee *et al.*, 2008), we included the single putative effector RIC into the following phenotypic analysis. The *ric* knockout mutant (*Δric*) and the double mutant *Δrop2Δric* were generated and we quantified the number of early gametophores in *Δrop2*, *Δric*, and *Δrop2Δric*. In order to characterize the early events that take place during gametophore initiation, the early gametophores were divided in two categories based on their morphology, less than 4-cell stage (<4-cell) and equal or more than 4-cell stage (≥ 4-cell). and we examined the number of early gametophores per colony in a time course for 48/72/96 hours. After 48 hrs of BAP treatment, wildtype presented on average 66±18 <4-cell early gametophores (n=7 colonies; ~80

filaments per colony), while *Δric* and *Δrop2Δric* produced more <4-cell early gametophores compared to wildtype (86±8 for *Δric, n=4*; 93±13 for *Δrop2Δric,* n=3, Fig. **3a,b**). In contrast, *Δrop2* revealed a significantly lower amount of <4-cell early gametophores (3±2, n=4) under exactly the same conditions. The number of <4-cell early gametophores in wildtype, *Δric*, and *Δrop2Δric* showed a reduction from 48hrs to 96hrs, whereas *Δrop2* showed an increase from 48hrs to 96hrs (12±9, Fig. **3a,b**), demonstrating a suppression in gametophore initiation.

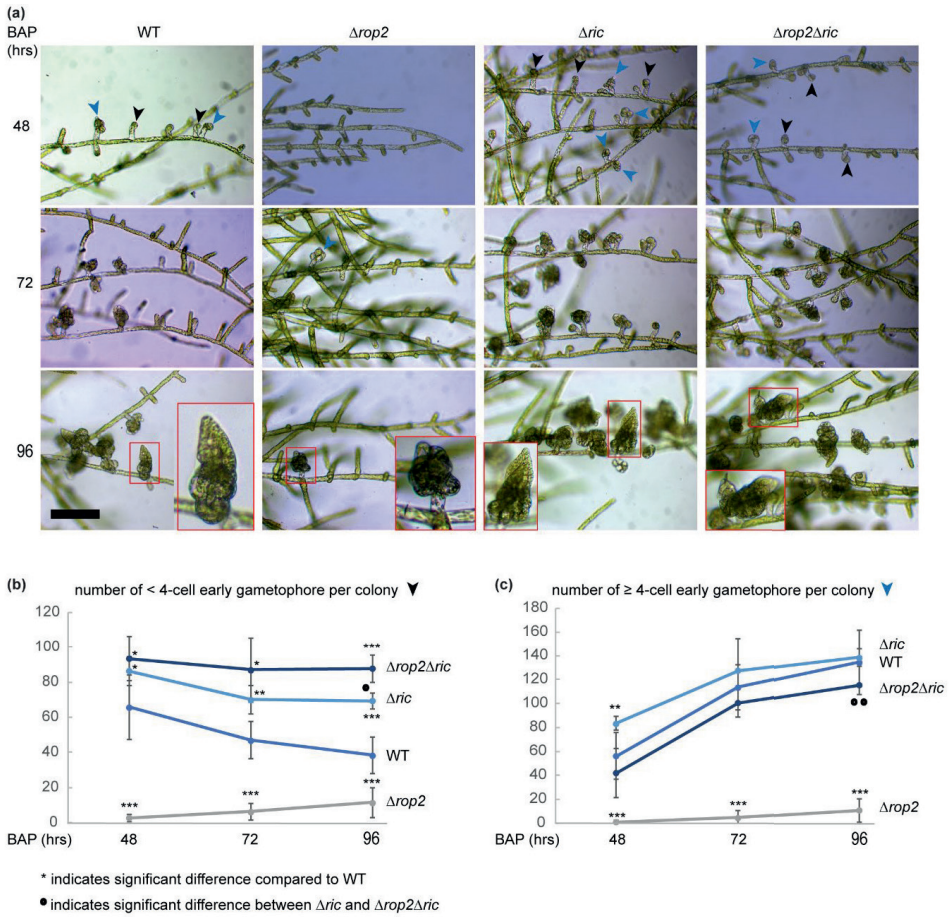

Figure 3. The defective gametophore initiation of *Δrop2* is restored by additively deleting *RIC*.

(a) Representative images of early gametophores induced with BAP treatment at indicated time point. Blue arrowheads indicate early gametophores with more than 4 cells, and black arrowheads indicate early gametophores with less than 4 cells. The example of leafy gametophores observed in wildtype, *Δric* and *Δrop2Δric* after 96 hrs of BAP treatment were depicted and zoomed in the red box; while the biggest early gametophore without leaf structure in *Δrop2* was depicted instead. Scale bar = 0.1 mm.

(b) and (c) Quantification of early gametophores with less than 4 cells (b) and equal or more than 4 cells. N = 7, 4, 4, 3 colonies for wildtype, *Δrop2, Δric,* and *Δrop2Δric*, respectively, and approximately 80 filaments were counted in one colony. * represents a significant difference (p <0.05) in comparison to wildtype, ** = p<0.01, and *** = p <0.001 by Welch's t-test; ● represents a significant difference (p <0.05) in comparison between *Δric* and *Δrop2Δric.* Sample dots at (c) without * or ● markers represented no statistical differences.

Early gametophores with equal or more than 4 cells (≥ 4-cell) were counted and showed an increase from 48 to 96 hrs in all tested lines. 48hrs after induction of gametophores, wildtype displayed 56±19, *Δric* had 83±5, and *Δrop2Δric* had 42±21 ≥ 4-cell early gametophores. In contrast, only 1±1 ≥ 4-cell early gametophores were induced in *Δrop2* (Fig. **3c**). After 96hrs, the number of ≥ 4-cell early gametophores increased to 135±27 in wildtype, 139±7 in *Δric*, and 116±0.7 in *Δrop2Δric*, while *Δrop2* maintained a lower amount of early gametophores (11±10). Moreover, the developing gametophores in wildtype, *Δric*, and *Δrop2Δric* displayed the first leafy structure at 96 hrs after induction, but still, no leafy gametophore could be observed in *Δrop2* (Fig. **3a**, red box). These results demonstrated that ROP2 is required for gametophore initiation and development, while RIC acts as a suppressor since *Δric* and *Δrop2Δric* showed a significantly higher amount of <4-cell early gametophores compared to wildtype. The defective gametophore initiation in *Δrop2* is restored by deleting *RIC*.

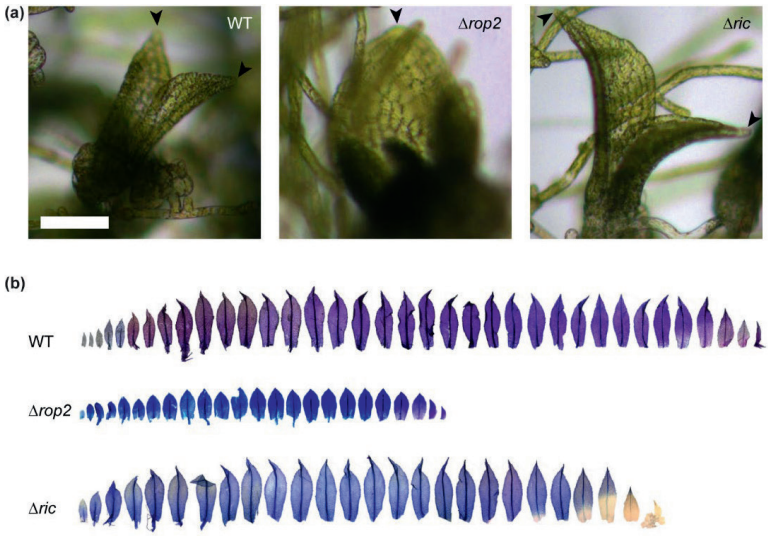

Figure 4. Gametophore development is defective in *rop2* deletion.
(a) Early gametophore development at 7 days posts BAP treatment in indicated lines. Black arrowheads indicate the leaf tip in each line, which is pointy in wildtype and *Δric* but rounded in *Δrop2*. Scale bar = 0.1 mm.
(b) Leaves of indicated lines were dissected from the biggest gametophore in a 6-weeks colony and stained with Toluidine blue.

Gametophore development is defective in *rop2* deletion

In addition to gametophore initiation, we further addressed whether ROP2 was required throughout the development of gametophores until they reach a mature state. We tracked the growth of early gametophores of examined lines *(Δrop2* and *Δric*) until 7 days after BAP treatment. *Δric* developed leafy gametophores that appeared indistinguishable from wildtype gametophores. The leaf expansion of wildtype and *Δric* revealed an elongated leaf shape with a pointy leaf tip (Fig. **4a**, arrowheads). In the *Δrop2* mutant, the few delayed early gametophores still developed into leafy gametophores, which showed a different leaf morphology compared to wildtype leaves. The leaf

shape of *Δrop2* appeared to be rounded without a pointy leaf tip, which reflected an irregular leaf expansion in longitudinal and lateral axis (Fig. **4a**).

To further characterize gametophore development, we analysed leaf shape and numbers in ~6-weeks-old plants of wildtype, *Δrop2,* and *Δric*. In wildtype gametophores, leaves show different morphological characteristics along their longitudinal axis, that can be correlated with gametophore age. Basal leaves (formed in young gametophores) are smaller, have a smooth border and lack a midrib; intermediate leaves (formed in pre-adult gametophores) are bigger (but have not yet reached maximum size), retain the smooth surface and contain a partial midrib; finally the apical leaves (formed in adult gametophores) reach maximum size, have a serrated border and a midrib that goes all along the longitudinal axis. Leaf shape and number in the *Δric* mutant was undistinguishable to wildtype, whereas *Δrop2* exhibited smaller and fewer leaves (Fig. **4b**). In wildtype and *Δric* gametophores, all the stages of leaves and their morphological characteristics described were observed, and there were no significant differences. In contrast, besides being smaller no leaves with apical/adult characteristics were observed in *Δrop2*. After the initial basal leaves, all of the remaining leaves displayed smooth borders and partial midribs. Furthermore, not only their morphology but also their size was comparable to wildtype intermedia/pre-adult leave (Fig. **4b**). These results demonstrated the necessity of ROP2 in leaf development and gametophore maturation.

ROP2 promotes the chloronema-to-caulonema transition in a RIC-independent manner

To address if the decrease in gametophore formation in *Δrop2* may be caused by aberrant filament growth, we characterized filament growth in *Δrop2*. To address if ROP2 is essential for the chloronema-to-caulonema transition, we measured the cell length of the sub-apical cells and the orientation of the first cross wall, since these two parameters have been reported to distinguish chloronema from caulonema cells (Ashton *et al.*, 1979; Coudert *et al.*, 2019). Chloronema cells grow shorter with transverse cross walls, whereas caulonema cells grow longer with oblique cross walls (Ashton *et al.*, 1979). 6-day-old moss filaments of *Δrop2* and *Δrop2Δric* appeared to have shorter cells with transverse cross walls, in contrast to wildtype and *Δric* that formed longer cells with mostly oblique cross walls (Fig. **5a**, white arrowheads.) The cell length of sub-apical cells in *Δrop2* and *Δrop2Δric* were significantly shorter compared to wildtype and *Δric* (n=74, 95±11 µm for *Δrop2;* n=51, 94±13 µm for *Δrop2Δric*; n=42, 134±18 µm for wildtype; n=43, 125±13 µm for *Δric*, Fig. **5b**). The orientation of cross walls in *Δrop2* and *Δrop2Δric* exhibited nearly all transverse patterns while wildtype and *Δric* showed smaller angles reflecting oblique divisions (n=35, 77±13 degree for *Δrop2;* n=31, 74±14 degree for *Δrop2Δric*; n=18, 51±11 degree for wildtype; n=25, 53±9 degree for *Δric*, Fig. **5c**). These results demonstrated that ROP2 is required for facilitating the chloronema-to-caulonema transition in a RIC-independent manner. It is noteworthy that the double mutant *Δrop2Δric* produced numerous early gametophores while its filament growth resembled the defective chloronema-to-caulonema transition in *Δrop2.* This result implies that the defective gametophore initiation in *Δrop2* is not simply caused by the impaired chloronema-to-caulonema transition.

Transcriptional analysis of ROPs and RIC in protonema cells and early gametophores

Loss-of-function analysis of ROPs and RIC demonstrated that ROP2 is required for protonema cell type transition and gametophore initiation, but its functional interplay with RIC specifically manifested during gametophore initiation.

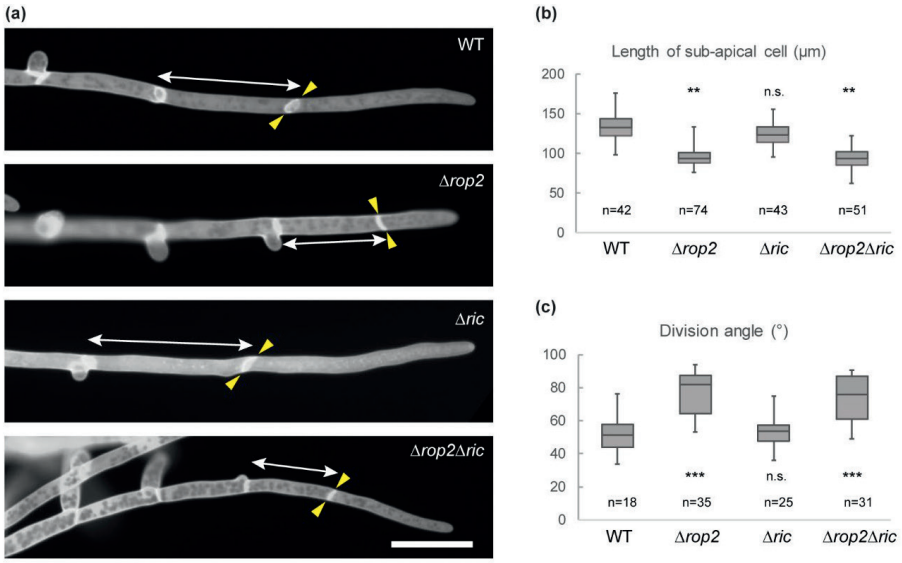

Figure 5. ROP2 promotes the chloronema-to-caulonema transition in a RIC-independent manner.
(a) Representative images of a filamentous cell of indicated lines. 6-days old moss tissues were stained with calcofluor white and imaged using Nikon 80i microscope with UV filter set. The white double arrows depict the sub-cellular lengths, and the yellow arrowheads indicate the cross walls where the division angle was measured. Scale bar = 100 μm.
(b) The length of sub-apical cells and the division angle of the first cross walls (c) as indicated in (a) in relative to the tip cell axis were measured in ImageJ. ** represents a significant difference (p<0.01) and *** = p <0.001 in comparing to WT by Welch's t-test.

To further validate whether a tissue-specific role of the ROP2-RIC interaction in gametophore initiation correlated with the regulation of their expression, we investigated transcript levels of all ROPs and RIC in wildtype protonema tissues and early gametophore-induced tissues. In protonema tissues, transcription level of *ROP3* and *ROP4* were ~7-fold and 3-fold higher than *ROP1* and *ROP2* mRNA levels, while *RIC* transcript was barely detected (Fig. **6a**). Conversely, transcription of the low-expressed *ROP1* and *ROP2* in protonema was up-regulated about 2-fold and *RIC* was induced around 6-fold in early gametophores (BAP treatment for 40 hrs), whereas *ROP3* and *ROP4* transcript levels did not show significant changes (Fig. **6b**). It must be noted that due to technical limitations, some protonema tissue was included in early gametophore-induced tissues during sample collection (Fig. **6c**), which may result in underestimation of the induction of *ROP1*, *ROP2* and *RIC* mRNA in early gametophore-induced tissues. Given that early gametophore formation was induced by BAP, it may be that the up-regulation could be triggered by a direct response to BAP rather than gametophore formation itself. To test if *ROP* and *RIC* are directly induced by BAP, we performed short, exogenous treatment with a higher concentration (10μM) of BAP for 30 minutes. The transcript levels of the *ROPs* and *RIC* showed no significant changes with this BAP treatment, implying that the up-regulation of *ROP1*, *ROP2*, and *RIC* in the early gametophore-induced tissues corresponds to gametophore initiation (Fig. **6d**).

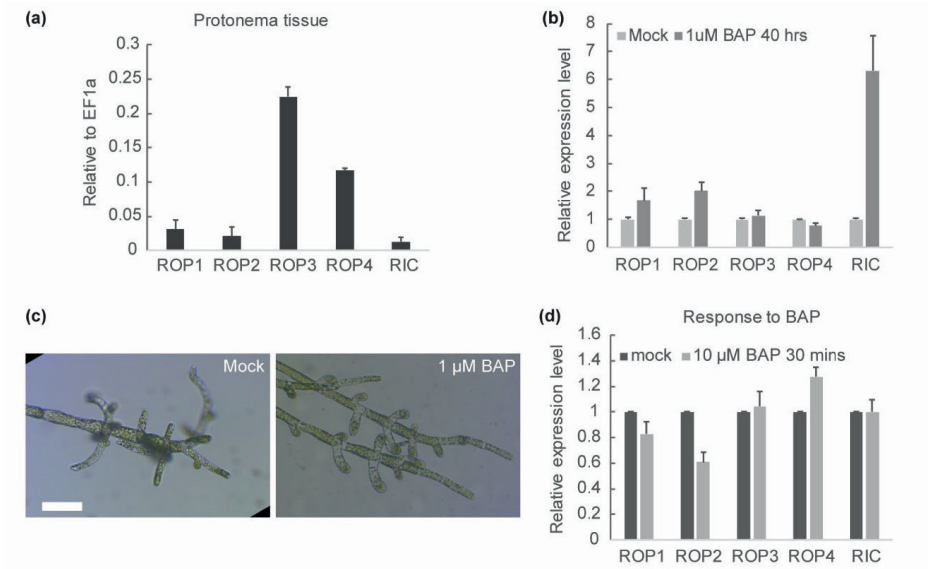

Figure 6. Transcriptional analysis of ROPs and RIC in protonema and early gametophores.

(a) The relative transcription level of ROPs and RIC genes in 7-day-old wild-type (WT) moss protonema tissues was quantified by quantitative real-time PCR analysis, normalized to that of EF1α. Error bars represent s.e.m.

(b) Tissues possess only protonema filament (Mock) and early gametophore-induced filaments (1μM BAP 40 hrs) were collected for RNA extraction and quantitative RT-PCR. The relative expression is first normalized to that of EF1α, and the mock sample was then used as a reference to examine expressional changes upon gametophore induction. Error bars = s.e.m.

(c) Representative images of moss tissues in the absent (mock) and present of 1 μM BAP treatment for 40 hrs. Scale bar = 50 μm.

(d) The relative transcript level of ROPs and RIC genes in response to BAP treatment. 7-day-old WT protonema tissues were transferred to liquid medium supplied with 10 μM BAP for 30 minutes, and moss tissues were directly collected for RNA extraction and qRT-PCR analysis. All expressional levels were first normalized to EF1α and compared to mock control. Error bars represent s.e.m.

Discussion

We report here that ROP2, but not other ROPs, is required to facilitate diverse developmental transitions during the development of the moss *Physcomitrella.* This includes chloronema-to-caulonema transition, gametophore initiation, and gametophore maturation. Among these events, the deletion of *ric* in *Δrop2* restored the defect in gametophore initiation, but not the filamentous transition. The functional involvement of RIC in a ROP2-dependent process correlated well with its transcriptional induction upon gametophore initiation, while *RIC* expression was hardly detected in filamentous tissues. Our data support that a ROP2/RIC interaction module specifically acts in gametophore initiation but not in filament development, and this module is locally active during gametophore initiation. Altogether, here we illustrated novel functions of ROP2 protein in developmental transitions, and also demonstrated a tissue-specific functional interplay of ROP2-RIC during gametophore initiation.

The ROP-RIC signalling pathway may be regulated via transcriptional control during gametophore initiation. We show that the transcript level of *ROP1*, *ROP2*, and *RIC* are up-regulated in 2-cell to 4-cell early gametophores. Induction of *RIC* expression has also been shown in previous microarray expression analysis performed on 4-cell early gametophores (Frank & Scanlon, 2015). In *Arabidopsis*, overexpression of *ROPs* or potential activators belonging to the family of guanine exchange factors (GEFs) results in swollen pollen tubes, and the tip cell swelling is also showed in moss filaments when overexpressing moss ROPs (Li *et al.*, 1999; Gu *et al.*, 2006; Ito *et al.*, 2014). These results suggest that excess ROP activity may lead to cell swelling. Whether the elevated expression of *ROP1*, *ROP2*, and *RIC* in early gametophores accounts for the cell swelling remains elusive.

RIC transcription was induced upon gametophore formation, and phenotypic analysis revealed that the deletion of *RIC* complemented the defect in gametophore initiation of *Δrop2*. These results suggest a functional interplay between ROP2 and RIC. We suspect that RIC-mediated suppression of gametophore initiation is in turn inhibited by its interaction with ROP2, which explains the opposite phenotypes of gametophore initiation in *Δrop2* and *Δric.*

We found that the apical accumulation of ROPs is diffused to the lateral side of the swelling gametophore initial cell. To dissect the causal relationship between ROPs re-localization and cell swelling, proteins that control the ROPs localization upon swelling should be identified. A recent study in root hair growth demonstrates that the ROPs activator GEF3 plays an essential role in positioning ROPs at the emerging root hair initiation domain (Denninger *et al.*, 2019). In early gametophores (the 4-cell stage), transcriptomic analysis reveals that the expression of two moss GEFs are highly activated (Frank & Scanlon, 2015), implying their potential role in regulating ROPs during gametophore initiation.

During filamentous growth, *Δrop2* appeared to impair the chloronema-to-caulonema transition since *Δrop2* filaments showed chloronema characteristics at the point where wildtype and *Δric* already displayed caulonema features instead. This defective transition resembled wildtype plants treated with low concentrations (10nM) of cytokinin (Coudert *et al.*, 2019), implying that the subcellular cytokinin level might be elevated in *Δrop2*. In contrast, auxin has been reported to stimulate caulonema growth (Ashton *et al.*, 1979). Recently, an auxin reporter line in *Physcomitrella* was reported (Thelander *et al.*, 2019), while cytokinin reporter has not yet been presented in moss. To uncover the mechanism underlying the chloronema-to-caulonema transition of *Physcomitrella*, the possible interplay between ROP2 and distinct hormone signalling pathways may be addressed using fluorescent reporters or responsive genes that allow the read-out of cellular cytokinin and auxin levels and signalling in *Δrop2* filaments.

Materials and Methods

Plasmids and cloning procedures

Plasmids used were generated using standard restriction-ligation cloning procedures and were verified by sequencing as described before (de Keijzer *et al.*, 2017). For construction of sYFP tagging constructs for each ROP gene and RIC knockout, regions of approximately 1 kb before and after the start codon of the encoding gene were amplified by PCR and digested with restriction enzymes and ligated into correspondingly digested pNter-sYFP vector for sYFP tagging and ploxP_Hyg vector or ploxP_Bsd for RIC knockout (de Keijzer *et al.*, 2017). Knockout of ROPs and RIC was verified by genotyping PCR.

Plant growth conditions and transformation

Wildtype of *Physcomitrella patens* (Gransden strain) (Ashton & Cove, 1977) was used as a standard line for the observation of bud formation. *Physcomitrella* tissues were routinely grown on BCDAT plates under continuous light at 25°C as described before (Nishiyama *et al.*, 2000). Quantification of gametophore was performed with 3-weeks old colonies of indicated lines grown on the same BCDAT plates. Plasmids were linearized and introduced into the genome by homologous recombination using PEG-mediated protoplast transformation (Nishiyama *et al.*, 2000). Correct insertion events were characterised by PCR.

For general imaging of early gametophores, protonemal tissue was grown on BCD medium in glass bottom dishes (Yamada *et al.*, 2016) for 3 days under continuous white light, then moved to red light (light transmission with wavelength > 600 nm) for another 3 days. After 3days red light growth, the dish was moved back to white light and supplied with ½ liquid BCD medium containing 1µM benzylaminopurine (BAP). Early gametophores were imaged between 30 to 48 hrs after BAP induction. Similar growth condition was performed for gametophore initiation analysis, but the time course of observation was between 48 to 96 hrs. For the analysis of filamentous cell type transition, we used exactly the same growth condition that plant was grown on BCD medium in glass bottom dishes for 6 days, and directly stained with Calcofluor White (10µg/ml) for imaging and quantification.

For gametophore development analysis, moss colonies grown on BCDAT plates with continuous white light illumination for 3 weeks were dissected. For leaf shape characterization, the biggest gametophore was picked from a 6-weeks colony and stained with Toluidine Blue for overnight.

For expressional analysis, wildtype tissue was freshly cultured on BCDAT plate with cellophane for 7 days and collected for RNA extraction and quantitative RT-PCR. For hormone treatment assay, the collected 7-day-old tissues were transferred to liquid BCD medium supplied with 10µM BAP for 30 minutes. For the expressional analysis in early gametophores, the early gametophore formation was synchronized and induced under controlled light and BAP treatment as described before (Aoyama *et al.*, 2012). In brief, plant tissue was cultured on BCDATG (BCDAT medium supply with 0.5% glucose) plate under unilateral red light for 2 weeks, at which the emergence of secondary branch was inhibited. After 2 weeks, plates were released from red light to continuous white light and submerged with liquid ½ BCD medium in the absent or present of BAP supply. Early gametophore formation was induced by BAP treatment, and secondary filaments were developed in the absence of BAP. After 40 hours of treatment, filaments with approximately 8-cells from the tip of a filament were collected for following RNA extraction.

Fluorescence microscopy and staining

For sYFP-ROPs localization characterization, live-cell imaging was performed on a Leica SP8X-SMD confocal microscope equipped with a hybrid single molecule detector (HyD) and an ultrashort pulsed white-light laser (WLL; 50%; 1 ps at 40 MHz frequency). The Leica Application Suite X was used as a software platform and imaging was conducted with a HC PL APO CS2 63x/1.20 water immersion objective, scan speed of 400 Hz and a resolution of 1024 x 1024 pixels and standard acquisition mode of the hybrid detector. sYFP was excited with the 514 nm laser line (10% laser output) of the WLL and the emitted light detected by HyD SMD 1 at 495-550 nm (gain 250). To remove autofluorescence in the YFP-channel (495-550 nm), time-gating was activated on detector HyD SMD 1 at a gate reference

wavelength of 514 nm. For imaging, gate opening times were selected such that no autofluorescence was detectable in the YFP-channel in wildtype tissues as a reference setting. Images were captured with frame averages of eight times. Single median plane focused on the cell outline was captured. All image analysis was performed using ImageJ.

For filamentous cell imaging, tissues were stained with calcofluor white solution right before image acquirement and were imaged on a Nikon Eclipse 80i system equipped with a Uvico-VIS (RappOpto Electronics) light source with HXP R 120 W/45 C VIS-white lamp and halogen lamp for BF transmission. Images were standard made with a 5 Mpx Ds Fi 1 colour camera. Image was conducted with a 10x objective illuminated with a UV filter set (360 nm spectrum).

Statistical analysis

For statistical analysis of gametophore quantification (Fig. **2**), one-way ANOVA and Tukey's HSD test were used. For the measurement of filament phenotyping and the formation of early gametophores (Fig. **3** and Fig. **4**), Welch's t-test was performed.

Acknowledgements

We would like to thank Magdalena Bezanilla (Darthmouth College, USA) for the important materials. The work has been financially supported by the Earth and Life Sciences Division ALW-VIDI (grant number: 864.13.008 to H.T. and J.V.)

Author Contributions

T.K. provided facilities and supporting materials. H.T., A.F., B.S., J.V., and V.W. planned and designed the research. H.T. and A.F. generated experimental materials. H.T. and A.F. performed experiments and conducted data analysis. H.T., A.F., V.W., J.V., and B.S. wrote the manuscript.

References

Aoyama T, Hiwatashi Y, Shigyo M, Kofuji R, Kubo M, Ito M, Hasebe M. 2012. AP2-type transcription factors determine stem cell identity in the moss Physcomitrella patens. *Development* **139**(17): 3120-3129.

Ashton N, Cove D. 1977. The isolation and preliminary characterisation of auxotrophic and analogue resistant mutants of the moss, Physcomitrella patens. *Molecular and General Genetics MGG* **154**(1): 87-95.

Ashton NW, Grimsley NH, Cove DJ. 1979. Analysis of gametophytic development in the moss, Physcomitrella patens, using auxin and cytokinin resistant mutants. *Planta* **144**(5): 427-435.

Bascom JC, Burkart GM, Mallett DR, O'Sullivan JE, Tomaszewski AJ, Walsh K, Bezanilla M. 2019. Systematic survey of the function of ROP regulators and effectors during tip growth in the moss Physcomitrella patens. *J Exp Bot* **70**(2): 447-457.

Burkart GM, Baskin TI, Bezanilla M. 2015. A family of ROP proteins that suppress actin dynamics and are essential for polarized growth and cell adhesion. *J Cell Sci*: jcs. 172445.

Chen X, Friml J. 2014. Rho-GTPase-regulated vesicle trafficking in plant cell polarity. *Biochemical Society Transactions* **42**(1): 212-218.

Coudert Y, Novák O, Harrison CJ. 2019. A KNOX-Cytokinin Regulatory Module Predates the Origin of Indeterminate Vascular Plants. *Current Biology* **29**(16): 2743-2750. e2745.

Craddock C, Lavagi I, Yang Z. 2012. New insights into Rho signaling from plant ROP/Rac GTPases. *Trends Cell Biol* **22**(9): 492-501.

de Keijzer J, Kieft H, Ketelaar T, Goshima G, Janson ME. 2017. Shortening of microtubule overlap regions defines membrane delivery sites during plant cytokinesis. *Current Biology* **27**(4): 514-520.

Denninger P, Reichelt A, Schmidt VA, Mehlhorn DG, Asseck LY, Stanley CE, Keinath NF, Evers J-F, Grefen C, Grossmann G. 2019. Distinct RopGEFs successively drive polarization and outgrowth of root hairs. *Current Biology* **29**(11): 1854-1865. e1855.

Eklund DM, Svensson EM, Kost B. 2010. Physcomitrella patens: a model to investigate the role of RAC/ROP GTPase signalling in tip growth. *J Exp Bot* **61**(7): 1917-1937.

Etienne-Manneville S. 2004. Cdc42-the centre of polarity. *Journal of Cell Science* **117**(8): 1291-1300.

Feiguelman G, Fu Y, Yalovsky S. 2018. ROP GTPases structure-function and signaling pathways. *Plant Physiol* **176**(1): 57-79.

Frank MH, Scanlon MJ. 2015. Cell-specific transcriptomic analyses of three-dimensional shoot development in the moss Physcomitrella patens. *Plant J* **83**(4): 743-751.

Fu Y, Gu Y, Zheng Z, Wasteneys G, Yang Z. 2005. Arabidopsis interdigitating cell growth requires two antagonistic pathways with opposing action on cell morphogenesis. *Cell* **120**(5): 687-700.

Fu Y, Wu G, Yang Z. 2001. Rop GTPase–dependent dynamics of tip-localized F-actin controls tip growth in pollen tubes. *The Journal of Cell Biology* **152**(5): 1019-1032.

Fu Y, Xu T, Zhu L, Wen M, Yang Z. 2009. A ROP GTPase signaling pathway controls cortical microtubule ordering and cell expansion in Arabidopsis. *Current Biology* **19**(21): 1827-1832.

Gu Y, Fu Y, Dowd P, Li S, Vernoud V, Gilroy S, Yang Z. 2005. A Rho family GTPase controls actin dynamics and tip growth via two counteracting downstream pathways in pollen tubes. *J Cell Biol* **169**(1): 127-138.

Gu Y, Li S, Lord EM, Yang Z. 2006. Members of a novel class of Arabidopsis Rho guanine nucleotide exchange factors control Rho GTPase-dependent polar growth. *The Plant Cell* **18**(2): 366-381.

Gu Y, Vernoud V, Fu Y, Yang Z. 2003. ROP GTPase regulation of pollen tube growth through the dynamics of tip-localized F-actin. *J Exp Bot* **54**(380): 93-101.

Harrison CJ, Roeder AH, Meyerowitz EM, Langdale JA. 2009. Local cues and asymmetric cell divisions underpin body plan transitions in the moss Physcomitrella patens. *Curr Biol* **19**(6): 461-471.

Ito K, Ren J, Fujita T. 2014. Conserved function of Rho-related Rop/RAC GTPase signaling in regulation of cell polarity in Physcomitrella patens. *Gene* **544**(2): 241-247.

Kremers G-J, Goedhart J, van Munster EB, Gadella TW. 2006. Cyan and yellow super fluorescent proteins with improved brightness, protein folding, and FRET Förster radius. *Biochemistry* **45**(21): 6570-6580.

Lee YJ, Szumlanski A, Nielsen E, Yang Z. 2008. Rho-GTPase–dependent filamentous actin dynamics coordinate vesicle targeting and exocytosis during tip growth. *The Journal of Cell Biology* **181**(7): 1155-1168.

Li H, Lin Y, Heath RM, Zhu MX, Yang Z. 1999. Control of pollen tube tip growth by a Rop GTPase–dependent pathway that leads to tip-localized calcium influx. *The Plant Cell* **11**(9): 1731-1742.

Lin D, Ren H, Fu Y. 2015. ROP GTPase-mediated auxin signaling regulates pavement cell interdigitation in Arabidopsis thaliana. *Journal of integrative plant biology* **57**(1): 31-39.

Molendijk AJ, Bischoff F, Rajendrakumar CSV, Friml J, Braun M, Gilroy S, Palme K. 2001. Arabidopsis thaliana Rop GTPases are localized to tips of root hairs and control polar growth. *The EMBO Journal* **20**(11): 2779-2788.

Moody LA. 2019. The 2D to 3D growth transition in the moss Physcomitrella patens. *Curr Opin Plant Biol* **47**: 88-95.

Nagawa S, Xu T, Lin D, Dhonukshe P, Zhang X, Friml J, Scheres B, Fu Y, Yang Z. 2012. ROP GTPase-dependent actin microfilaments promote PIN1 polarization by localized inhibition of clathrin-dependent endocytosis. *PLoS biology* **10**(4): e1001299.

Nishiyama T, Hiwatashi Y, Sakakibara K, Kato M, Hasebe M. 2000. Tagged mutagenesis and gene-trap in the moss, Physcomitrella patens by shuttle mutagenesis. *DNA research* **7**(1): 9-17.

Thelander M, Landberg K, Sundberg E. 2019. Minimal auxin sensing levels in vegetative moss stem cells revealed by a ratiometric reporter. *New Phytologist*.

Vidali L, Bezanilla M. 2012. Physcomitrella patens: a model for tip cell growth and differentiation. *Curr Opin Plant Biol* **15**(6): 625-631.

Wu G, Gu Y, Li S, Yang Z. 2001. A Genome-Wide Analysis of Arabidopsis Rop-Interactive CRIB Motif–Containing Proteins That Act as Rop GTPase Targets. *The Plant Cell* **13**(12): 2841-2856.

Xu T, Dai N, Chen J, Nagawa S, Cao M, Li H, Zhou Z, Chen X, De Rycke R, Rakusová H. 2014. Cell surface ABP1-TMK auxin-sensing complex activates ROP GTPase signaling. *Science* **343**(6174): 1025-1028.

Xu T, Wen M, Nagawa S, Fu Y, Chen J-G, Wu M-J, Perrot-Rechenmann C, Friml J, Jones AM, Yang Z. 2010. Cell surface-and rho GTPase-based auxin signaling controls cellular interdigitation in Arabidopsis. *Cell* **143**(1): 99-110.

Yalovsky S, Bloch D, Sorek N, Kost B. 2008. Regulation of membrane trafficking, cytoskeleton dynamics, and cell polarity by ROP/RAC GTPases. *Plant Physiol* **147**(4): 1527-1543.

Yamada M, Miki T, Goshima G 2016. Imaging mitosis in the moss Physcomitrella patens. *The Mitotic Spindle*: Springer, 263-282.

Yang Z. 2002. Small GTPases: versatile signaling switches in plants. *The Plant Cell* **14**(suppl 1): S375-S388.

Yang Z, Fu Y. 2007. ROP/Rac GTPase signaling. *Curr Opin Plant Biol* **10**(5): 490-494.

Zhou Z, Shi H, Chen B, Zhang R, Huang S, Fu Y. 2015. Arabidopsis RIC1 severs actin filaments at the apex to regulate pollen tube growth. *The Plant Cell*: tpc. 114.135400.

Chapter 5

The directionality of wounding-induced cell reprogramming in moss leaves

Han Tang[1,2], Koen Hoogendoorn[2], Tijs Ketelaar[1], and Joop E.M. Vermeer[3,4]

[1] Laboratory of Plant Developmental Biology, Wageningen University & Research, Wageningen, The Netherlands
[2] Laboratory of Cell Biology, Wageningen University & Research, Wageningen, The Netherlands
[3] Plant Cell Biology, Department of Plant and Microbial Biology and Zurich Basel Plant Science Center, University of Zürich, 8008 Zürich, Switzerland
[4] Present address: Laboratory of Cell and Molecular Biology, Institute of Biology, University of Neuchâtel, 2000 Neuchâtel, Switzerland

Abstract

Cell regeneration is a widely conserved response to repair parts of injured bodies or to form new organs in both animals and plants. At the initial stage of regeneration, cells need to reprogram their identity, followed by cell proliferation and re-differentiation. Hormones and wounding itself have been identified as key elements for cell reprogramming. In many cases, cell regeneration takes place at wounding sites, suggesting that the wounding may be a primary trigger to initiate cell reprogramming. However, how cells sense and transmit wound stimuli to induce cell reprogramming remains largely unknown. In this study, we used laser ablation to precisely damage cells in phyllids, the leaf-like structure of the moss *Physcomitrella patens* and observed the response of adjacent cells. We found that adjacent cells respond to wounding by cell reprogramming with the acquisition of new cell characteristics and cell cycle reactivation. Most observed cell reprogramming occurred in the cells directly in contact with the wounding site. Cell reprogramming preferentially occurred in the cells positioned axially with respect to the wounding site, demonstrating that cell reprogramming (1) is locally induced and (2) has a directional tendency. To further dissect the underlying mechanism of this directionality, we monitored cytoskeleton dynamics since it has been reported that the cytoskeleton of cells surrounding the wounding site rearranges in response to wounding. We observed that in these cells both microtubule and actin filaments rearranged. The reorganization of the cytoskeleton was only observed in the parts of the cells that were in direct contact with the wounding site and not in other parts of the cells. However, all surrounding cells showed the cytoskeletal reorganization, which was inconsistent with the observed axial directionality of cell reprogramming. The differences in the directionalities of the cytoskeletal reorganization and the cell reprogramming suggest that the cell reprogramming might not be correlated with cytoskeleton reorganization, but rather depends on other mechanisms. One possible mechanism could be the modulation of symplastic connections to regulate intercellular transport of yet unidentified biochemical cues.

Introduction

In animals and plants, regeneration is a widely conserved response to repair parts of an injured body or to form new organs (Sugimoto *et al.*, 2011). Plants mainly regenerate in two modes: *de novo* organogenesis and somatic embryogenesis. During *de novo* organogenesis, plants regenerate to form new organs from either *in vivo* wounding sites or *in vitro* explanted tissues (Ikeuchi *et al.*, 2016). Wounding in most studied cases is induced by cutting or cell death induced by laser ablation (Ishikawa, M. *et al.*, 2011; Ikeuchi *et al.*, 2016; Sato *et al.*, 2017). The differentiated cells on the wounding sites reprogram to non-differentiated callus and subsequently develop into new meristem cells that ultimately generate new organs. The other mode is somatic embryogenesis, where a somatic cell is isolated as a single cell and further develops into a zygote and embryo-like structure, which regenerates into a whole plant in the final step of the process. In both types of regeneration, a cell needs to reprogram its identity from a somatic cell to a stem cell that possesses totipotency. Subsequently, new organs can be further regenerated from the stem cell following cell divisions and differentiation (Ikeuchi *et al.*, 2016).

Plant cell reprogramming can be induced by hormone treatment and wounding at different levels. In both *de novo* organogenesis and somatic embryogenesis, treatment with a specific ratio of the phytohormones auxin and cytokinin has been demonstrated to trigger callus formation followed by

regeneration in distinct species (Green & Phillips, 1975; Novak *et al.*, 1989). Generally, treatment with a high ratio of auxin to cytokinin leads to root regeneration; while a high ratio of cytokinin to auxin induces shoot formation (Skoog & Miller, 1957). Interestingly, in the presence of hormones without additional wounding, the regeneration rate is much lower compared to when the hormone treatments are combined with wounding (Iwase *et al.*, 2015). This suggests that wounding enhances the reprogramming efficiency/frequency. In addition, plant cell reprogramming can also be induced by wounding in the absence of exogenous hormone treatment (Sugiyama, 2015). The distribution of endogenous auxin and cytokinin shows a characteristic response to wounding (Liu *et al.*, 2014). Upon wounding in the *Arabidopsis* leaf, auxin starts to accumulate at the wounding site and the amount of auxin gradually increases while new roots regenerate from the cutting site of the wounded leaf. Another study demonstrated that both auxin and cytokinin are enriched in the grafting junction where two cuts are reconnected through cellular reprogramming (Melnyk *et al.*, 2015). In addition to auxin and cytokinin, the wounding-response hormone jasmonic acid has been shown to fast and transiently increase at the wounding site in various plant species (Ahkami *et al.*, 2009).

At the molecular level, one APETALA2 (AP2)-type transcriptional regulator, *WOUND-INDUCED DEDIFFERENTIATION1* (*WIND1*) has been identified as a critical factor for wound-induced reprogramming. *WIND1* expression is activated upon wounding and promotes callus formation (Iwase *et al.*, 2011). Transient over-expression of *WIND1* induces callus formation that is able to regenerate shoots and roots in the absence of auxin and cytokinin, suggesting that WIND1 is sufficient to reprogram somatic cells. The direct target gene of WIND1 is identified as ENHANCER OF SHOOT REGENERATION1 (ESR1), which encodes another AP2/ERF transcription factor in *Arabidopsis*. Upon wounding, the strong activation of ESR1 by WIND1 is crucial for callus formation and shoot regeneration (Iwase *et al.*, 2017). However, how somatic cells perceive wounding as a trigger to activate WIND1 and induce subcellular responses for reprogramming still remains elusive.

The difficulty to mechanistically study wounding-induced cell reprogramming is to precisely damage target cells without disturbing surrounding cells. Since the surrounding cells are the potential candidates for later cell reprogramming, the reprogramming should be the consequence of wounding-induced signal transduction rather than a side effect of the wounding procedure. Thus, to investigate wounding-induced cell reprogramming, two essential factors are the capacity of somatic cells to undergo reprogramming and a controllable, precise wounding system.

In this study, we used the moss *Physcomitrella patens* as our model system. It has long been known that the phyllids (leafy tissue, hereafter refer to leaves) of *Physcomitrella* are capable of reprogramming from somatic leaf cells into meristematic protonema cells (Cove & Knight, 1993). The single-cell layer feature of the moss leaves allowed us to use laser ablation to precisely wound cells without disturbing surrounding cells. Additionally, the 2-dimensional structure of the leaves makes it straightforward to observe cellular responses to wounding and to follow subsequent cellular reprogramming. Finally, the lattice of cell profiles of the *Physcomitrella* leaves made it possible to determine the directionality of distinct cellular responses, which would be challenging in puzzle-shaped pavement cells in *Arabidopsis* leaves or the multiple cell layers present in most tissues of vascular plants.

After ablation of cells in excised leaves, we found that two major types of cell reprogramming occurred resulting in the reestablishment of tip growth and cell division. The tip-growing cell has

been verified to result from a cell identity change from leaf cell to meristematic protonema cell (Ishikawa, Masaki *et al.*, 2011), whereas cell divisions appear to result from a direct reactivation of the cell cycle. Additionally, both types of cellular responses were mostly observed in the surrounding cells in contact with the wounding site and showed a specific axial directionality.

The observed axial directionality of cells that acquire new cellular characteristics as protonema cells implied that wounding may induce different responses in axial cells compared to the lateral cells. The most obvious difference between axial cells and lateral cells is the surface area of the interface with the wounding site. Therefore, one possible explanation for this difference may result from different levels of mechanical force perception from the ablated cells. It has been shown in *Arabidopsis* that the cell surrounding ablated cells reorganize their cortical microtubule cytoskeleton in response to the changes in the mechanical stress detected by these cells (Hamant *et al.*, 2008). Therefore, we investigated whether the cytoskeleton in moss reacts in a similar way to ablation of cells in the middle of the leaf. In addition, we were curious whether cytoskeleton dynamics differed in the axial cells compared to the lateral cells. We observed that the actin and microtubule cytoskeleton transiently reorganized towards the wounding site in both axial and lateral cells directly surrounding the wounded cells. Taken together, our work demonstrates that wounding-induced cell reprogramming has an axial directionality in moss leaves, which seems not to be correlated with a transient reorganization of the cytoskeleton in the surrounding cells.

Results

Laser ablation as a precise system to locally wound *Physcomitrella* leaves

To investigate the nature of wounding-induced cell reprogramming, a controllable wounding system is essential. Excised gametophore leaves without additional wounding have been shown to regenerate from the cut edge, however, the regeneration appeared to occur randomly in a few cells facing the cut site (Ishikawa, Masaki *et al.*, 2011). In our hands, the manual control of excision using a surgical blade or scissors was not precise. This made it very difficult to predict which cells could have the potential to regenerate until visible morphological changes or expression of a protonema-specific fluorescent marker occurred. To improve the wounding system to be able to investigate cell reprogramming, we set-up a laser-ablation system to precisely and locally generate wounding sites in the middle of excised *Physcomitrella* leaves. Taking advantage of the single-cell layer architecture of *Physcomitrella* leaves, we were able to ablate a rectangular area of cells without damaging any other perpendicular cells (Fig. **1**).

Preliminary tests regarding the size of the ablation area revealed that there was no difference between ablating 3, 6, and 12 cells in order to be able to trigger cell reprogramming. However, single cell ablation turned out not to be sufficient to induce cell reprogramming in cells adjacent to the wounding site. Since the shape of the 3-cell area was not symmetric and 12-cell areas were technically more difficult to ablate, we settled on a 6-cell area for the following experiments. To avoid any side effects from the excision itself, the target area to be ablated was chosen at about one-third of the leaf length from the tip of the excised leaf to keep it at a fair distance from the cut site. We never observed any reprogramming in the target area of excised leaves that were not exposed to ablation, indicating that induction of cell reprogramming mainly resulted from ablation wounding. This observation excluded the possibility that the reprogramming in the target area was influenced by factors other than the laser ablation.

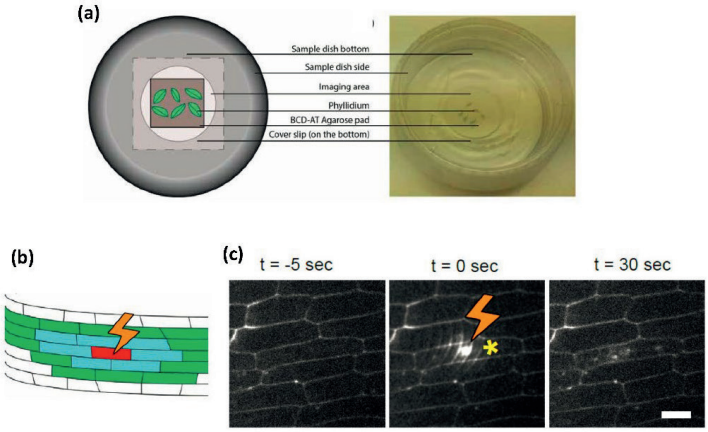

Fig. 1 System development to generate the precise wounding site in moss leaves by laser ablation.
(a) Schematic and actual overview of laser ablation sample. Excised leaves from 4-weeks-old gametophore were deposited on an agar block, which was then placed upside down in the middle of an imaging dish with coverslip bottom. The outer area was filled in with medium for nutrient supply.
(b) Schematic overview of an ablation site. The area around the ablation site was colour coded with the ablated cell in red, the first radial surrounding layer in cyan and the second surrounding layer in green.
(c) Example images of laser ablation site. Cell outlines of one moss leaf were stained with propidium iodide and observed at t=0 by spinning disk microscopy. The ablated cell in the middle panel was indicated by a yellow asterisk, and the bright dot showed the target site of the laser beam. Auto-fluorescence emitted from the ablated cell was shown in the right panel. T = 0 is the timing of ablation, scale bar = 10 μm.

For successful laser ablation followed by live-cell imaging, it was imperative that an excised leaf was as flat as possible. To achieve a flat imaging plane, leaves had to be immobilized, which made incubation in liquid medium impossible. After experimentation with different sample preparation methods to flatten leaves as much as possible, we s selected a method which involved placed 5-10 excised leaves on a small block of solidified growth medium using 3% agar. The agar block with the excised leaves was then carefully transferred to an imaging chamber equipped with a coverslip on a bottom hole, which makes it suitable for observation on an inverted microscope (Fig. **1a**). Gently placing the agar block against the coverslip resulted in flattened leaves between the agar block and the coverslip. The bottom of the imaging chamber not covered by the agar block was filled with warm growth medium containing agar that connects with the agar block for nutrients supply and humidity maintenance. This setup allowed us to ablate and observe the leaves for up to at least five consecutive days without any visible detrimental effects. We used this setup to precisely wound an area of six cells in detached leaves. To minimize possible heat stress to adjacent cells, we targeted the cell-cell junctions within the six-cell area, which resulted in an efficient wounding of only the targeted cells. Cell death was detectable by leakage of cellular contents, burst of detectable organelles and an increase in auto-fluorescence of dead cells. (Fig. **1b,c**). Therefore, we were able to precisely target cells to kill and clearly recognize them. Once cell death was confirmed in the ablated cells, we focused on the cellular responses of the surrounding cells.

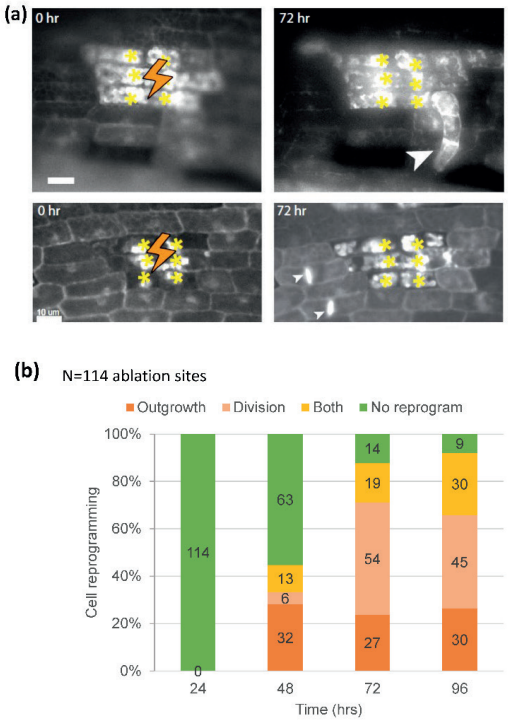

Fig. 2. Laser ablation induces surrounding cells to reprogram by tip growth or division.
(a) Representative images of six-cells ablation site. Fluorescence-tagged LifeAct-GFP mCherry-Tubulin line was used. Due to the interference of autofluorescence emitted from chloroplast in the red channel, here only green channel is shown. T=0 is the timing of laser ablation where ablated cells emitted strong auto-fluorescence was marked by yellow asterisks. Cell reprogramming recognized by tip cell outgrowth or newly formed cell division planes was shown with enriched LifeAct-GFP on the division planes as white arrowheads indicated. Scale bar = 10 µm.
(b) Quantitative result of cell reprogramming in the first radial layer of surrounding cells. The occurrence of cell reprogramming was monitored every 24 hours post ablation, where the occurrence of tip cell outgrowth, new division event, and the appearance of tip growth concurrent with new divisions was presented in the stacked bars, respectively. N=114 ablation sites in >8 independent experiments. The sample numbers for each category were marked in the bar with the proportional indication in the y-axis.

Wounding-induced cell reprogramming is a local and directional response

During leaf cell reprogramming at the cut edge, it has been demonstrated that this process induces a re-activation of the cell cycle and the acquisition of protonema characteristics such as tip cell growth (Ishikawa, Masaki *et al.*, 2011; Sugiyama, 2015). To determine whether the laser ablation of a six-cell area in the middle of an excised leaf could induce cell reprogramming in the surrounding cells, we monitored whether these cells would undergo cell division or re-establish tip growth. The latter would indicate that leaf cells change their identity from a leaf cell to a protonema cell and also re-activation of the cell cycle, whereas the cell division implies re-activation of their cell cycle. These two cellular responses were considered as representative outcomes of the cell reprogramming (Fig. **2a**). Four days after laser ablation, we observed that in most samples, at least one cell surrounding the wounding site had responded to the ablation. In 26% of the cases, which displayed tip cell growth characteristics, and 40% of the cases showed new cell divisions (N=114, Fig. **2b**). Notably, another 26% of the reprogramming cell appeared to proceed both tip cell growth and cell division. In some cases (30 out of 114, 26%) we noticed that not only one, but multiple surrounding cells underwent reprogramming. In sum, 92% of total examined ablation samples revealed wounding-induced cell division reactivation and/or protonema outgrowth.

Next, we asked whether every surrounding cell has an equal chance to undergo cellular reprogramming. To test this, we counted the number of reprogrammed cells and the total amount of surrounding cells in the first and second radial layers, respectively. Then we calculated the

reprogramming probability by dividing the number of reprogramming cells by the total amount of surrounding cells in the first and second radial layers, separately. We found that the probability of cellular reprogramming in the first radial layer of surrounding cells was significantly higher than that in the second layer (Fig. **3a**, student t-test, 20% and 5% for the first and second radial layer of cells). The radial layer of surrounding cells was demonstrated in the drawn ablation site outline at the right upper corner of Figure 3a. The probability of cellular reprogramming in the non-ablation leaves was used as a control, which revealed that almost no reprogramming occurred in these cells (Fig. **3a**).

Next, we asked if there is a directional tendency in wounding-induced cell reprogramming. This directionality was scored by measuring the angle between the centre of the reprogramming cell and the centre of the wounding site. We reoriented the leaf images with the leaf tip toward the right and drew a line between the centre of the reprogramming cell and ablation site. The angle between these two lines was measured (Fig. **3b**). This revealed that the cellular reprogramming in the first radial layer of surrounding cells showed an apparent directionality toward the proximal-distal axis in relation to the ablation site. In other words, the cells located on both apical sites of the ablation area showed a significantly higher chance to reprogram (Fig. **3b**). Taken together, these results suggest that wounding-induced cell reprogramming is a local and directional response.

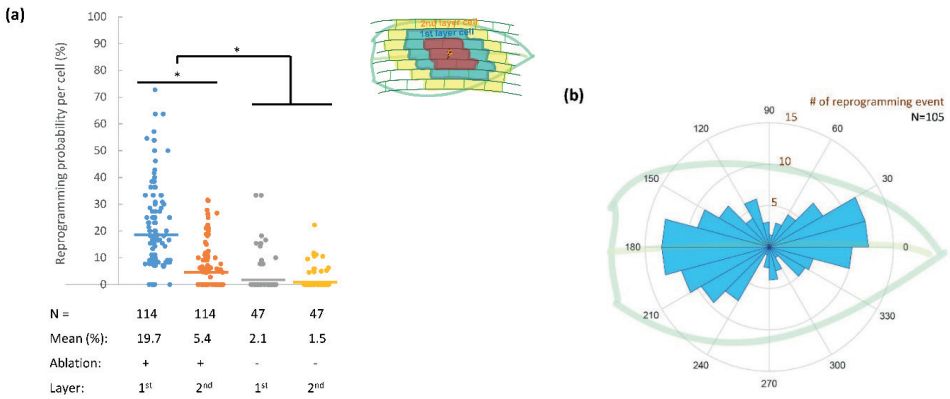

Fig. 3. Wounding-induced cell reprogramming is locally induced with axial directionality.
(a) Among 114 ablation sites and 47 non-ablated sites as control, reprogramming probability per cell was calculated in the first and second radial layers of surrounding cells, which were represented in blue and yellow in the drawing figure on the right corner panel. The number of reprogrammed cells was divided by the total number of surrounding cells in every single leaf to give the probability. * represents a significant difference ($P < 0.05$) between three means of each dataset using Student's two-tailed t-tests, and the horizontal line represented the mean of each group. The schematic representation of a leaf with laser ablation is shown at top-right panel. Red area in the middle marks laser ablation site; the blue area marks the first radial layer of surrounding cells; and the yellow area depicts the second radial layer of surrounding cells.
(b) Distribution of angles of reprogramming cells. All the ablated leaves were re-oriented to place the tips of leaves toward the right as 0 degrees, as shown in the blue outline depicted the leafy shape, thereafter the angle between the centre of ablation site and the reprogramming cells were measured. Numbers marked around the graph indicated the degree, and the number in brown represented the frequency of reprogramming events.

The markers of the microtubule and actin cytoskeleton locally and transiently accumulate on the cell surface facing toward ablation-killed cells

What causes the axial directionality of the wounding-induced cell reprogramming? The most apparent difference between axial and lateral cells was the length of the interface in contact with the ablation site. This area was shorter in axial cells compared to the lateral cells. Because mechanical stimulation on adjacent cells resulting from laser ablation has been shown in *Arabidopsis* (Hamant *et al.*, 2008; Sampathkumar *et al.*, 2014), it was expected that the axial and lateral cells perceived a mechanical stimulus caused by laser ablation. Due to the difference in interface length with the ablation site, it is plausible that the axial and lateral cells perceive different levels of mechanical stimuli. This primary difference in sensing of mechanical perturbation may ultimately lead to the directional tendency of the cell reprogramming. The mechanical perturbation can be visualized through the rearrangement of the cytoskeleton, as reported for *Arabidopsis* pavement cells and cells within the apical meristem (Hamant *et al.*, 2008; Sampathkumar *et al.*, 2014) Therefore, we used fluorescent markers to monitor the responses of both microtubule and actin filaments in the first radial layer of surrounding cells during laser ablation.

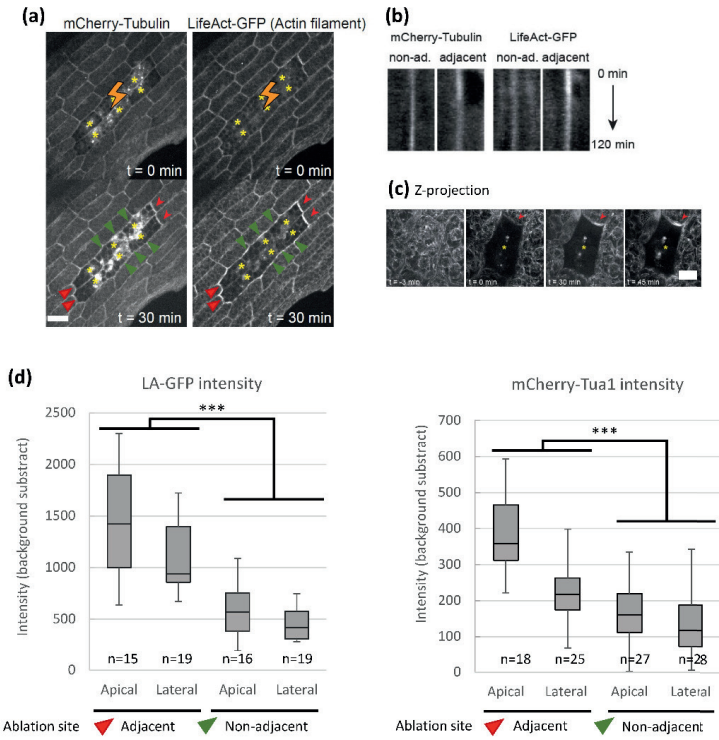

Fig. 4. Signals of cytoskeletal markers in the first radial layer of surrounding cells locally and transiently accumulate on the interface in contact with the ablated site.

(a) Representative images of microtubule marker mCherry-α-tubulin and actin filaments marker LifeAct-GFP in response to laser ablation. Laser ablation was applied at t = 0 min to the target cells marked by yellow asterisks. The signals of both cytoskeletal markers were enriched in the interface in contact with the ablation site of the

first radial layer of surrounding cells, of which the red arrowheads depicted the accumulation in axial cells and the green arrowheads depicted that in lateral cells. Scale bar = 10 µm.
(b) Representative kymograph of mCherry-α-Tubulin and LifeAct-GFP in adjacent cells and non-adjacent cells was presented by depicting a line perpendicularly cross the cell membrane of a randomly chosen non-adjacent cell versus an adjacent axial cell as indicated by the red arrowheads in (a), where the signal in the middle of kymograph revealed the appearance of indicated cytoskeleton on the membrane along time course as indicated. Both signals appeared to accumulate on the membrane of the adjacent cell for around 40 mins and diminished in the end, while no obvious enrichment was shown in the non-adjacent cell.
(c) Max projection of z-stacked images of LifeAct-GFP signal before and after laser ablation. The ablated cell was marked by a yellow asterisk, and the accumulation of LifeAct-GFP signal was indicated by the red arrowhead. Scale bar = 5 µm.
(d) The quantitative intensity of both cytoskeletal markers was measured by drawing lines (~10 µm) along with the cell membrane of randomly chosen non-adjacent and adjacent cells with the indicated sample number. The intensity was measured at 30 mins post ablation. Both microtubule and actin filaments presented differences in non-adjacent and adjacent cells with statistical significance. The horizontal line in the box denotes the median value of all measured area. *** represents a significant difference (P <0.001) between non-adjacent and adjacent cells datasets using Student's two-tailed t-tests.

We observed that the markers of both microtubules and actin filaments in the first radial layer of surrounding cells locally accumulated on the cell periphery facing the ablation site (Fig. **4a**). This re-localization of the cytoskeletal markers only occurred in the first radial layer of surrounding cells, and the localization pattern returned back to the pre-ablation situation after two hours (Fig. **4b**). To visualize the fine structure of actin filaments in response to wounding, we carefully observed the marker of actin filaments using 3D-imaging tracked before and after laser ablation (Fig. **4c**). Notably, all cells in the first radial layer surrounding the ablation site revealed the accumulation of cytoskeletal markers on the interfaces with the ablation site without showing any apparent directionality (Fig. **4d**). In contrast to cell reprogramming, the response of the cytoskeletal markers to laser ablation is a quick, transient, and non-directional effect occurring only in the first radial layer of surrounding cells. Although both the cell reprogramming and cytoskeletal rearrangement occurred mainly in the first radial layer cells, the difference in directionality may suggest that the cytoskeleton response is not related to the triggering of cell reprogramming, but rather a direct and transient response to mechanical stimulation.

Discussion

In this study, we developed an experimental system to precisely wound moss leaf cells by laser ablation, which induced a cellular reprogramming into tip growing protonema cells or reactivated the cell cycle in the cells surrounding the wounding site. Both types of observed responses were shown to have an axial directionality. Indeed, moss leaf cells are capable of reprogramming and it was shown that cellular reprogramming in one isolated leaf cell inhibits the reprogramming capacity of its neighbour (Sato *et al.*, 2017). This inhibitory effect revealed a similar axial directional tendency as the induction of reprogramming described in the current study. Adjacent cells in contact with a reprogramming cell in the axial side have a lower chance to reprogram in than that in the lateral side (Sato *et al.*, 2017), suggesting that the transduction of inhibitory signals may also possess an axial directionality. These results suggest that in *Physcomitrella*, both the induction and repression of cellular reprogramming possesses a directionality. What could determine the directionality? We monitored the quick wounding response as revealed by rearrangement of the cytoskeleton, which

has been shown to rearrange due to mechanical stimulation of surrounding cells (Hamant *et al.*, 2008; Sampathkumar *et al.*, 2014). If this quick response of the cytoskeleton rearrangement primes the cells to reprogram, it should occur in a similar axial directional pattern. However, it turned out that the quick cytoskeleton rearrangement response did not display any obvious directional tendency. Although there is a clear polarization of both the actin and microtubule markers towards the wounding site, the resolution of our images does not exclude the accumulation of cytoplasm that contains unbound markers rather than localized polymerization responses. This suggests that the cytoskeleton rearrangement most likely is not the trigger for the directional cellular reprogramming.

What other mechanisms could underlie this directionality of cellular reprogramming? One possibility could be the distribution of the phytohormones auxin and cytokinin, two critical hormones for cell regeneration in tissue cultures (Skoog & Miller, 1957). The flux of auxin mainly depends on the distribution of its membrane-localized transporters belonging to the PIN-FORMED (PIN) protein family (Blilou *et al.*, 2005; Wiśniewska *et al.*, 2006). There are four PIN homologous genes encoded in the *P. patens* genome, PpPINA-PpPIND. The studies on the localization of *Physcomitrella* PINs in moss leaves revealed distinct patterns in the basal and the apical half of the leaf (Viaene *et al.*, 2014). PpPINA localizes uniformly on all sites of the cells at the basal half of the leaf, whereas it accumulates only on the apical site of each cell in the apical half of the leaf (Viaene *et al.*, 2014). For our experiments, we usually used the apical half of leaf, where the directional cell reprogramming occurred. Thus, the axial directionality of the cell reprogramming could be correlated with PIN localization. One possible hypothesis is that the auxin might re-distribute in response to wounding, which could ultimately lead to directional cell reprogramming. Therefore, it would be interesting to characterize the localization of PpPINA in response to the wounding response.

Another possible regulatory mechanism for directional cell reprogramming could be cell-cell communication via symplastic connections. The intercellular transport in moss leaves has been shown to exhibit a basal-apical directionality (Kitagawa & Fujita, 2015). In this study, a transgenic line expressing a diffusible photo-activated fluorescent protein was used to probe symplastic transport through plasmodesmata. Fluorescence was activated in a single cell in the middle of a detached leaf and the diffusion of the fluorescent protein was observed after a few hours (Kitagawa & Fujita, 2015). Only cells located at the basal and apical position of the activated single cell showed visible fluorescence, demonstrating the axial directionality of protein diffusion through plasmodesmata. The presence of plasmodesmata in moss leaf cells has been verified by callose staining and revealed a higher density at the apical side compared to the lateral side of cells (Regmi *et al.*, 2017), consistent with the axial direction of the observed diffusion of the fluorescent protein. Different lines of evidence suggest that small molecule diffusion in moss leaves possess a similar directionality as cell reprogramming e.g. the plasmodesmata are only present in the walls of the long axis (de Keijzer *et al.*, 2017). This implies that the wounding site may be a source for an unidentified wounding signal. The higher diffusion efficiency in the axial direction could then leads to the directional cell reprogramming. However, what is the nature of the wounding signal? Is the signal indeed transported through plasmodesmata? How do the signals induce the cell reprogramming in the receiving cells? Further studies are required to clarify the involvement of cell-cell transportation in the wounding-induced cell reprogramming.

The cell reprogramming mainly takes place in the surrounding cells in direct contact with the ablation zone and appears to have an axial directionality, which makes the axial cells of the wounding site

good candidates with a high potential to reprogram. The predictable cell reprogramming within four days post ablation makes it possible to investigate cell reprogramming in real-time. The subcellular reactions in these axial cells in response to wounding can be dissected in combination with other techniques such as laser dissection, RNA sequencing, and time-lapse imaging with specific reporters. The information collected from different experiments will shed new light on mysterious mechanisms of the wounding-induced cell reprogramming.

Material and methods

Plant material and growth conditions

For the preparation of all samples, small pieces of *P. patens* protonema tissue were transferred onto 0.9% agar BCD-AT plates and incubated for four weeks at 25°C under continuous light. For the ablation experiments a LifeAct-GFP, mCherry-Tubulin line was used to visualize the reorganization of both the actin and the microtubules after the ablation procedure.

Laser ablation sample preparation

Four-week-old gametophores were picked from *P. patens* colonies and carefully deposited into a drop of Milli-Q™ water to prevent the leaves from dehydrating and sticking to tools used to manipulate tissue. The rhizoids, as well as the top and bottom leaves, were removed using a razor blade because pre-existing damage to these areas is likely due to the picking of the gametophore. Individual leaves were excised from the remaining structure at about 1/3 of the leaf length from its base and stored in Milli-Q™ water droplets. Excised leaves tips were carefully picked up with tweezers at the cut site to prevent extra damage, especially to the fragile tip, and transferred onto a pad of 3.6% agar BCD-AT. The pad was then positioned with the leaves against the coverslip of a 35mm sample dish (MatTek Corporation, Ashland, MA, USA). A drop of water was deposited against the agar pad, which expelled any air bubbles that remained under the pad. To provide the leaves with sufficient nutrients, the pad was covered by a cap of a 15ml falcon tube to prevent the leaves from heat stress caused by the hot 1.2% agar BCD-AT that was poured around the cap. After the medium solidified, the cap was removed resulting in an approximately 0.5 cm gap band inside the edge of the sample dish. The gap between the pad and the outer BCD-AT was filled in with 1.2% agar BCD-AT to connect the pad and the outer medium.

Laser ablation procedure

Samples were scanned for flat, unfolded leaves in a Roper spinning disc confocal microscope on a Nikon Eclipse body (de Keijzer *et al.*, 2017). The area on one-third from the distal part of the flat excised leaves was chosen for ablation with rectangular target regions. To ablate selected cells, we used a high-powered pulsed Teem photonics SNG-03E 532nm laser with a 1000ns pulse length with the attenuating polarizer set to 340°. Based on the results of the preliminary test regarding the size of the ablation site, a 6-cell area was fixed as the standard size for ablation. To avoid damaging adjacent cells, the target site of the laser ablation was focused on the central part of the chosen 6-cell rectangular area, especially the cell-cell junctions. Bright field live-cell imaging was used on all ablated cells to confirm whether a cell died. A cell was clearly dead when the leakage of the cell contents or the shrinkage of intracellular organelles became visible. The other indicator was the emission of the strong auto-fluorescence from dead cells, which was detected with 561nm laser excitation.

Sample imaging

For time-lapse imaging of cytoskeletal markers, samples were imaged in a Roper spinning disc confocal microscope for 2 hrs with 2 minutes intervals. The fluorescence images were taken using the 491nm laser for the LifeAct-GFP images and the 561nm laser for the mCherry-Tubulin images. For cell reprogramming imaging, the observation was conducted on a ZEISS axiovert 200M epifluorescence microscope equipped with a Qimaging retiga EX camera. DIC and fluorescence images were taken at a 20x (pixel size: 6.45/20 = 0.3225 µm) magnification using a halogen lamp at 5.9V with a minimum field diaphragm diameter.

Statistics

Statistical analyses were conducted using SPSS (IBM Corp, 2013). Due to working with mostly categorical data, normal distributions could not be assumed. Therefore, the non-parametric Kruskall-Wallis test was used in most cases. In the few cases where binary data was collected (regeneration vs no regeneration etc.), a chi-square test was used when expected counts were higher than five. If expected counts are lower than five, Fisher's exact test yields more accurate results and was used instead (Fisher, 1922). Expected counts were calculated by SPSS from 2x2 contingency tables by applying the following formula:

$$expected_{i,j} = \frac{\sum column_i}{\sum total} * \sum row_j$$

For multiple comparison testing, a Bonferroni correction was applied (Shaffer, 1995).

Acknowledgements

We thank Marcel Janson in Cell Biology group for support and discussion.

Author Contributions

H.T. and T.K. planned and designed the research. H.T. and K.H. performed experiments and conducted data analysis. H.T., T.K., and J.V. wrote the manuscript.

References

Ahkami AH, Lischewski S, Haensch KT, Porfirova S, Hofmann J, Rolletschek H, Melzer M, Franken P, Hause B, Druege U. 2009. Molecular physiology of adventitious root formation in Petunia hybrida cuttings: involvement of wound response and primary metabolism. *New Phytologist* **181**(3): 613-625.

Blilou I, Xu J, Wildwater M, Willemsen V, Paponov I, Friml J, Heidstra R, Aida M, Palme K, Scheres B. 2005. The PIN auxin efflux facilitator network controls growth and patterning in Arabidopsis roots. *Nature* **433**(7021): 39.

Cove DJ, Knight CD. 1993. The moss Physcomitrella patens, a model system with potential for the study of plant reproduction. *The Plant Cell* **5**(10): 1483.

de Keijzer J, Kieft H, Ketelaar T, Goshima G, Janson ME. 2017. Shortening of microtubule overlap regions defines membrane delivery sites during plant cytokinesis. *Current Biology* **27**(4): 514-520.

Fisher RA. 1922. On the interpretation of χ 2 from contingency tables, and the calculation of P. *Journal of the Royal Statistical Society* **85**(1): 87-94.

Green C, Phillips R. 1975. Plant Regeneration from Tissue Cultures of Maize 1. *Crop Science* **15**(3): 417-421.

Hamant O, Heisler MG, Jönsson H, Krupinski P, Uyttewaal M, Bokov P, Corson F, Sahlin P, Boudaoud A, Meyerowitz EM. 2008. Developmental patterning by mechanical signals in Arabidopsis. *Science* **322**(5908): 1650-1655.

IBM Corp N. 2013. IBM SPSS statistics for windows. *Version 22.0*.

Ikeuchi M, Ogawa Y, Iwase A, Sugimoto K. 2016. Plant regeneration: cellular origins and molecular mechanisms. *Development* **143**(9): 1442-1451.

Ishikawa M, Murata T, Sato Y, Nishiyama T, Hiwatashi Y, Imai A, Kimura M, Sugimoto N, Akita A, Oguri Y. 2011. Physcomitrella cyclin-dependent kinase A links cell cycle reactivation to other cellular changes during reprogramming of leaf cells. *The Plant Cell*: tpc. 111.088005.

Ishikawa M, Murata T, Sato Y, Nishiyama T, Hiwatashi Y, Imai A, Kimura M, Sugimoto N, Akita A, Oguri Y, et al. 2011. Physcomitrella cyclin-dependent kinase A links cell cycle reactivation to other cellular changes during reprogramming of leaf cells. *Plant Cell* **23**(8): 2924-2938.

Iwase A, Harashima H, Ikeuchi M, Rymen B, Ohnuma M, Komaki S, Morohashi K, Kurata T, Nakata M, Ohme-Takagi M. 2017. WIND1 promotes shoot regeneration through transcriptional activation of ENHANCER OF SHOOT REGENERATION1 in Arabidopsis. *The Plant Cell* **29**(1): 54-69.

Iwase A, Mita K, Nonaka S, Ikeuchi M, Koizuka C, Ohnuma M, Ezura H, Imamura J, Sugimoto K. 2015. WIND1-based acquisition of regeneration competency in Arabidopsis and rapeseed. *J Plant Res* **128**(3): 389-397.

Iwase A, Mitsuda N, Koyama T, Hiratsu K, Kojima M, Arai T, Inoue Y, Seki M, Sakakibara H, Sugimoto K. 2011. The AP2/ERF transcription factor WIND1 controls cell dedifferentiation in Arabidopsis. *Current Biology* **21**(6): 508-514.

Kitagawa M, Fujita T. 2015. A model system for analyzing intercellular communication through plasmodesmata using moss protonemata and leaves. *J Plant Res* **128**(1): 63-72.

Liu J, Sheng L, Xu Y, Li J, Yang Z, Huang H, Xu L. 2014. WOX11 and 12 are involved in the first-step cell fate transition during de novo root organogenesis in Arabidopsis. *The Plant Cell* **26**(3): 1081-1093.

Melnyk CW, Schuster C, Leyser O, Meyerowitz EM. 2015. A developmental framework for graft formation and vascular reconnection in Arabidopsis thaliana. *Current Biology* **25**(10): 1306-1318.

Novak F, Afza R, Van Duren M, Perea-Dallos M, Conger B, Xiaolang T. 1989. Somatic embryogenesis and plant regeneration in suspension cultures of dessert (AA and AAA) and cooking (ABB) bananas (Musa spp.). *Bio/Technology* **7**(2): 154.

Regmi KC, Li L, Gaxiola RA. 2017. Alternate modes of photosynthate transport in the alternating generations of Physcomitrella patens. *Frontiers in Plant Science* **8**: 1956.

Sampathkumar A, Krupinski P, Wightman R, Milani P, Berquand A, Boudaoud A, Hamant O, Jönsson H, Meyerowitz EM. 2014. Subcellular and supracellular mechanical stress prescribes cytoskeleton behavior in Arabidopsis cotyledon pavement cells. *Elife* **3**: e01967.

Sato Y, Sugimoto N, Hirai T, Imai A, Kubo M, Hiwatashi Y, Nishiyama T, Hasebe M. 2017. Cells reprogramming to stem cells inhibit the reprogramming of adjacent cells in the moss Physcomitrella patens. *Sci Rep* **7**(1): 1909.

Shaffer JP. 1995. Multiple hypothesis testing. *Annual review of psychology* **46**(1): 561-584.

Skoog F, Miller C 1957. Chemical regulation of growth and organ formation in plant tissues cultured. *Vitro, Symp. Soc. Exp. Biol*.

Sugimoto K, Gordon SP, Meyerowitz EM. 2011. Regeneration in plants and animals: dedifferentiation, transdifferentiation, or just differentiation? *Trends Cell Biol* **21**(4): 212-218.

Sugiyama M. 2015. Historical review of research on plant cell dedifferentiation. *J Plant Res* **128**(3): 349-359.

Viaene T, Landberg K, Thelander M, Medvecka E, Pederson E, Feraru E, Cooper ED, Karimi M, Delwiche CF, Ljung K. 2014. Directional auxin transport mechanisms in early diverging land plants. *Current Biology* **24**(23): 2786-2791.

Wiśniewska J, Xu J, Seifertová D, Brewer PB, Růžička K, Blilou I, Rouquié D, Benková E, Scheres B, Friml J. 2006. Polar PIN localization directs auxin flow in plants. *Science* **312**(5775): 883-883.

Chapter 6

General discussion

Han Tang[1,2]

[1] Laboratory of Plant Developmental Biology, Wageningen University & Research, Wageningen, The Netherlands
[2] Laboratory of Cell Biology, Wageningen University & Research, Wageningen, The Netherlands

General discussion

To study the control of cell division in time and space in basal land plants, we used *Physcomitrella patens* as our model system, which grows as filamentous protonema cells together with the emergence of branch filaments. The predictable cell growth pattern and division timing make this a suitable system to investigate cytokinesis and developmental processes (**Chapter 1**). In this thesis, we first describe the role of the tethering complex during cytokinesis in pre-prophase band (PPB)-lacking filamentous cells **(Chapter 2)**. We then address the geometric features of division planes during the transition from 2-dimensional (2D) to 3-dimensional (3D) growth. **(Chapter 3)**. Next, we investigated the contribution of polarity proteins during gametophore initiation **(Chapter 4)**. Finally, a controllable wounding system was developed to study cell reprogramming in excised moss leaves **(Chapter 5)**, as a start to elucidate the interplay of cell reprogramming and cell division control in the early land plant lineage.

1. The regulation in the orientation of the division plane

To investigate molecular components involved in the final step of cell division, cytokinesis, when dividing cells are physically separated by forming a precisely oriented cross wall in between. We identified one specific subunit of the tethering exocyst complex, Sec6, that plays an independent role apart from the complex **(Ch. 2)**. During cytokinesis, the microtubule-based phragmoplast guides vesicles delivery and cell plate formation by forming an overlapping region in the midline of the division (Lee & Liu, 2013). How the vesicles are guided and bridged to the overlapping region of phragmoplast was unclear. We present evidence that phragmoplast microtubule overlaps are essential for the distribution of the Sec6 subunit of the exocyst tethering complex. Abolishment of the microtubule overlaps leads to failure of Sec6 to localize to the midline of the future division site, clarifying the requirement of microtubule overlaps for Sec6 localization. We found that Sec6 perfectly co-localized with microtubules before anaphase and concentrated to the overlapping region of phragmoplast prior to the arrival of vesicles. Attenuation of Sec6 expression resulted in a reduced amount of recruited vesicles and the Sec6-interacting membrane anchoring protein KEULE to the overlapping region of phragmoplast at the initiation of cytokinesis (Tang *et al.*, 2019). Therefore, our results reinforce the idea that the phragmoplast serves as a scaffold to recruit proteins and membranous materials to the division midline, where Sec6 may bridge microtubule overlaps and vesicles for cell plate formation.

Once arrived to the site of cell plate formation, the exocyst complex is required for vesicles tethering and membrane fusion across kingdoms (Wang *et al.*, 2002; Fendrych *et al.*, 2010; Heider & Munson, 2012). In yeast and mammalian cells, the exocyst complex is associated with vesicles and delivered at the division plane (Wu & Guo, 2015). The fluorescent-labelled subunits Sec3a, Sec5b, and membranous vesicles were observed to arrive simultaneously at the median plane of a dividing protonema cell, which supports the notion that the association of vesicles and at least in part of the exocyst complex could be conserved in *Physcomitrella*. Among exocyst subunits, Sec6 has been identified to interact with cytokinesis-specific SNARE protein KEULE in *Arabidopsis*, where the interaction between exocyst complex and SNAREs facilitates vesicles tethering and membrane fusion (Wu *et al.*, 2013). We have found that the interaction between Sec6 and KEULE is conserved in *Physcomitrella*, where the C-terminal interacting domain of KEULE is also highly conserved and sufficient to interact with Sec6. Knockdown of the only subunit Sec6 in *Physcomitrella* revealed

defective cell cross walls and a lower amount of vesicle accumulation at the division site, suggesting an evolutionarily conserved function in vesicle tethering and membrane fusion.

The determination of the orientation of the division plane has been demonstrated to rely on two plant specialized microtubule structures, the PPB and the phragmoplast (Oliferenko *et al.*, 2009; Li *et al.*, 2015; Lipka *et al.*, 2015). However, the orientation of the cell division planes can exhibit normal positioning in the absence of a PPB in *Arabidopsis* mutants and in *Physcomitrella* filamentous tissues, suggesting that other PPB-independent mechanisms exist (Doonan *et al.*, 1987; Schaefer *et al.*, 2017). To properly orient the developing cell plate, some landmark proteins e.g. MAP65-4, TANGLED, and Ran-GAP1 reside on the parental cortex and have been demonstrated to guide the phragmoplast and drive correct cell plate insertion (Cleary & Smith, 1998; Xu *et al.*, 2008; Li *et al.*, 2017). However, how are they recruited and functioning at the cortical site is still unclear. Our evidence that exocyst subunits appear to localize at the cortical membrane as punctate structures, where the future cell plate insertion takes place might help to investigate PPB-independent mechanisms underlying the control of the division plane orientation. Relevant questions to address are (1) whether cortically localized exocyst subunits are required for cell plate insertion; (2) whether the subunits of the exocyst complex bind/recruit known resident proteins at the insertion site, and (3) how different exocyst complex subunits are recruited to the cortical division site.

To answer these questions, mutations in cortically localized exocyst subunits that specifically disrupt their cortical localization are required. To dissect the role of the cortical localization in cell plate guidance, the cell plate insertion and the orientation of the division plane should be analysed in these mutants. The identified exocyst subunits at the parental cortex before cell plate attachment, and their potential interplay with known resident proteins e.g. MAP65-4, TANGLED, and Ran-GAP1 (Cleary & Smith, 1998; Xu *et al.*, 2008; Li *et al.*, 2017) may further our understanding of mechanisms underlying the regulation and guidance of the orientation of cell division planes.

2. Cell divisions as a marker for cell fate transition

Previous studies regarding the transition from filaments to gametophores mainly focused on an oblique division and follow-up development (Harrison *et al.*, 2009; Perroud *et al.*, 2014; Moody *et al.*, 2018). Approximately 5% of branch cells acquire a new cell fate as a gametophore initial cell that commences the transition from 2D to 3D growth. However, a gametophore initial cell should already have acquired its new cell fate prior to cell swelling and the oblique division (Harrison *et al.*, 2009). We investigated this cell fate transition in the moss life cycle, which starts from an asymmetric cell division in filamentous cells, by characterizing the properties of just-divided filamentous cells **(Ch. 3)**. We managed to quantitatively predict the cell fate of a gametophore initial cell prior to visible swelling, much earlier compared to previous studies (Harrison *et al.*, 2009). The identified parameters, the cell width of an initial cell and the angle of the transition division plane, enable us to recognize gametophore initials with high confidence. Additionally, we identified a fluorescent marker that was highly expressed in the filamentous cell, but appeared to be switched off in gametophore cells, allowing us to predict the cell fate of a gametophore initial cell.

Based on our results, we are now able to predict a gametophore initial cell at the stage prior to swelling, which provides a powerful tool to investigate this developmental transition at early stages. We can now synchronize and recognize gametophore initials within a short timeframe, which makes it possible to induce multiple gametophore initiation simultaneously and harvest gametophore initial

cells and parental cells for comprehensive transcriptional analysis e.g. single-cell sequencing (Denyer *et al.*, 2019; Kubo *et al.*, 2019). Questions remain to answer are (1) Whether the parental cells of a branch and a gametophore initial cell exhibit differences in terms of transcriptional regulation; (2) What key regulators are responsible for the cell swelling and cell fate acquirement of a gametophore initial cell could be addressed with such an approach. Furthermore, it would allow the identification of genetic networks that lead to different characteristics in cell division plane and cell swelling of gametophore initial cells. Further functional studies will provide insights into molecular mechanisms underlying the 2D-to-3D transition.

The orientation of division planes was identified as a geometric difference that distinguishes a gametophore initial cell from a branch initial cell. Because the PPB is lacking in filamentous cells, the orientation of the transition division plane must be regulated by PPB-independent mechanisms. It is interesting to note that computational modelling in Arabidopsis embryos indicates that hormone-dependent microtubule stabilization mechanisms and a geometrically favoured orientation of the cortical microtubule array associated with cell shape are sufficient to predict the division planes of the first four divisions (Chakrabortty *et al.*, 2018). Hence, cytoskeletal elements can already predict cell division planes prior to PPB formation, and an interesting question is whether filamentous cells in moss possess predictive cytoskeletal structures that may be translated by other (PPB-independent) mechanisms.

To induce gametophore formation, it has long been known that plant hormones, auxin and cytokinin, are essential for gametophore induction (Ashton *et al.*, 1979). To demonstrate whether and how hormones contribute to the onset of the developmental transition, the distribution of auxin and cytokinin should be monitored during the gametophore initiation. The marker line bearing fluorescent-tagged actin filaments and microtubule is available and used in Chapter 5, and recently an auxin reporter line in *Physcomitrella* was reported (Thelander *et al.*, 2019). A cytokinin reporter has not yet been presented in moss, but three receptors have been identified to respond to cytokinin. Mutation of three receptor genes leads to lack of gametophore formation (von Schwartzenberg *et al.*, 2015). These available materials make it possible to investigate the roles of cytoskeletal arrangement and hormone signalling pathways in the 2D-to-3D growth transition in the near future.

3. Polarization mechanisms and fate transition

During the 2D-to-3D transition, a pronounced morphological change is that gametophore initial cells swell after the division. This cell shape change and the loss of tip growth suggest that the intrinsic polarity of a gametophore initial cell may change during this process. Rho GTPases including subfamilies such as Cdc42, Rac, and Rho are known as key regulators for polarity control across kingdoms (Etienne-Manneville, 2004; Feiguelman *et al.*, 2018). Plants contain only a single subfamily Rho GTPases, termed Rho-of-Plant (ROPs). These ROPs regulate cell polarity through interacting with distinct effectors e.g. RICs (Rho-interactive CRIB motif-containing proteins) and ICR1 (Interactor of Constitutive active ROPs 1) (Lavy *et al.*, 2007; Zhou *et al.*, 2015; Feiguelman *et al.*, 2018).

In an attempt to link the morphological changes observed in gametophore initial cells to causative molecular pathways, we investigated the role of ROP proteins during the 2D to 3D transition through (1) characterization of their localization and (2) loss-of-function phenotypic analyses (**Ch. 4**). In *Physcomitrella,* only four ROPs (ROP1 to ROP4) and one putative effector RIC were identified based on sequence similarity (Burkart *et al.*, 2015; Bascom *et al.*, 2019). We showed that all four ROPs

proteins are localized at the plasma membrane of tip growing cells, whereas the apical enrichment is dispersed to the lateral side along with the swelling of gametophore initial cells. The apex-enriched localization of moss ROPs shown in this thesis (Ch.4, Fig. 1) is similar to what has been reported for other tip growing cells such as root hairs or pollen tubes (Molendijk *et al.*, 2001; Gu *et al.*, 2003), indicating a conserved role in supporting polar growth in *Physcomitrella* (Burkart *et al.*, 2015). The dispersed distribution of ROPs at the plasma membrane concurrent with the swelling of gametophore initial cells (Ch.4, Fig. 1), which suggests a correlation between ROPs localization and cell shape change.

The causal relationship between cell swelling and the disperse localization of ROP proteins is not yet clear. Based on previous studies regarding the function of ROPs in polarity control, we propose that the polarity of a gametophore initial cell may be changed via redistribution of ROPs at the plasma membrane. Another possibility is that the diffusion of ROPs at the plasma membrane can be a consequence of a polarity change. To determine the causal relationship between ROPs localization and cell swelling, what proteins control the ROPs localization upon swelling should be identified. Only the GTP-bound active ROPs localize to the plasma membrane, and the GEFs (guanine exchange factors) activate ROPs by promoting GDP-to-GTP exchange (Berken *et al.*, 2005). Thus, GEFs could be one of the strong candidates that activate and thereby regulate ROPs distribution during cell swelling. In a previous study, transcriptomic analysis showed that two moss GEFs are dramatically up-regulated in 4-cell early gametophores (Frank & Scanlon, 2015), which supports the idea that GEFs may regulate ROPs at the initial stage of gametophore development.

During tip cell growth, the apical polarity is supported by apex-enriched ROPs where it promotes actin assembly and thereby facilitate polarized exocytosis (Gu *et al.*, 2003; Cole & Fowler, 2006; Craddock *et al.*, 2012; Shao & Dong, 2016). In contrast, during the 2D to 3D transition in moss, a swelling gametophore initial cell appears to lose its apical polarity. Therefore, the exocyst complex and cytoskeleton are suspected to be involved in this process. The localization of Sec6 in a swelling gametophore initial cell will demonstrate if the polarized exocytosis is diffused. Along with the swelling of gametophore initial cells, the reorganization of actin filaments was observed and this showed that the apical enrichment of actin filaments is lost (Ch.6, Fig. **1**). In moss, the apical enrichment of actin filaments has been reported to support protonema polarized cell growth (Augustine *et al.*, 2011; Vidali & Bezanilla, 2012), suggesting that the loss of this apical structure indicates an alteration in intracellular polarity. A change in polarity has been demonstrated to be a trigger for asymmetric divisions in angiosperms (Casimiro *et al.*, 2001; Dong *et al.*, 2009), hence we suspect the alteration of polarity in gametophore initial cells is likely a prerequisite of the oblique division.

During the observation of early gametophore development, we found that ROPs localize to the cell plate forming site and thereafter decorate the cross walls, which is reminiscent of the localization patterns of the exocyst complex (Ch.4, Fig.1). Additionally, the examined exocyst subunits reside at the cell division site on the parental plasma membrane (Ch.2 Fig 1), where ROP GTPase activating proteins (GAPs) have been reported to accumulate by binding with mitosis-specific kinesin POKs (Stockle *et al.*, 2016). Because exocytosis in the cell apex is polarized via ROPs, it is plausible to hypothesize that active ROPs may recruit the exocyst complex to the site of cell plate formation.

To test the functional interplay between ROPs and the exocyst complex during cytokinesis, fluorescent-labelling of exocyst complex in *rop* mutants and reciprocal constructs should be generated and analysed in this process.

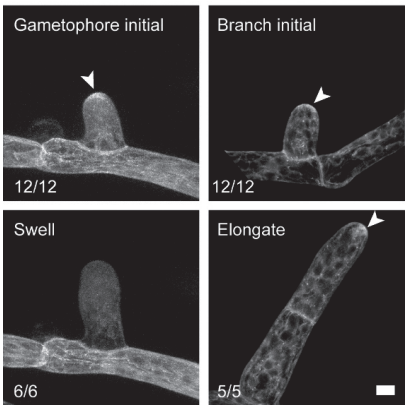

Figure 1. Actin filaments lose polar accumulation during the swelling of a gametophore initial cell.

Representative images of a gametophore and a branch initial cell with LifeAct-GFP labelled actin filaments (AFs) and in indicated stages. White arrowheads depicted the apical accumulation of AFs. N = number of images obtained / n = displayed typical distribution are shown at lower left. Scale bar = 10 µm.

The loss-of-function analyses showed that the *rop2* mutant reveals severe defects in gametophore initiation and development, which is rescued by deleting *PpRIC* in the *rop2* knockout background (*Δrop2Δric*). These data indicate involvement of a ROP2-RIC module in gametophore formation although it remains to be shown whether this is a direct effect of ROP action in the gametophore initial. Such a proof is important because we observed that, during filamentous cell growth, both *Δrop2Δric* and *Δrop2* display an impaired chloronema-to-caulonema transition. The *Δric* mutant resembles wildtype filaments, which indicates that the requirement of ROP2 in filament development is RIC-independent. Transcriptional analysis revealed that *RIC* expression is activated upon gametophore initiation, whereas the *RIC* transcript is almost undetectable in protonema. Together, our data support that a tissue-specific module of ROP2-RIC is active in gametophore formation that might be under transcriptional control.

The involvement of small GTPases in cell fate transition has been reported in animal cells, where the apical-restricted active small GTPases drives the cell mobility and thereby facilitate epithelial-to-mesenchymal transitions, which is crucial in embryonic development and tissue remodelling (Hay, 1995; Clay & Halloran, 2013). However, the direct functions of ROPs in cell fate transition in plants have not been established yet. Although a direct link between the function of ROP2 in polarity regulation and its requirement in developmental transitions remains elusive, our study paves the way for future studies addressing this issue.

4. Cellular reprogramming involves local stimulation of cell division

To investigate cell division control during cell reprogramming in basal land plants, we deployed a controllable wounding system by laser ablation in *Physcomitrella* **(Ch. 5)**. Upon wounding in gametophore-derived leaves, cell reprogramming takes place to reverse leaf cells to protonema cells along with tip growth (Prigge & Bezanilla, 2010). This is accompanied by re-activation of the cell cycle (Ishikawa *et al.*, 2011). Reprogrammed protonema cells ultimately develop into an entirely new plant (Prigge & Bezanilla, 2010). We performed laser ablations targeted to the middle of the single-cell layer of dissected moss leaves, which allowed us to track cell reprogramming in the cells surrounding the wounding site. We observed that cell reprogramming is not induced randomly but appears to be

restricted within one cell layer of the surrounding cells with an axial directionality along leaf axis, providing new evidence of a spatial control of cell reprogramming control.

The axial directionality of cell reprogramming in moss leaves also appeared in an observed inhibitory effect (Sato *et al.*, 2017). This study revealed that a reprogramming cell inhibits apical but not lateral adjacent cells to reprogram (Sato *et al.*, 2017). We suspect that this directionality could be correlated to directional hormone distribution or cell-cell communication. Moss auxin efflux transporters (PpPIN) have been shown to be polarly localized at the apical sites of leaf cells in the apical half of the leaf (Viaene *et al.*, 2014), where we deployed laser ablation. Therefore the axial auxin transport correlates with the axial directionality of cell reprogramming and may contribute to this process. Besides hormones, symplastic transport via plasmodesmata in moss leaves has been shown to possess an axial directionality. When a photoactivated fluorescence marker is stimulated in a single cell located in the middle of the leaf, the fluorescence signal displays an axial directional movement (Kitagawa & Fujita, 2015). To test if directional-transported hormones or other plasmodesmata-mediated molecules contribute to directional cell reprogramming, mutations in hormone transporters or plasmodesmata regulation should be generated and their capacity and directionality of cell reprogramming should be examined.

A fraction of surrounding cells (60%) progress to reprogramming along with tip cell growth, while some re-activate cell divisions (45%) but do not grow out as new filamentous cells within 96hrs. This observation raises further questions: (1) What is the identity of these divided cells; (2) why does laser ablation induce different cell responses in surrounding cells? To address these questions, molecular markers of leaf cells and protonemata cells are required. Protonema-specific marker have been reported for moss, which are specifically expressed in protonemata tissue but not in gametophores (Ishikawa *et al.*, 2011). At the margin of excised moss leaves, this marker gene is activated before visible cell elongation or division (Ishikawa *et al.*, 2011), which suggests that a leaf cell may already reprogram to a protonema cell prior to division or outgrowth. Laser ablations can be performed in this marker line to test whether activation of the marker gene can be detected prior to re-activation of the cell cycle.

5. Interplay between ROPs and the exocyst complex

In cell growth and polarity control, a role of small GTPases in regulating the exocyst complex is demonstrated in diverse organisms (Guo *et al.*, 2001; Moskalenko *et al.*, 2002; Sugihara *et al.*, 2002). During tip growth in plants, cell polarity is maintained by apically localized active ROPs that coordinate actin assembly and thus facilitate polarized exocytosis at cell apex (Molendijk *et al.*, 2001; Gu *et al.*, 2003). In yeast, small GTPases have been identified to directly interact with specific subunits of the exocyst complex and spatiotemporally regulate exocytosis by facilitating the exocyst complex assembly, vesicles tethering, and local activation (Wu *et al.*, 2008). Few studies have demonstrated the interaction between ROPs and subunits of the exocyst complex in plants. The interaction is indirectly mediated via the ROP effector ICR1, which interacts with AtROP6 and AtROP10 and binds to the exocyst subunit Sec3. Thus recruits this ICR1-Sec3 complex to the plasma membrane in *Arabidopsis* (Lavy *et al.*, 2007). The stomatal opening of *Arabidopsis* is negatively regulated by AtROP2, which is activated by light and interacts with effector RIC7 (Jeon *et al.*, 2008). The active RIC7 directly binds to and inhibits exocyst subunit EXO70B1, which positively regulates stomatal opening (Hong *et al.*, 2016).

In *Physcomitrella*, functional interplay between ROPs and the exocyst complex has not been described yet. This study reveals similar localization patterns of ROPs proteins and exocyst subunits at the apex of tip growing cells, which suggest their conserved working module to support polarized growth as shown in pollen tube and root hair (Molendijk *et al.*, 2001; Gu *et al.*, 2003). Suppression of *ROP* or *Sec6* expression by RNA silencing revealed similar tip growth phenotypes, indicating their essential role in polarized growth (Burkart *et al.*, 2015; Tang *et al.*, 2019).

During the 2D-to-3D transition, we have found that apically accumulated ROP proteins at the plasma membrane disperse laterally in a gametophore initial cell along with cell swelling, which suggests a polarity change. The exocyst complex is essential for the maintenance of tip growth since mutations in exocyst subunit Sec6 lead to swollen tips. The swollen branch cells upon Sec6 suppression resemble the swelling of gametophore initial cells (Ch.2, Fig. S6). Therefore, it is conceivable that the exocyst complex is functioning downstream of ROPs to modulate polarized exocytosis and facilitate the swelling of gametophore initial cells. To test this hypothesis, the localization patterns and functional study of the exocyst subunits should be examined in *rop* mutant background with a focus on the gametophore initiation.

In sum, we investigated different aspects of cell division control in the moss *P.patens*. We identified a role of exocyst subunit Sec6 in bridging the cytoskeletal network and membranous compartments during cytokinesis **(Ch. 2)**. We identified morphological characteristics that forecast a gametophore cell fate during a key 2D-3D developmental transition **(Ch. 3)**. We identified the involvement of polarity regulating ROP proteins in this transition as well as in filament development **(Ch. 4)**. Lastly, we found that cellular reprogramming involves local stimulation of cell divisions with an axial directionality in moss leaves **(Ch. 5)**.

References

Ashton NW, Grimsley NH, Cove DJ. 1979. Analysis of gametophytic development in the moss, Physcomitrella patens, using auxin and cytokinin resistant mutants. *Planta* **144**(5): 427-435.

Augustine RC, Pattavina KA, Tüzel E, Vidali L, Bezanilla M. 2011. Actin interacting protein1 and actin depolymerizing factor drive rapid actin dynamics in Physcomitrella patens. *The Plant Cell* **23**(10): 3696-3710.

Bascom JC, Burkart GM, Mallett DR, O'Sullivan JE, Tomaszewski AJ, Walsh K, Bezanilla M. 2019. Systematic survey of the function of ROP regulators and effectors during tip growth in the moss Physcomitrella patens. *J Exp Bot* **70**(2): 447-457.

Berken A, Thomas C, Wittinghofer A. 2005. A new family of RhoGEFs activates the Rop molecular switch in plants. *Nature* **436**(7054): 1176.

Burkart GM, Baskin TI, Bezanilla M. 2015. A family of ROP proteins that suppress actin dynamics and are essential for polarized growth and cell adhesion. *J Cell Sci*: jcs. 172445.

Casimiro I, Marchant A, Bhalerao RP, Beeckman T, Dhooge S, Swarup R, Graham N, Inzé D, Sandberg G, Casero PJ, et al. 2001. Auxin Transport Promotes Arabidopsis Lateral Root Initiation. *The Plant Cell* **13**(4): 843-852.

Chakrabortty B, Willemsen V, Zeeuw Td, Liao C-Y, Weijers D, Mulder B, Scheres B. 2018. A microtubule-based mechanism predicts cell division orientation in plant embryogenesis. *bioRxiv*.

Clay MR, Halloran MC. 2013. Rho activation is apically restricted by Arhgap1 in neural crest cells and drives epithelial-to-mesenchymal transition. *Development* **140**(15): 3198-3209.

Cleary AL, Smith LG. 1998. The Tangled1 gene is required for spatial control of cytoskeletal arrays associated with cell division during maize leaf development. *The Plant Cell* **10**(11): 1875-1888.

Cole RA, Fowler JE. 2006. Polarized growth: maintaining focus on the tip. *Curr Opin Plant Biol* **9**(6): 579-588.

Craddock C, Lavagi I, Yang Z. 2012. New insights into Rho signaling from plant ROP/Rac GTPases. *Trends Cell Biol* **22**(9): 492-501.

Denyer T, Ma X, Klesen S, Scacchi E, Nieselt K, Timmermans MC. 2019. Spatiotemporal developmental trajectories in the Arabidopsis root revealed using high-throughput single-cell RNA sequencing. *Dev Cell* **48**(6): 840-852. e845.

Dong J, MacAlister CA, Bergmann DC. 2009. BASL controls asymmetric cell division in Arabidopsis. *Cell* **137**(7): 1320-1330.

Doonan JH, Cove DJ, Corke FMK, Lloyd CW. 1987. Pre-prophase band of microtubules, absent from tip-growing moss filaments, arises in leafy shoots during transition to intercalary growth. *Cell Motility* **7**(2): 138-153.

Etienne-Manneville S. 2004. Cdc42-the centre of polarity. *Journal of Cell Science* **117**(8): 1291-1300.

Feiguelman G, Fu Y, Yalovsky S. 2018. ROP GTPases structure-function and signaling pathways. *Plant Physiol* **176**(1): 57-79.

Fendrych M, Synek L, Pečenková T, Toupalová H, Cole R, Drdová E, Nebesářová J, Šedinová M, Hála M, Fowler JE. 2010. The Arabidopsis exocyst complex is involved in cytokinesis and cell plate maturation. *The Plant Cell*: tpc. 110.074351.

Frank MH, Scanlon MJ. 2015. Cell-specific transcriptomic analyses of three-dimensional shoot development in the moss Physcomitrella patens. *Plant J* **83**(4): 743-751.

Gu Y, Vernoud V, Fu Y, Yang Z. 2003. ROP GTPase regulation of pollen tube growth through the dynamics of tip-localized F-actin. *J Exp Bot* **54**(380): 93-101.

Guo W, Tamanoi F, Novick P. 2001. Spatial regulation of the exocyst complex by Rho1 GTPase. *Nature cell biology* **3**(4): 353.

Harrison CJ, Roeder AH, Meyerowitz EM, Langdale JA. 2009. Local cues and asymmetric cell divisions underpin body plan transitions in the moss Physcomitrella patens. *Curr Biol* **19**(6): 461-471.

Hay ED. 1995. An overview of epithelio-mesenchymal transformation. *Cells Tissues Organs* **154**(1): 8-20.

Heider MR, Munson M. 2012. Exorcising the exocyst complex. *Traffic* **13**(7): 898-907.

Hong D, Jeon BW, Kim SY, Hwang JU, Lee Y. 2016. The ROP 2-RIC7 pathway negatively regulates light-induced stomatal opening by inhibiting exocyst subunit Exo70B1 in Arabidopsis. *New Phytologist* **209**(2): 624-635.

Ishikawa M, Murata T, Sato Y, Nishiyama T, Hiwatashi Y, Imai A, Kimura M, Sugimoto N, Akita A, Oguri Y, et al. 2011. Physcomitrella cyclin-dependent kinase A links cell cycle reactivation to other cellular changes during reprogramming of leaf cells. *Plant Cell* **23**(8): 2924-2938.

Jeon BW, Hwang J-U, Hwang Y, Song W-Y, Fu Y, Gu Y, Bao F, Cho D, Kwak JM, Yang Z. 2008. The Arabidopsis small G protein ROP2 is activated by light in guard cells and inhibits light-induced stomatal opening. *The Plant Cell* **20**(1): 75-87.

Kitagawa M, Fujita T. 2015. A model system for analyzing intercellular communication through plasmodesmata using moss protonemata and leaves. *J Plant Res* **128**(1): 63-72.

Kubo M, Nishiyama T, Tamada Y, Sano R, Ishikawa M, Murata T, Imai A, Lang D, Demura T, Reski R. 2019. Single-cell transcriptome analysis of Physcomitrella leaf cells during reprogramming using microcapillary manipulation. *Nucleic acids research* **47**(9): 4539-4553.

Lavy M, Bloch D, Hazak O, Gutman I, Poraty L, Sorek N, Sternberg H, Yalovsky S. 2007. A novel ROP/RAC effector links cell polarity, root-meristem maintenance, and vesicle trafficking. *Current Biology* **17**(11): 947-952.

Lee Y-RJ, Liu B. 2013. The rise and fall of the phragmoplast microtubule array. *Curr Opin Plant Biol* **16**(6): 757-763.

Li H, Sun B, Sasabe M, Deng X, Machida Y, Lin H, Julie Lee YR, Liu B. 2017. Arabidopsis MAP65-4 plays a role in phragmoplast microtubule organization and marks the cortical cell division site. *New Phytol* **215**(1): 187-201.

Li S, Sun T, Ren H. 2015. The functions of the cytoskeleton and associated proteins during mitosis and cytokinesis in plant cells. *Frontiers in Plant Science* **6**(282).

Lipka E, Herrmann A, Mueller S. 2015. Mechanisms of plant cell division. *Wiley Interdiscip Rev Dev Biol* **4**(4): 391-405.

Molendijk AJ, Bischoff F, Rajendrakumar CSV, Friml J, Braun M, Gilroy S, Palme K. 2001. *Arabidopsis thaliana* Rop GTPases are localized to tips of root hairs and control polar growth. *The EMBO Journal* **20**(11): 2779-2788.

Moody LA, Kelly S, Rabbinowitsch E, Langdale JA. 2018. Genetic Regulation of the 2D to 3D Growth Transition in the Moss Physcomitrella patens. *Curr Biol* **28**(3): 473-478 e475.

Moskalenko S, Henry DO, Rosse C, Mirey G, Camonis JH, White MA. 2002. The exocyst is a Ral effector complex. *Nature cell biology* **4**(1): 66.

Oliferenko S, Chew TG, Balasubramanian MK. 2009. Positioning cytokinesis. *Genes & development* **23**(6): 660-674.

Perroud PF, Demko V, Johansen W, Wilson RC, Olsen OA, Quatrano RS. 2014. Defective Kernel 1 (DEK1) is required for three-dimensional growth in Physcomitrella patens. *New Phytol* **203**(3): 794-804.

Prigge MJ, Bezanilla M. 2010. Evolutionary crossroads in developmental biology: Physcomitrella patens. *Development* **137**(21): 3535-3543.

Sato Y, Sugimoto N, Hirai T, Imai A, Kubo M, Hiwatashi Y, Nishiyama T, Hasebe M. 2017. Cells reprogramming to stem cells inhibit the reprogramming of adjacent cells in the moss Physcomitrella patens. *Sci Rep* **7**(1): 1909.

Schaefer E, Belcram K, Uyttewaal M, Duroc Y, Goussot M, Legland D, Laruelle E, de Tauzia-Moreau M-L, Pastuglia M, Bouchez D. 2017. The preprophase band of microtubules controls the robustness of division orientation in plants. *Science* **356**(6334): 186-189.

Shao W, Dong J. 2016. Polarity in plant asymmetric cell division: Division orientation and cell fate differentiation. *Dev Biol* **419**(1): 121-131.

Stockle D, Herrmann A, Lipka E, Lauster T, Gavidia R, Zimmermann S, Muller S. 2016. Putative RopGAPs impact division plane selection and interact with kinesin-12 POK1. *Nat Plants* **2**: 16120.

Sugihara K, Asano S, Tanaka K, Iwamatsu A, Okawa K, Ohta Y. 2002. The exocyst complex binds the small GTPase RalA to mediate filopodia formation. *Nature cell biology* **4**(1): 73.

Tang H, de Keijzer J, Overdijk EJ, Sweep E, Steentjes M, Vermeer JE, Janson ME, Ketelaar T. 2019. Exocyst subunit Sec6 is positioned by microtubule overlaps in the moss phragmoplast prior to cell plate membrane arrival. *J Cell Sci* **132**(3): jcs222430.

Thelander M, Landberg K, Sundberg E. 2019. Minimal auxin sensing levels in vegetative moss stem cells revealed by a ratiometric reporter. *New Phytologist*.

Viaene T, Landberg K, Thelander M, Medvecka E, Pederson E, Feraru E, Cooper ED, Karimi M, Delwiche CF, Ljung K, et al. 2014. Directional auxin transport mechanisms in early diverging land plants. *Curr Biol* **24**(23): 2786-2791.

Vidali L, Bezanilla M. 2012. Physcomitrella patens: a model for tip cell growth and differentiation. *Curr Opin Plant Biol* **15**(6): 625-631.

von Schwartzenberg K, Lindner A-C, Gruhn N, Šimura J, Novák O, Strnad M, Gonneau M, Nogué F, Heyl A. 2015. CHASE domain-containing receptors play an essential role in the cytokinin response of the moss Physcomitrella patens. *J Exp Bot* **67**(3): 667-679.

Wang H, Tang X, Liu J, Trautmann S, Balasundaram D, McCollum D, Balasubramanian MK. 2002. The multiprotein exocyst complex is essential for cell separation in Schizosaccharomyces pombe. *Molecular biology of the cell* **13**(2): 515-529.

Wu B, Guo W. 2015. The exocyst at a glance. *J Cell Sci* **128**(16): 2957-2964.

Wu H, Rossi G, Brennwald P. 2008. The ghost in the machine: small GTPases as spatial regulators of exocytosis. *Trends Cell Biol* **18**(9): 397-404.

Wu J, Tan X, Wu C, Cao K, Li Y, Bao Y. 2013. Regulation of cytokinesis by exocyst subunit SEC6 and KEULE in Arabidopsis thaliana. *Molecular plant* **6**(6): 1863-1876.

Xu XM, Zhao Q, Rodrigo-Peiris T, Brkljacic J, He CS, Müller S, Meier I. 2008. RanGAP1 is a continuous marker of the Arabidopsis cell division plane. *Proceedings of the National Academy of Sciences* **105**(47): 18637-18642.

Zhou Z, Shi H, Chen B, Zhang R, Huang S, Fu Y. 2015. Arabidopsis RIC1 severs actin filaments at the apex to regulate pollen tube growth. *The Plant Cell*: tpc. 114.135400.

Summary

Cell division and cell growth are essential for the development of all living organisms. Cells can produce identical daughter cells through proliferative symmetric divisions. Alternatively, they can produce daughter cells acquiring different cell fates through formative asymmetric cell divisions. Symmetric divisions account for the majority of the body expansion, whereas asymmetric divisions are crucial for the production of different tissue types. Due to the immobility of plant cells, the spatiotemporal control of cell divisions demands tight coordination with developmental cues and environmental stimuli. In **Chapter 1**, I introduce mechanisms that control plant cell divisions throughout development at cellular and tissue level. At cellular level, I focus on the final step of cell division, cytokinesis, which physically separates two daughter cells by building a new cross wall in between. At the tissue level, I review the regulation of asymmetric cell divisions including the orientation of the division plane, polarity establishment, and cell identity acquisition in angiosperms. Although we have acquired knowledge from angiosperms, the regulation of cell divisions in early land plants has not been studied in detail. I discuss the utility of the model bryophyte *Physcomitrella patens*, which has a powerful genetic toolset and single-cell-layer tissues easily observable through microscopy, and thus is highly suitable to investigate both generalities and differences of cell division control in an evolutionary manner.

In **Chapter 2**, we investigate the link between cytoskeletal structures and the cell plate deposition machinery during cytokinesis. During cytokinesis, two antiparallel sets of microtubules overlap with their plus ends at the midline of dividing cells. This microtubule configuration is referred to as the phragmoplast. Membranous material-carrying vesicles are delivered to the phragmoplast midplane where they fuse with each other for *de novo* cell plate formation. Centrifugal phragmoplast expansion thereby promotes the radial outgrowth of a disc-shaped membrane compartment. To investigate how microtubule overlaps are linked to membranous material deposition, we have focused on the exocyst, a vesicle tethering protein complex, which is involved in cell plate formation in *Arabidopsis*. We first survey the localization patterns of distinct exocyst subunits during cell division and show that subunit Sec6 localizes to microtubule overlaps prior to the arrival of vesicles. By induced silencing of MAP65, a microtubule- associated protein that is essential for overlap formation, we show that MAP65 supported microtubule overlaps are essential for Sec6 positioning. We demonstrate that the interaction between Sec6 and the membrane fusion component KEULE is conserved in moss. Suppression of *Sec6* expression shows lower abundance of membranous material-carrying vesicles and KEULE at phragmoplast midplane, which suggests a role of Sec6 in bridging the phragmoplast and vesicle fusion machinery.

Physcomitrella is a suitable system to study the integration of cell division control into developmental progression, since moss protonema cells execute a growth transition from a filament to a reproductive gametophore in a single-cell-layer tissue. In **Chapter 3**, we shift our focus to this transition. In *Physcomitrella*, a protonema cell may either branch out to form a new filament or transit into a gametophore, where the cell division control is the basis of these processes. A protonema cell undergoes an asymmetric cell division (transition division) to produce a gametophore initial cell. After the transition division, a gametophore initial cell swells and performs an oblique division. It has been proposed that a gametophore initial cell may already acquire its new cell fate prior to the swelling. To investigate the differences between gametophore and branch initial cells before swelling, we examine morphological changes by geometric analysis during the gametophore

initiation. We characterize and quantify two geometric cues: the width of the initial cell and the angle of the transition division plane, which are sufficiently distinguished a gametophore from a branch initial cell. We also identify a fluorescent marker that specifically switches off in gametophore initial cells before swelling, which allows us to predict gametophore cell fate at the initial stage with high confidence. Our results implicate that the parent cell of a gametophore initial cell possesses different properties from that of a branch initial cell. This study provides a new tool for mechanistic investigation of the 2D-to-3D growth transition at early stages in both parental cells and gametophore initial cells.

The swelling of a gametophore initial cell reflects an intracellular polarity change. In plants, polarized growth and polarity control are mainly regulated by widely conserved Rho-GTPase polarity proteins, in plants called Rho-of-Plants (ROPs). In **Chapter 4,** we aim to unravel the potential roles of ROPs in gametophore formation. We characterize the localization patterns of moss ROPs and find that during gametophore initiation, all the four moss ROPs display an apical accumulation at the plasma membrane of a gametophore initial cell but diffuse laterally along with the cell swelling. In loss-of-function analyses, the deletion of each single *ROP* reduces gametophore number, but the deletion of *rop2* (Δ*rop2)* shows the most severe defects. Δ*rop2* reveals aberrant gametophore initiation and leave development, and these defects are rescued by knocking out the single putative ROPs effector, RIC, in the Δ*rop2* background. Additionally, along with tip growth, protonema cells undergo a cell type transition from chloronema to caulonema fate with different differentiation characteristics. Our filament phenotype analysis shows that ROP2 promotes the chloronema-to-caulonema transition in a RIC-independent manner. This result suggests that the ROP2-RIC interplay is only relevant for specific developmental stages. Transcriptional analysis shows an induction of *ROP1*, *ROP2*, and *RIC* during gametophore initiation, while *RIC* is barely detected in filaments. These results support that a ROP2/RIC interaction module specifically acts in gametophore initiation but not in filament development, and this module is locally active during gametophore initiation. Altogether, here we demonstrate novel functions of the ROP proteins in developmental transitions, and also illustrate a tissue-specific functional interplay of ROP2-RIC during gametophore initiation.

Wounding-induced cell reprogramming is usually accompanied by reactivation of cell division to regenerate tissues. In **Chapter 5,** we aim to develop a controllable system in moss, using excised leaves, to gain knowledge about wounding-induced cell reprogramming. We use laser ablation to induce cell death in the middle of excised moss leaves, and we track the progress of cell reprogramming in cells surrounding the laser-wounding site. We find that cell reprogramming is not randomly induced, but is restricted to the first radial layer of cells surrounding the ablation site. Among them, cells positioned in the proximal-distal axis in relation to the ablation site have a higher chance to reprogram than lateral cells, indicating an axial directionality of cell reprogramming. Next, we investigate if the cytoskeletal network in surrounding cells responds to wounding. We find that the fluorescent markers of actin filaments and microtubules in the first radial layer cells transiently accumulate on the cell surface towards the ablation site without a directional tendency. Taken together, wounding-induced cell reprogramming reveals an axial directionality in moss leaves, which seems uncorrelated with the transient reorganization of the cytoskeleton in the surrounding cells.

In **Chapter 6**, we discuss the contribution of our work to different aspects of cell division control. We have found that exocyst subunit Sec6 may link the cytoskeletal network and membranous materials to initiate cytokinesis. During the 2D-to-3D growth transition, we identified markers as a new tool for

recognizing gametophore initial cells at early stages. We verified novel functions of ROP2 in two developmental transitions with different RIC dependency. We found that cellular reprogramming in excised moss leaves involves local stimulation of cell divisions with an axial directionality. Finally, the interplay between ROPs and the exocyst complex is discussed.

Acknowledgements

It is a great pleasure to finish such a long journey, and here I would like to express my gratefulness to all the people who support me along with my PhD path.

First I would like to deliver my deep appreciations to my supervisor team: Joop, Ben, Viola, and Tijs. **Tijs**, thank you so much for your unconditional support at the initial phase. At that uncertain moment it was you to provide me the first chance to join the CLB group, and we shared a great time on the exocyst project. **Joop**, nothing would happen without you. I enjoyed every skype meeting we have had as well as when you were around. You were always so nice and supportive no matter what happened, from which you encouraged me and taught me a lot in both scientific and life aspects. I am thankful to have you as my promotor during this PhD period. **Viola**, it was you to pick me up when I was lost. Your positive and energetic characteristics lightened up my path, where you guided me how to work on science in a broad view. You showed me how to lead a team with open-minded discussion, collaborative work, and help each other. It was my pleasure to work with you, and I would never forget our celebration for the first paper baby we delivered together. **Ben**, I clearly remember the first time I went to you for extra advice on supervision, and you might not know how meaningful your friendly replied "yes" to me. I treasured every chance to learn more from you. During my thesis writing, you always made time for me. Even when you have only few minutes between two meetings, you still ran to me with all the drafts and comments on hand. I enjoyed a lot to translate your handwriting on my draft and realized how lucky I am to have you as my promotor. You showed me how to work effectively, ask fundamental but important questions, and be a good scientist. Thank you all for your supervision and guidance.

Next I would like to thank all members of the CLB group, present and past, for all your kind helps and warm companionship through my PhD period. **Henk**, it was my pleasure to have you around with all the technical support in lab, and your reminder of taking care of myself with a kind smile always made me feel warm. **Ale**, we have opposite working styles, but eventually we compensate each other and work it out very well. I owe you a big thank you for your kind collaborative and honest characteristics, and all the brainstorms we have had together. **Marcel**, thank you for your practical support on microscope and teaching tasks. From your courses I learned how to guide students during the practical courses, where you showed your patience to diverse students. **Norbert**, you were always busy but you still made time to come over and care about my progress once a while, which I deeply appreciated it. Your professional support on microscope and the wonderful dinner you invited me delighted my PhD. **Hannie**, you always impressed me with your teaching profession, and your advice on holiday plans also expanded our experiences in the Netherlands. Many thanks for your accompany and I will treasure the sweet memory of playing game with Fenna during the X'mas dinner at your place. **Bela**, you were so positive and gave nice suggestions during our work discussion, and I also enjoyed hearing interesting stories you told in our gathering party. It was a great time to have you around. **Otto**, your big smile always pleased my day. I loved to listen to your adventure stories and your enthusiasm in plant researches. You are a sweet person and I enjoyed working with you very much. **Peter**, I could tell you love moss as much as I am, and I believe that can connect us

for the rest of our moss career. I wish you all the best with your moss factory and thank you for bringing all the new systems here. **Kiki**, thanks a lot for the management and assistant that keep the lab well-organized, your delicious baking products are more attractive to me though. **Marie-Jose**, thank you very much for everything you helped me with high efficiency, and also for organizing all the cards and gifts, you are absolutely the best secretary. **Elysa**, you showed me how to fight for ourselves and how Dutch people deal with strong argument directly. All the troubleshooting, moss transformation, lab works we have been through reminding me how did we develop our skills together with each other. I am very grateful to receive your useful suggestions when I was lost. **Jeroen**, I learned everything about moss, microscope, data analysis from you. It was a nice experience of collaboration with you on the Sec6 project, I sincerely wish you a bright future with your advanced skills and brilliant ideas. **Kris**, I missed the time we spent together during the coffee break. You always convinced me that a coffee break is a must, where we can guess a kiwi pattern every day. Your invitation to some dance or music events brought us to somewhere we would never be, which generates special memories for us.

I would like to deliver my thankfulness to all the master students who have worked with me. **Maikel**, **Els**, **Koen**, and **Kilian**, I enjoyed working with you very much and appreciate your contribution to this thesis. Thank you for giving me a chance to learn how to supervise students with different characters, and grew together with me.

I am grateful to have many nice people around me in my PhD daily life. MOB friends: **Wouter, Jac, Henk, Olga, Erik, Renze, Rik, Huchen, Anneke, Wenkun, Jelle, Renan, Vera, Menno, Yuda, Titis, Jorge, Marijn, Mengmeng,** and **Kavya**, I enjoyed every moment we sang the song together for a birthday cake or any occasion we have celebrated in the cozy coffee room. Thank you all for help and warm smiles you have sent to me in the hallway. **Martinus**, **Zhichun**, and **Xu**, I am glad to have you as my neighbour. The traditional Chinese foods you have shared with me really cheered me up when I was down.

My teammates in Invicta H3, **Peter, Bert, Marcel, Mathijs, Koen, Rijk, Piet,** and coach **Ellen**, I missed the training and tournaments we have had together. It was fun and enjoyable to play volleyball with you guys, which is a wonderful memory to bring back to Taiwan.

Big thanks to my dear friends around in Wageningen, **Momo, Dandan, Chia-Kai, Tze-Yi, Jimmy, Ya-Fen, Chang-Lin, Chia-Chi, I-Chiao, Hsuan, and Peng-Ying**. Your warm supports and companionship lightened up my heart along this long journey. All the nights we spent together with loud laugh and interesting topics brought me enormous joy, which always empowered me with the courage to move on. I appreciated it from my deep heart.

My paranymphs, Aniek and Jieyu, thank you for your practical supports on my big day. **Aniek**, I was grateful for the countless pancakes you made for me. The pancake lunches we had really encouraged me to deal with difficulties bravely, and I appreciated your patience to listen to all my complaining. I wish you all the best in any aspect of life, and we will certainly have another pancake party in the near future. **Jieyu**, it is so nice to have you around as my neighbour. You are such a lovely girl and I

enjoyed chatting with you very much. I am happy to share PhD life with you and thanks a lot for your sweet encouragement in the past few years.

My beloved **mom and papa**, thank you so much for your understanding of my decision. I am sorry to let you wait for a bit longer time than expected, but I hope at the moment you would be proud of me. For all the unconditional love and supports overseas, it is my great honour to present this thesis to you as a gift. My twin sister, **Ning**, and our **Pudding** dog, I would never achieve it without you. Your optimism, encouragement, and sweet personality brought me a wonderful life, now and past. Deep thanks for taking care of mommy and daddy, which allows me to pursue my scientific dream abroad.

A special thank is given to my dear husband, **Kuan-Ju**. No matter what happened, I know you will be there for me. Your faith in science, hard work in the lab, and the combination of confidence and humble in a soft heart show me how is an excellent scientist developed. Thank you for taking care of me, practically and mentally. You lifted me up when I was drowning, and you always knew how to cheer me up with hand-made sweet cards and date arrangement. I appreciate the destination that brought you to me, which made me tough and tender to face everything we encountered together.

About the author

Han was born on 21st September 1983 in Buenos Aires, Argentina. She lived and grew up in Taipei, Taiwan. She was interested in biology subject since junior high school. During her senior high school stage, she obtained a chance to join a research group as a part-time internship in Academia Sinica for one year. This short period stimulated her interests in scientific research.

After graduation from high school, she was enrolled in the Department of Plant Pathology and microbiology of National Taiwan University (NTU), where she built up her background knowledge regarding plant physiology, molecular biology, biochemistry, and plant pathology. She spent three and half a year to obtain her bachelor degree, and directly enrolled in a Taiwan International Graduate Program (TIGP) in Academia Sinica to pursue her PhD. She joined the Molecular and Biological Agricultural Sciences (MBAS) program in 2005 and start her first research work in Dr. Yu-Chan Chao's group in the Institute of Molecular Biology. She used the insect cell line like a factory where genetic-engineered recombinant Baculovirus can infect and express foreign proteins for application. She worked on a long non-coding RNA involved in reactivation of a latency state of virus and successfully generated a cell line with latent virus infection, which became an essential material for the group. In 2008, she changed her research topic and worked with Dr. Chao-Wen Wang in the Institute of Plant and Microbial Biology. She learned the background knowledge of cell biology and practical techniques by using a budding yeast system. She established a lipid analysis system including lipid extraction, visualization, and quantification. After two years, she decided to move to more complex organisms, thus she switched her choice again and work on the model plant Arabidopsis for about three years in Dr. Tien-Shin Yu's group. She expanded her viewpoint from simple single cell to a complex tissue and organ levels by studying long-distance light signalling transported from illuminated leaves to dark-treated shoot apex. She finished her first manuscript and submitted near the end of her PhD period, however, due to personal issue she did not complete it.

In 2014, together with her husband, she moved to Wageningen, the Netherlands. After a gap around half a year, she contacted Dr. Tijs Ketelaar in the chair group of Cell Biology in the Wageningen University. Tijs offered her an opportunity to help some laboratory work in CLB group for few months, and afterwards, Dr. Joop Vermeer offered her a PhD position in the same group. From Aug 2015 to Oct 2019, she got the second chance to pursue her dream in scientific research. At the first two years, she investigated the role of a protein Sec6 during the formation of cell division plane. She learned a new model system, *Physcomitrella patens*, and obtained practical skills about microscopy imaging and analysis. Later she shifted her focus to cell fate transition during a developmental switch in moss, which was supervised by Dr. Ben Scheres and Dr. Viola Willemsen. She established a system to investigate the correlation between cell division planes and cell fates. The outcome of her PhD research is present in this thesis.

List of publications

1. Y.-L. Wu*, C.P. Wu*, **Han Tang**, C.-H. Chang, H.-H. Chen and Y.-C. Chao. The Early Gene *hhi1* Reactivates *Heliothis zea* Nudivirus1 in Latently Infected Cells. *Journal of Virology***.** (2010) 84:1057-1065.

2. **Han Tang**, Jeroen de Keijzer, Elysa Overdijk, Els Sweep, Maikel Steentjes, Joop E. Vermeer, Marcel E. Janson, and Tijs Ketelaar. Exocyst subunit Sec6 is positioned by microtubule overlaps in the moss phragmoplast prior to the arrival of cell plate membrane. *Journal of Cell Science***.** (2019) 132.3: jcs222430.

3. **Han Tang**, Kilian Duijts, Magdalena Bezanilla, Ben Scheres, Joop E.M. Vermeer, and Viola Willemsen. Geometric cues forecast the switch from 2D-to-3D growth in *Physcomitrella patens***.** *New Phytologist***.** (2019) in press.

4. Elysa J.R. Overdijk, **Han Tang**, Jan Willem Borst, Francine Govers, and Tijs Ketelaar. Time-gated confocal microscopy reveals accumulation of exocyst subunits at the plant-pathogen interface. *Journal of Experimental Botany*. (2019) in press.

5. **Han Tang***, Alejandra Freire Rios*, Tijs Ketelaar, Ben Scheres, Joop E.M. Vermeer, and Viola Willemsen. The roles of ROP2 and RIC in *Physcomitrella patens* gametophore formation. In preparation.

Education Statement of the Graduate School Experimental Plant Sciences

Issued to: Han Tang
Date: 24 January 2020
Group: Laboratory of Plant Developmental Biology & Laboratory of Cell Biology
University: Wageningen University & Research

1) Start-Up Phase	date	cp
► **First presentation of your project**		
Characterization of exocyst complex in moss	16 Oct 2015	1.5
► **Writing or rewriting a project proposal**		
► **Writing a review or book chapter**		
► **MSc courses**		
Subtotal Start-Up Phase		1.5

2) Scientific Exposure	date	cp
► **EPS PhD student days**		
EPS PhD student days Get2Gether, Soest, The Netherlands	28-29 Jan 2016	0.6
EPS PhD student days Get2Gether, Soest, The Netherlands	15-16 Feb 2018	0.6
► **EPS theme symposia**		
EPS theme 1 'Developmental Biology of Plants', Wageningen University, The Netherlands	21 Jan 2016	0.3
EPS theme 1 'Developmental Biology of Plants', Leiden University, The Netherlands	28 Feb 2017	0.3
EPS theme 1 'Developmental Biology of Plants', Wageningen University, The Netherlands	30 Jan 2018	0.3
► **Lunteren Days and other national platforms**		
Annual meeting 'Experimental Plant Sciences', Lunteren, The Netherlands	11-12 Apr 2016	0.6
Annual meeting 'Experimental Plant Sciences', Lunteren, The Netherlands	10-11 Apr 2017	0.6
Annual meeting 'Experimental Plant Sciences', Lunteren, The Netherlands	9-10 Apr 2018	0.6
Annual meeting 'Experimental Plant Sciences', Lunteren, The Netherlands	8-9 Apr 2019	0.6
► **Seminars (series), workshops and symposia**		
Seminar Siobhan Bredy	9 Sep 2015	0.1
Seminar Olivier Harmant	15 Mar 2016	0.1
Seminar Niels Galjart	12 May 2016	0.1
Seminar Sabine Muller	9 Sep 2016	0.1
Seminar Daniel von Wangenheim	11 Oct 2016	0.1
Seminar Magalena Bezanilla	6 Nov 2017	0.1
Seminar Jiri Friml	17 Dec 2018	0.1
Symposium: Dutch Biophysics meeting, Veldhoven, The Netherlands	2-3 Oct 2017	0.6
Workshop: Breeding for sustainability, Wageningen, The Netherlands	20 Nov 2018	0.3
► **Seminar plus**		
► **International symposia and congresses**		
Workshop: EMBO workshop: New model systems for early land plant. Vienna, Austria	22-24 Jun 2016	0.9
Symposium: The plant and microbial cytoskeleton. Gordon conferences, Andover, NH, US	14-19 Aug 2016	1.3
Symposium: Symposium Dynamics Plant Dev. & Evol. Zurich, Switzerland	30 Nov 2017	0.5
Workshop: EMBO workshop: New shores in land plant evolution. Lisbon, Portugal	20-23 Jun 2018	1.1
Symposium: Japan-Taiwan Plant Biology. Nagoya, Japan	14-16 Mar 2019	0.9
Symposium: iMoss meeting. Madrid, Spain	9-12 Jul 2019	0.9
► **Presentations**		
Poster: Evo-devo of plant cell differentiation Workshop: EMBO workshop: New model systems for early land plant. Vienna, Austria	22-24 Jun 2016	1.0
Poster: Evo-devo of plant cell differentiation Symposium: The plant and microbial cytoskeleton. Gordon conferences, Andover, NH, US	14-19 Aug 2016	1.0
Poster: mechanical perturbation of plant tissue triggers repgrogramming of cells Symposium: Dutch Biophysics meeting. Veldhoven, The Netherlands	2-3 Oct 2017	1.0
Poster: Geometric cues forecast the 2D-to-3D transition in *Physcomitrella patens* Symposium: Japan-Taiwan Plant Biology. Nagoya, Japan	14-16 Mar 2019	1.0
Talk: The exocyst subunit Sec6 kickstarts vesicle assembly during cytokinesis ALW meeting 'Experimental Plant Sciences', Lunteren, The Netherlands	10-11 Apr 2017	1.0
Talk: The directionality of wounding-induced cell reprogramming in moss leaves EPS PhD student days Get2Gether, Soest, The Netherlands	15-16 Feb 2018	1.0
Talk: The role of ROPs and RIC during asymmetric cell division in bud formation of *Physcomitrella patens* Workshop: EMBO workshop: New shores in land plant evolution. Lisbon, Portugal	20-23 Jun 2018	1.0
Talk: Geometric cues forecast the switch from 2D-to-3D growth in *Physcomitrella patens* Symposium: iMoss meeting. Madrid, Spain	9-12 Jul 2019	1.0
► **IAB interview**		
► **Excursions**		
EPS PhD Council company visit to Koppert	26 Oct 2018	0.2
Subtotal Scientific Exposure		19.9

E

3) In-Depth Studies	date	cp
► **Advanced scientific courses & workshops**		
The power of RNA-seq	10-12 Feb 2016	0.8
Introduction to R for statistical analysis	20-21 Feb 2019	0.6
► **Journal club**		
PDB-MOB journal club	2018 - 2019	1.0
► **Individual research training**		
Yeast-2-Hybrid in Business Unit Bioscience, WUR	2015	1.5
Subtotal In-Depth Studies		3.9

4) Personal Development	date	cp
► **General skill training courses**		
Project and time management	4, 18 Nov, 16 Dec 2016	1.5
EPS PhD introduction course	16 Feb 2017	0.3
Efficient writing strategies	Oct - Dec 2016	1.3
WGS PhD workshop Carousel	7 Apr 2017	0.3
WIAS course survival guide to peer review	2 Jun 2017	0.3
PhD competence assessment	13 Jun 2017	0.3
PhD peer consultation	30 Jan 2018	0.6
Scientific writing	9 Jan - 27 Feb 2018	1.2
The essentials of scientific writing and presenting	4, 18 May 2018	0.6
Scientific publishing	11 Oct 2018	0.3
Critical thinking and argumentation	23 Oct 2018	0.3
Supervising BSc and MSc thesis students	24 Oct, 13, 16 Nov 2018	0.6
Writing Propositions for your PhD	27 Nov 2018	0.0
Last stretch of the PhD program	27 Nov 2018	0.0
Reviewing a scientific paper	29 Nov 2018	0.1
► **Organisation of meetings, PhD courses or outreach activities**		
► **Membership of EPS PhD Council**		
Subtotal Personal Development		7.7

TOTAL NUMBER OF CREDIT POINTS*	**33.0**

Herewith the Graduate School declares that the PhD candidate has complied with the educational requirements set by the Educational Committee of EPS with a minimum total of 30 ECTS credits.

** A credit represents a normative study load of 28 hours of study.*

E

This research was performed at the Laboratory of Cell Biology and the Laboratory of Plant Developmental Biology, Wageningen University & Research, the Netherlands and financially supported by the Earth and Life Sciences Council (ALW) of the Netherlands Organization for Scientific Research (NWO; ALW-VIDI 864.13.008).

Cover and layout design: Han Tang & ProefschriftMaken

Printed by: ProefschriftMaken